Form factors for semileptonic $\mathrm{B_s} \to \mathrm{K}\ell\nu$ decays in lattice QCD

DISSERTATION

zur Erlangung des akademischen Grades
doctor rerum naturalium
(Dr. rer. nat.)
im Fach Physik
Spezialisierung: Theoretische Physik

eingereicht an der
Mathematisch-Naturwissenschaftlichen Fakultät
der Humboldt-Universität zu Berlin

von
Herrn Dipl.-Phys. Felix Tobias Bahr

Präsident der Humboldt-Universität zu Berlin
Prof. Dr. Jan-Hendrik Olbertz

Dekan der Mathematisch-Naturwissenschaftlichen Fakultät
Prof. Dr. Elmar Kulke

Gutachter/innen:
1. Prof. Dr. Rainer Sommer
2. Priv.-Doz. Dr. Oliver Bär
3. Prof. Dr. Sinéad Ryan

Tag der mündlichen Prüfung: 18.06.2015

Abstract

We present an exploratory study of the calculation of the form factor $f_+(q^2)$ for the semileptonic decay $\mathrm{B_s} \to \mathrm{K}\ell\nu$ in large-volume lattice QCD simulations with two dynamical sea quark flavours using $O(a)$ improved Wilson fermions. We discuss the computation of relevant two- and three-point functions and consider complementary methods how these can be combined to obtain the form factor. In particular, we put forward the strategy of a combined fit in which data of all correlators enter and which has as fit parameters energies and amplitudes of the correlators and the form factor.

The b quark is treated in HQET; our present analysis focuses on the static limit. Meanwhile, we have developed the code and performed the measurements of all needed $O(1/m_\mathrm{h})$ corrections which will be used as soon as their coefficients will have been computed by the ALPHA collaboration. In order to be able to measure the form factor at the same value of the momentum transfer q^2 on all ensembles, we impose twisted boundary conditions on the s and b quarks that allow for a free tuning of the quark momenta and thus of q^2. We perform measurements on a subset of $N_\mathrm{f} = 2$ CLS gauge configurations, obtaining the form factor at three different lattice spacings and roughly the same pion mass of about 330 MeV. Using these, we carry out a continuum extrapolation and observe that it is relatively flat in a^2. A measurement at a different pion mass indicates that quark mass effects are small. We compare our continuum value of the form factor with recently published results of other collaborations and observe a good agreement.

Keywords:
Lattice QCD, HQET, form factors, b physics

Zusammenfassung

Wir präsentieren eine Forschungsstudie zur Berechnung des Formfaktors $f_+(q^2)$ für den semileptonischen Zerfall $B_s \to K\ell\nu$ in Gitter-QCD-Simulationen im großen Volumen mit zwei dynamischen Seequark-Flavours mit $O(a)$-verbesserten Wilson-Fermionen. Wir diskutieren die Berechnung relevanter Zwei- und Dreipunkt-Funktionen und betrachten komplementäre Methoden diese zu kombinieren, um den Formfaktor zu erhalten. Insbesondere stellen wir die Strategie eines kombinierten Fits vor, in den Datenpunkte aller Korrelatoren eingehen und der als Fitparameter Energien, Amplituden und den Formfaktor hat.

Das b-Quark wird in HQET behandelt; unsere momentane Analyse konzentriert sich auf den statischen Grenzfall. Indes haben wir den Code für alle nötigen $O(1/m_h)$-Korrekturen entwickelt und die Messungen dieser durchgeführt; sie werden verwendet werden, sobald ihre Koeffizienten von der ALPHA-Kollaboration bestimmt worden sein werden. Um den Formfaktor auf allen Ensembles bei dem gleichen Wert des Impulsübertrags q^2 bestimmen zu können, führen wir getwistete Randbedingungen für das s- und das b-Quark ein, die ein freies Einstellen der Quarkimpulse und damit von q^2 ermöglichen. Wir führen Messungen auf einer Untermenge von $N_f = 2$ CLS Eichkonfigurationen durch und erhalten den Formfaktor bei drei verschiedenen Gitterabständen und etwa gleicher Pionmasse von ungefähr 330 MeV. Wir benutzen diese, um eine Kontinuumsextrapolation durchzuführen, und beobachten, dass diese relativ flach in a^2 ist. Eine Messung bei einer unterschiedlichen Pionmasse deutet an, dass Quarkmassen-Effekte klein sind. Wir vergleichen unseren Kontinuumswert des Formfaktors mit kürzlich veröffentlichten Ergebnissen anderer Kollaborationen und stellen eine gute Übereinstimmung fest.

Schlagw?ter:
Gitter-QCD, HQET, Formfaktoren, b-Physik

Contents

1 Introduction

The world of elementary particles is theoretically described by quantum field theories incorporated in the Standard Model (SM) of particle physics. It is gauge invariant under an $\mathrm{SU}(3)_\mathrm{c} \times \mathrm{SU}(2)_\mathrm{I} \times \mathrm{U}(1)_\mathrm{Y}$ group. Electroweak interactions are characterised by the $\mathrm{SU}(2)_\mathrm{I} \times \mathrm{U}(1)_\mathrm{Y}$ group of electroweak isospin and hypercharge, strong interactions are governed by the $\mathrm{SU}(3)_\mathrm{c}$ colour group, and in which fields dubbed *quarks* and *gluons* participate.

Electromagnetic interactions are described by Quantum Electrodynamics (QED). It can very well be treated in perturbation theory (PT), that is, an expansion in the coupling α_em, which is roughly constant as a function of energy, $\alpha_\mathrm{em} \approx 1/137$ at zero energy, $\alpha_\mathrm{em} \approx 1/128$ at the mass of the W boson ($\approx 80\,\mathrm{GeV}$). The theory of strong interactions is formulated in the framework of Quantum Chromodynamics (QCD). Here, the coupling α_s is a function of the energy of the process considered. It is small, and thus a good expansion parameter, for processes at high energies, $O(10\text{–}100\ \mathrm{GeV})$, or small distances. That is, in this regime, particles couple very weakly among each other, and thus can be considered (nearly) free. This property is known as *asymptotic freedom*. For processes at low energies, $O(100\ \mathrm{MeV})$, or large distances, however, α_s is of order 1 and thus perturbation theory can no longer be applied reliably. Here, particles couple strongly and one is in the regime known as *confinement*, where quarks are confined to within a hadron.

The six quarks that nature has invented cover a mass range spanning several orders of magnitude, from a few MeV for the up and down quark up to around 170 GeV for the top quark. It, in fact, is too heavy to hadronise, since because of its high mass, it decays before it can form a hadronic bound state. Thus, the heaviest quark that can form hadrons is the bottom or *beauty* quark, with a mass of around 4 GeV. Therefore, b physics, that is, the dynamics of hadrons containing a beauty quark, is a particularly special and interesting field of research. To compute hadronic quantities (intrinsically, confined particles), a fully non-perturbative treatment is necessary. A powerful tool for non-perturbative calculations is Lattice QCD. In this thesis, we will use it to compute semileptonic decays of $\mathrm{B_s}$ mesons to kaons, that is, of a meson containing a b and an (anti-)s quark, the b quark decays to a u quark via the weak interaction, with the s a spectator quark, that is, it does not participate in the short-distance weak process.

1.1 The CKM matrix and the $|V_\mathrm{ub}|$ puzzle

The CKM matrix, named after the authors of the works in which it was first described, Cabibbo [1], and Kobayashi and Maskawa [2], collects the strengths of weak flavour chang-

ing quark decays:

$$V_{\mathrm{CKM}} = \begin{pmatrix} V_{\mathrm{ud}} & V_{\mathrm{us}} & V_{\mathrm{ub}} \\ V_{\mathrm{cd}} & V_{\mathrm{cs}} & V_{\mathrm{cb}} \\ V_{\mathrm{td}} & V_{\mathrm{ts}} & V_{\mathrm{tb}} \end{pmatrix}, \tag{1.1}$$

where V_{ij} is the strength of quark flavour change from flavour i to flavour j. In this section, we review some of its properties and parameterisations, detailed, for example, in reference [3]. In the SM, the CKM matrix is a unitary matrix. Testing its unitarity is therefore a powerful way of probing the SM. Unitarity predicts that

$$\sum_i V_{ij} V_{ik}^* = \delta_{jk} \quad \text{and} \quad \sum_j V_{ij} V_{kj}^* = \delta_{ik}. \tag{1.2}$$

Six different combinations of i, j, k will give 0, the most prominent of which is

$$V_{\mathrm{ud}} V_{\mathrm{ub}}^* + V_{\mathrm{cd}} V_{\mathrm{cb}}^* + V_{\mathrm{td}} V_{\mathrm{tb}}^* = 0. \tag{1.3}$$

To each of these combinations corresponds a unitarity triangle, an example of which we discuss below, compare figure 1.1. They all have the same area which is a measure for CP violation. It is given by $J/2$, where J is the Jarlskog invariant [4], defined by

$$\mathrm{Im}(V_{ij} V_{kl} V_{il}^* V_{kj}^*) = J \sum_{m,n} \epsilon_{ikm} \epsilon_{jln}. \tag{1.4}$$

In what is sometimes referred to as the "Standard" parameterisation [5], the CKM matrix reads:

$$V_{\mathrm{CKM}} = \begin{pmatrix} c_{12}c_{13} & s_{12}c_{13} & s_{13}\,\mathrm{e}^{-\mathrm{i}\,\delta} \\ -s_{12}c_{23} - c_{12}s_{23}s_{13}\,\mathrm{e}^{\mathrm{i}\,\delta} & c_{12}c_{23} - s_{12}s_{23}s_{13}\,\mathrm{e}^{\mathrm{i}\,\delta} & s_{23}c_{13} \\ s_{12}s_{23} - c_{12}c_{23}s_{13}\,\mathrm{e}^{\mathrm{i}\,\delta} & -c_{12}s_{23} - s_{12}c_{23}s_{13}\,\mathrm{e}^{\mathrm{i}\,\delta} & c_{23}c_{13} \end{pmatrix}, \tag{1.5}$$

where $s_{ij} = \sin\theta_{ij}$, $c_{ij} = \cos\theta_{ij}$ with the three Euler angles θ_{ij} and a phase δ associated with CP violation. Changing variables [6]

$$s_{12} = \lambda, \quad s_{23} = A\lambda^2, \quad s_{13}\,\mathrm{e}^{-\mathrm{i}\,\delta} = A\lambda^3(\rho - \mathrm{i}\,\eta), \tag{1.6}$$

one arrives at the Wolfenstein parameterisation [7], defined as an expansion in λ, usually given up to λ^3:

$$V_{\mathrm{CKM}} = \begin{pmatrix} 1 - \lambda^2/2 & \lambda & \lambda^3 A(\rho - \mathrm{i}\,\eta) \\ -\lambda & 1 - \lambda^2/2 & \lambda^2 A \\ \lambda^3 A(1 - \rho - \mathrm{i}\,\eta) & -\lambda^2 A & 1 \end{pmatrix}. \tag{1.7}$$

Now one can define

$$\bar{\rho} = \rho(1 - \lambda^2/2), \quad \bar{\eta} = \eta(1 - \lambda^2/2); \tag{1.8}$$

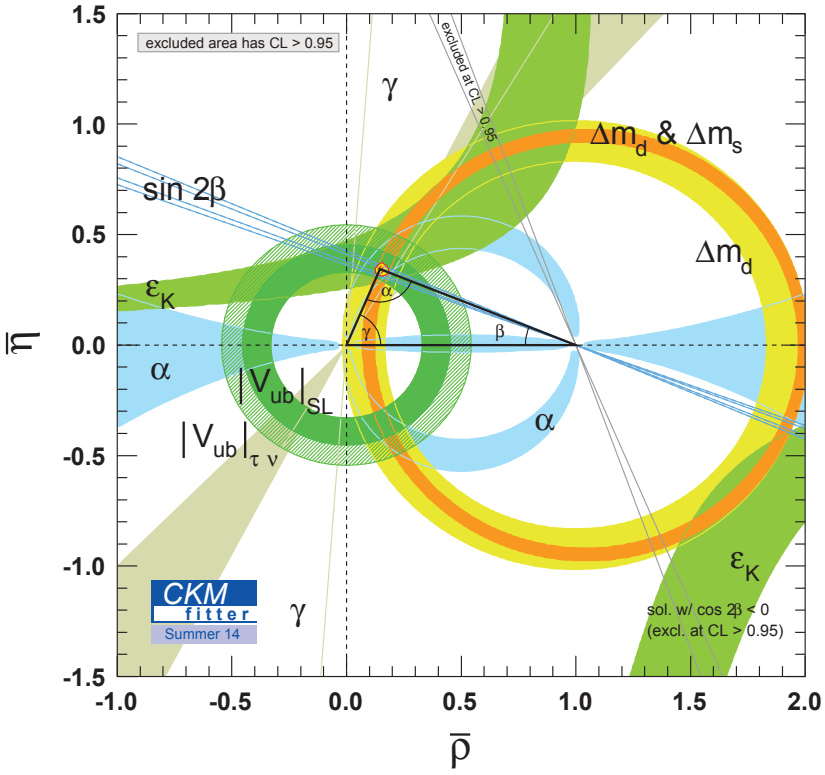

Figure 1.1: Unitarity triangle in the $\bar{\rho}\,\bar{\eta}$-plane. Picture taken from the CKMfitter group [8].

$\bar{\rho}$ and $\bar{\eta}$ now span a plane in which it is popular to plot a unitarity triangle, figure 1.1, along with the various constraints on its parameters.

The matrix element $|V_{ub}|$ is one of the least well-known CKM matrix elements. In fact, there is an ongoing $\sim 2-3\sigma$ discrepancy in the value of $|V_{ub}|$ determined from different decays[1]. The recent PDG report [3] lists these as[2]:

- $|V_{ub}| = (4.41 \pm 0.15^{+0.15}_{-0.19}) \times 10^{-3}$ from inclusive $B \to X_u \ell\nu$ decays;
- $|V_{ub}| = (3.28 \pm 0.29) \times 10^{-3}$ from exclusive $B \to \pi\ell\nu$ decays;
- $|V_{ub}| = (4.22 \pm 0.42) \times 10^{-3}$ from $B \to \tau\nu$ decays.

Understanding this discrepancy is an open challenge for the particle physics community. For this, both experimental and theoretical input is needed. Experiments are ongoing or planned [9–11]. Let us mention at this point that this topic has been the subject of recent overviews, for example references [12–14] and the monumental work of reference [15].

Let us discuss the $|V_{ub}|$ determination from $B \to \tau\nu$ decays a little further. The quantity accessible in experiments is the branching fraction $\mathcal{B}(B \to \tau\nu)$, which is related to $|V_{ub}|$

[1] Note that in equation (2.15), V_{ub}^2 enters. Thus, one can only give values for $|V_{ub}|$.
[2] Here and in the following, if two errors are given, the first error is statistical and the second error is systematic.

Collaboration	Tag	$\mathcal{B}(B \to \tau\nu) \times 10^4$	$\lvert V_{ub}\rvert \times 10^3$	Reference
Belle	semileptonic	$1.25 \pm 0.28 \pm 0.27$	4.4 ± 1.4	[17]
Belle	hadronic	$0.72^{+0.27}_{-0.25} \pm 0.11$	3.4 ± 1.3	[18]
BaBar	semileptonic	$1.7 \pm 0.8 \pm 0.2$	5.2 ± 2.5	[19]
BaBar	hadronic	$1.83^{+0.53}_{-0.49} \pm 0.24$	5.3 ± 1.6	[20]

Table 1.1: Values for $\mathcal{B}(B \to \tau\nu)$ as determined by Belle and BaBar collaborations using different tagging methods and the corresponding values of $|V_{ub}|$.

via

$$\mathcal{B}(B \to \tau\nu) = \frac{G_F^2 m_B m_\tau^2}{8\pi}\left(1 - \frac{m_\tau^2}{m_B^2}\right)^2 f_B^2 |V_{ub}|^2 \tau_B, \tag{1.9}$$

where $G_F = 1.1663787(6) \times 10^{-5}\,\mathrm{GeV}^{-2}$ [3] is the Fermi constant, m_B, m_τ are the masses of the B meson and τ lepton, respectively, f_B is the decay constant of the B meson and τ_B is its lifetime. The PDG value of $|V_{ub}|$ given above is computed using the world average of $\mathcal{B}(B \to \tau\nu) = (1.14 \pm 0.27) \times 10^{-4}$. However, to illustrate the wide spread there is in measuring this quantity experimentally, in table 1.1, we list the values determined by the Belle and BaBar collaborations using semileptonic or hadronic tagging methods for particle reconstruction. We compute $|V_{ub}|$ using [3] $m_{B^\pm} = 5.27925(26)$ GeV, $m_\tau = 1.77682(16)$ GeV, $\tau_{B^\pm} = 1.638(4) \times 10^{-12}\,\mathrm{s}$ and [16] $f_B = 0.1905(42)$ GeV for each of the given branching fractions. For simplicity, we assume that the branching fractions are the only contributing source of uncertainty to $|V_{ub}|$. While we will not discuss these values any further, they serve to demonstrate that the determination of $|V_{ub}|$ is still afflicted by large uncertainties that will need to be controlled in order to understand the underlying physical processes.

$|V_{ub}|$ enters in semileptonic decays like for example $B \to \pi\ell\nu$, $B_s \to K\ell\nu$, where, in the quark picture, the b quark is converted to a u quark via a W boson, while the $\bar{d}$ or $\bar{s}$ is a spectator, see figure 1.2.

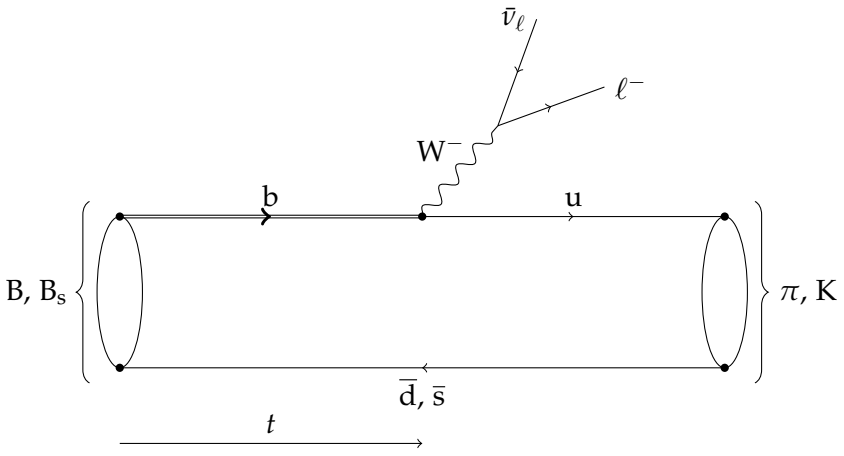

Figure 1.2: Schematic representation of semileptonic decays $B \to \pi\ell\nu$, $B_s \to K\ell\nu$

As already noted, processes like these are intrinsically non-perturbative in nature and this calls for a thorough treatment in lattice QCD. We comment on this in the next section. First efforts to compute semileptonic B to light meson decays on the lattice were made more than twenty years ago and it has been an active field of research since [21–27].

Only recently, however, have large-volume unquenched lattice simulations become feasible, and papers have been published on this topic [28–32]. And, browsing through the `arXiv` on a sunny afternoon, one encounters several ongoing works [33–37] in this field. Furthermore, effort has been put into the form factor computation in light cone sum rules [38–42].

1.2 Lattice QCD and HQET

Lattice QCD is a very valuable tool in QCD physics since it allows non-perturbative calculations of physical quantities from first principles. In a lattice QCD calculation, $|V_{\mathrm{ub}}|$ is not directly computable. Instead, one can compute the hadronic part of an interaction process, parameterised by form factors. Then, only when combined with experimentally measured decay rates, which contain the full real world process information, can input from lattice QCD be used to extract $|V_{\mathrm{ub}}|$. We will focus on this and explain in some detail the underlying principles in chapter 2.

We note the wide range of scale of QCD:

$$m_\pi \approx 140 \text{ MeV} \ldots m_{\mathrm{B}} \approx 5 \text{ GeV}. \tag{1.10}$$

If we wish to simulate QCD on a lattice with extent L and lattice spacing a, we then realise the following scale inequality:

$$L^{-1} \ll m_\pi, \ldots, m_{\mathrm{B}} \ll a^{-1}, \tag{1.11}$$

which needs to be fulfilled in order for both finite-volume (infrared) effects and lattice spacing (ultraviolet) effects to be controlled. Finite-volume effects appear at $O(\mathrm{e}^{-Lm_\pi})$ [43] and it has been shown [44] that for

$$Lm_\pi \gtrsim 4, \tag{1.12}$$

they are at the percent level. Condition (1.12) is satisfied for all lattices on which we will simulate. For the second part of inequality (1.11), we would need $m_{\mathrm{B}} \ll 1/a$, that is, lattice spacings fine enough to accommodate a B meson. While today's finest lattices in fact almost reach $m_{\mathrm{B}} \approx 1/a$, the "much greater" part of the inequality is still far from accessible with the present computing resources. This indicates the need for a framework in which one can still simulate B mesons reliably. One such tool is Heavy Quark Effective Theory (HQET) [45–48], which will be used in this thesis to treat the b quark.

In this thesis, we consider semileptonic $\mathrm{B_s} \to \mathrm{K}$ decays instead of $\mathrm{B} \to \pi$, because the K is heavier than a π and can in lattice simulations thus be held at (or near) its physical

mass, hence suffering less from chiral effects, as a pion on a lattice, much heavier than its physical mass, would. As of now, however, the process $B_s \to K$ has not been measured experimentally [13], and hopes are that measurements will become available from future B factories. Meanwhile, it offers an opportunity for lattice QCD to make predictions on certain quantities which eventually can be compared to experiment. In the long run, one would of course like to simulate $B \to \pi$ as well, since this is where experimental data is available.

In this thesis, while for definiteness, when labelling quarks as u, b, s and mesons as K, B_s, we restrict ourselves to the decay $B_s \to K$, it is trivial to adopt equations and expressions also to the decay $B \to \pi$ by replacing $s \rightsquigarrow d$, $K \rightsquigarrow \pi$ and $B_s \rightsquigarrow B$. The only places where an actual changes occurs is where we insert explicit properties of the s quark, the kaon and the B_s meson, that is, their masses. Then one would have to numerically adapt $\kappa_s \rightsquigarrow \kappa_d$, $m_K \rightsquigarrow m_\pi$, $m_{B_s} \rightsquigarrow m_B$.

The program code which computes the quantities discussed in this thesis is located as a `git` repository in
`/afs/ifh.de/group/alpha/bup/alpha/git_repositories/codes/ddhqet-fabiob_ftbahr.git`. Whenever we give directory paths in this thesis as `~/...`, they are relative to this directory.

The rest of this thesis is organised as follows. In chapter 2, we discuss the general strategy of how the input from a lattice QCD calculation can be used to obtain $|V_{ub}|$. In chapter 3, we give a brief overview of the foundations of lattice QCD and introduce some features thereof. In chapter 4, we present an introduction to HQET, which we will apply to perform our calculations. In chapter 5, we detail all necessary ingredients and then combine them to construct the quantities which we want to measure. In chapter 6, we describe our analysis and explain how we obtain the form factors from the raw data. In chapter 7, we perform a continuum extrapolation of our lattice data and compare the continuum form factor to recently published works of two collaborations. Finally, in chapter 8, we summarise and and give an outlook towards the future. Some technical calculations and figures have been relegated to the appendix.

2 From the form factors to $|V_{ub}|$

In this chapter we explain how to obtain $|V_{ub}|$ with the form factors as input obtained from a lattice calculation. For this, we also need experimentally determined decay rates. While for the decay $B_s \to K$ these are not yet available, we still discuss the general procedure here. It can be applied once experimental decay rates become available for $B_s \to K$, or be trivially extended to the case of $B \to \pi$ decays.

2.1 Definition of the form factors

The matrix element of physical interest can be parameterised by two form factors,

$$\langle K(p_K^\mu)|\hat{V}^\mu|B_s(p_{B_s}^\mu)\rangle = (p_{B_s}^\mu + p_K^\mu) f_+(q^2) + (p_{B_s}^\mu - p_K^\mu) f_-(q^2). \tag{2.1}$$

This parameterisation is given by the Lorentz structure of the matrix element: It depends on two four-vectors, p_K^μ and $p_{B_s}^\mu$, so any parameterisation of it is a linear combination of the same two four-vectors multiplying two unknown scalar form factors. In its more common form, equation (2.1) reads

$$\langle K(p_K^\mu)|\hat{V}^\mu|B_s(p_{B_s}^\mu)\rangle = f_+(q^2)\left[p_{B_s}^\mu + p_K^\mu - \frac{m_{B_s}^2 - m_K^2}{q^2} q^\mu\right] + f_0(q^2)\frac{m_{B_s}^2 - m_K^2}{q^2} q^\mu, \tag{2.2}$$

with

$$q^\mu = p_{B_s}^\mu - p_K^\mu \tag{2.3}$$

and the vector current

$$\hat{V}^\mu = \hat{\bar{\psi}}_u \gamma^\mu \hat{\psi}_b. \tag{2.4}$$

Let us point out here that equation (2.1) is written in Hilbert space and we have decorated operators with a hat. When we turn to computing the matrix element on the lattice, chapter 5, we will identify them with fermion fields which we write without a hat. Working in HQET, it is more convenient to consider a different form factor decomposition of the matrix element, namely in the B_s rest frame. That is, setting $v^\mu = (1,0,0,0)$, we have $p_{B_s}^\mu = m_{B_s} v^\mu$, and define

$$p_\perp^\mu = p_K^\mu - (p_K \cdot v) v^\mu . \tag{2.5}$$

Then, the energy of the light meson is given by

$$E_K = p_K \cdot v = \frac{m_{B_s}^2 + m_K^2 - q^2}{2m_{B_s}} \tag{2.6}$$

and the matrix element can be rewritten in terms of form factors $f_\parallel$ and $f_\perp$ as

$$\langle K(p_K^\mu)|\hat{V}^\mu|B_s(0)\rangle = \sqrt{2m_{B_s}}\left[v^\mu f_\parallel(E_K) + p_\perp^\mu f_\perp(E_K)\right], \tag{2.7}$$

with the relation to f_+ and f_0 being

$$f_+ = \frac{1}{\sqrt{2m_{B_s}}} f_\parallel(E_K) + \frac{1}{\sqrt{2m_{B_s}}}(m_{B_s} - E_K) f_\perp(E_K)\,, \tag{2.8a}$$

$$f_0 = \frac{\sqrt{2m_{B_s}}}{m_{B_s}^2 - m_K^2}\Big[(m_{B_s} - E_K) f_\parallel(E_K) + (E_K^2 - m_K^2) f_\perp(E_K)\Big]. \tag{2.8b}$$

We further note that

$$\langle K(p_K^\mu)|\hat{V}^0|B_s(0)\rangle = \sqrt{2m_{B_s}} f_\parallel(E_K)\,, \tag{2.9a}$$

$$\langle K(p_K^\mu)|\hat{V}^k|B_s(0)\rangle = \sqrt{2m_{B_s}} p_K^k f_\perp(E_K)\,. \tag{2.9b}$$

At this point we note that equation (2.2) is the relativistic QCD matrix element $\langle K|V^\mu|B_s\rangle_{rel}$. Relativistic states are normalised as [49]

$$\langle \vec{p}|\vec{p}'\rangle_{rel} = (2\pi)^3 2E(\vec{p})\delta(\vec{p} - \vec{p}'). \tag{2.10}$$

On the lattice we compute the matrix element in HQET; a suitable non-relativistic normalisation of states is

$$\langle \vec{p}|\vec{p}'\rangle_{NR} = 2(2\pi)^3\delta(\vec{p} - \vec{p}'). \tag{2.11}$$

Relativistic and non-relativistic states are then related via

$$\langle \vec{p}|\vec{p}'\rangle_{rel} = E(\vec{p})\,\langle \vec{p}|\vec{p}'\rangle_{NR}\,. \tag{2.12}$$

For the matrix element, this means that

$$\langle K|\hat{V}^\mu|B_s\rangle_{rel} = \sqrt{E_K m_{B_s}} \times \langle K|V^\mu|B_s\rangle_{NR}. \tag{2.13}$$

In chapter 5 we will show how to compute the non-relativistic HQET matrix element in a lattice QCD computation and hence be able to extract the form factors. Only after that, in chapter 7, we will convert this to the relativistic QCD matrix element as in equation (2.13).

This inspires us to do a dimensional analysis. From equation (2.10), a state $|\vec{p}\rangle_{rel}$ has mass dimension -1. $\hat{V}^\mu$, from equation (2.4), has mass dimension 3. Then, from equation (2.2), $\langle K|\hat{V}^\mu|B_s\rangle_{rel}$ has mass dimension 1. Consequently, the form factors f_+, f_0 are dimensionless. Equation (2.8a) then tells us that $f_\parallel$ has mass dimension $1/2$ and $f_\perp$ has $-1/2$.

Now, from equation (2.13), the HQET matrix element that we compute on the lattice is a dimensionless number. When we want to convert to the QCD matrix element in physical units, we have to remember equation (2.13).

2.2 Differential decay rates

The differential decay rates, which are accessible in experiments, are given by [15]

$$\frac{\mathrm{d}\Gamma}{\mathrm{d}q^2} = \frac{G_\mathrm{F}^2 |V_\mathrm{ub}|^2}{24\pi^3 m_{\mathrm{B_s}}^2} \left(1 - \frac{m_\ell^2}{q^2}\right)^2 |\vec{p}_\mathrm{K}| \left[\left(1 + \frac{m_\ell^2}{2q^2}\right) m_{\mathrm{B_s}}^2 \vec{p}_\mathrm{K}^2 |f_+(q^2)|^2 + \frac{3m_\ell^2}{8q^2} (m_{\mathrm{B_s}}^2 - m_\mathrm{K}^2)^2 |f_0(q^2)|^2 \right], \tag{2.14}$$

where m_ℓ is the lepton mass. In the limit of small lepton mass, $m_\ell \approx 0$, which for light leptons $\ell = \mathrm{e}, \mu$ is a good approximation, equation (2.14) simplifies to

$$\frac{\mathrm{d}\Gamma}{\mathrm{d}q^2} = \frac{G_\mathrm{F}^2 |V_\mathrm{ub}|^2}{192\pi^3 m_{\mathrm{B_s}}^3} \lambda^{3/2}(q^2) |f_+(q^2)|^2, \tag{2.15}$$

where

$$\lambda(q^2) = 4m_{\mathrm{B_s}}^2 \vec{p}_\mathrm{K}^2 = (m_{\mathrm{B_s}}^2 + m_\mathrm{K}^2 - q^2)^2 - 4m_{\mathrm{B_s}}^2 m_\mathrm{K}^2. \tag{2.16}$$

We note in particular that in equation (2.15) f_0 does not contribute.

Let us at this point make a general observation: In principle, it is sufficient for the extraction of $|V_\mathrm{ub}|$ to know both the experimentally determined decay rates and $f(q^2)$ from lattice QCD at the same single value of q^2. Since in practice, however, experimental data are provided over a range (of bins) of q^2, one can use the BCL parameterisation, which we discuss in the next section, to parameterise experimental decay rates as a continuous function of q^2, while as lattice QCD input we provide $f_+(q^2)$ at a single value of q^2. Let us stress that in any case, $|V_\mathrm{ub}|$ can only be obtained once experimental data are combined with the theoretically determined form factor $f_+(q^2)$.

2.3 BCL parameterisation

As a model independent parameterisation of the form factor, we choose the one presented by Bourrely, Caprini and Lellouch in reference [50]. Following this reference, we write the form factor f_+ as an expansion

$$f_+(q^2) = \frac{1}{1 - q^2/m_{\mathrm{B_s^*}}^2} \sum_{k=0}^{K-1} b_k \left[z^k - (-1)^{k-K} \frac{k}{K} z^K \right] \tag{2.17}$$

where $m_{\mathrm{B_s^*}} = 5.4158(15)$ GeV [3] is the mass of the first excited state of the $\mathrm{B_s}$ meson and

$$z(q^2, t_0) = \frac{\sqrt{t_+ - q^2} - \sqrt{t_+ - t_0}}{\sqrt{t_+ - q^2} + \sqrt{t_+ - t_0}} \tag{2.18}$$

with

$$\sqrt{t_+} = (m_{B_s} + m_K)\,, \tag{2.19a}$$
$$\sqrt{t_-} = (m_{B_s} - m_K)\,. \tag{2.19b}$$

While t_+ marks the B_sK threshold, note that the semileptonic region is

$$0 \leq q^2 \leq t_-. \tag{2.20}$$

The mapping function $z(q^2, t_0)$ in equation (2.18) is constructed such that it maps $q^2 > t_+$ to $|z| = 1$ while $q^2 < t_+$ are mapped to the real interval $z \in [-1, 1]$. While t_0 is an arbitrary parameter, if it is chosen to

$$t_{opt} \equiv (m_{B_s} + m_K)(\sqrt{m_{B_s}} - \sqrt{m_K})^2 \approx 15.27\ \text{GeV}^2, \tag{2.21}$$

the semileptonic region is mapped symmetrically to the real interval $|z| \leq 0.146$. In equation (2.17), there are K unknown parameters b_k which will be our fit parameters.

Imposing unitarity and crossing symmetry [50] leads to the condition:

$$\sum_{j,k=0}^{K} B_{jk}(t_0) b_j(t_0) b_k(t_0) \leq 1 \tag{2.22}$$

where the B_{jk} are known coefficients [50].

2.4 Determination of $|V_{ub}|$

In all cases, the parameterisation of the form factor in equation (2.17) is used. Then, a combined fit of theoretical and experimental input values is performed by minimising

$$\chi^2(b_k, |V_{ub}|) = \chi^2_{th} + \chi^2_{exp} \tag{2.23}$$

and respecting condition (2.22) with $N = K + 1$ fit parameters: $b_k, k \leq K - 1$ and $|V_{ub}|$. Schematically, χ^2 for the lattice data points is written as

$$\chi^2_{th} = \sum_{j,k} [f^{in}_j - f_+(q^2_j)] C^{-1}_{jk} [f^{in}_k - f_+(q^2_k)], \tag{2.24}$$

where f^{in} is the value of the form factor from the lattice computation and $f_+(q^2)$ is the form factor parameterised as in equation (2.17), with the covariance matrix of the lattice data C^{-1}_{jk}.

As already mentioned, experimental data are typically provided as branching ratios $\mathcal{B}^{in}$ in a given q^2 bin. The expression for differential decay rates $d\Gamma/dq^2$ is given in equation

(2.15). We need to integrate them over the given q^2 bins,

$$\int \mathrm{d}\Gamma = \int_{q^2_{\mathrm{low}}}^{q^2_{\mathrm{high}}} \mathrm{d}q^2 \frac{G_F^2 |V_{ub}|^2}{192\pi^3 m_{B_s}^3} \lambda^{3/2}(q^2) |f_+(q^2)|^2, \tag{2.25}$$

assuming a parameterisation of the form factor, equation (2.17). $|V_{ub}|$ and b_k are left as open parameters. Now, the resulting decay rates have mass dimension 1 and can be converted to dimensionless branching ratios $\mathcal{B}(f_+)$ by multiplying with the lifetime of the B_s meson, $\tau_{B_s} = 1.512(7) \times 10^{-12}\,\mathrm{s}$ [3],

$$\mathcal{B}(f_+) = \tau_{B_s} \times \int \mathrm{d}\Gamma \tag{2.26}$$

Then, we have

$$\chi^2_{\mathrm{exp}} = \sum_{j,k} [\mathcal{B}_j^{\mathrm{in}} - \mathcal{B}_j(f_+)] C^{-1}_{\mathcal{B}jk} [\mathcal{B}_k^{\mathrm{in}} - \mathcal{B}_k(f_+)]. \tag{2.27}$$

Here, $C^{-1}_{\mathcal{B}jk}$ is the covariance matrix of the experimental data provided together with the data.

3 Setup

In this chapter, we discuss the setup of lattice QCD and give the basic formulae needed to construct the framework in which we will present our later calculations.

3.1 Lattice QCD

We start our discussion by introducing the basic features of lattice QCD. First described by Wilson [51], the concept can nowadays be found neatly presented in the textbook of one's choice [52, 53]. The idea is that one discretises spacetime such that it is accommodated on a four-dimensional hypercube with spacing a between neighbouring sites, a total extent of L, and thus L/a lattice sites in each direction. One works in Euclidean spacetime. Usually, the extent of the three spacial directions is denoted by L while that in time direction is T. A parallel transporter between two lattice sites, a *link* at point x oriented in direction μ, is written as

$$U(x,\mu) \equiv U_\mu(x) \in \mathrm{SU}(N) \tag{3.1}$$

and is a matrix of the fundamental representation of the corresponding gauge group, which in the case of QCD is an $\mathrm{SU}(3)$. The gauge field is defined as the set of all links. A link with backward orientation is written as

$$U^\dagger(x,\mu) \equiv U(x+a\hat{\mu},-\mu). \tag{3.2}$$

One a defines a plaquette as

$$U(p) \equiv U_{\mu\nu}(x) = U(x,\mu)U(x+a\hat{\mu},\nu)U(x+a\hat{\nu},\mu)^\dagger U(x,\nu)^\dagger. \tag{3.3}$$

It is the shortest, non-trivial closed loop of links, the trace of which is gauge invariant. Wilson [51] used plaquettes to construct a lattice gauge action as

$$S_\mathrm{G}[U] = \frac{1}{g_0^2}\sum_p \mathrm{tr}\left\{1-U(p)\right\}, \tag{3.4}$$

where the sum is over all oriented plaquettes, meaning that any plaquette is counted only once, regardless of direction.

3.2 Wilson Quarks

Fermion fields $\psi(x)$ are Graßmann variables and reside on lattice points x. They carry colour, Dirac and flavour indices; hence, a fermion field can be written as

$$\psi_{c,\alpha,f}(x) \equiv \psi_k, \tag{3.5}$$

where $k = \{x/a, c, \alpha, f\}$, $k = 1, \ldots, n$, $n = \prod_\mu L_\mu/a \times 3 \times 4 \times N_\mathrm{f}$. While for definiteness, in this thesis, we will keep flavour indices explicit, for brevity we suppress all other indices unless explicitly noted. The full action is the sum of gauge action, S_G, discussed in the previous section, and fermion action, S_F,

$$S\left[U, \overline{\psi}, \psi\right] = S_\mathrm{G}[U] + S_\mathrm{F}\left[U, \overline{\psi}, \psi\right], \tag{3.6}$$

The naive fermion action is

$$S_\mathrm{F,naive}\left[U, \overline{\psi}, \psi\right] = a^4 \sum_x \overline{\psi}(x)\left(D + m_0\right)\psi(x), \tag{3.7}$$

where

$$D = \frac{1}{2}\left\{\gamma_\mu(\nabla^*_\mu + \nabla_\mu)\right\} \tag{3.8}$$

and derivatives and γ matrices are given in appendix A. This action, however, leads to the infamous doubling problem arising from the fact that the quark propagator associated with this Dirac operator has not only one pole, corresponding to a physical particle, but 16 poles within the Brillouin zone, which can be seen as unphysical "particles", commonly referred to as doublers. A possible way out is to use Wilson fermions, adding an additional Wilson term $-\frac{1}{2}a\nabla^*_\mu\nabla_\mu$ to the Dirac operator. That is, one replaces the naive Dirac operator by

$$D_\mathrm{W} = \frac{1}{2}\left\{\gamma_\mu(\nabla^*_\mu + \nabla_\mu) - a\nabla^*_\mu\nabla_\mu\right\}. \tag{3.9}$$

Adding the Wilson term removes the doublers, but it breaks chiral symmetry of the theory, which is only restored once the continuum limit is taken, $a \to 0$. Details can be found in references [54–56]. Then, the Wilson fermion action is

$$S_\mathrm{F}\left[U, \overline{\psi}, \psi\right] = a^4 \sum_x \overline{\psi}(x)\left(D_\mathrm{W} + m_0\right)\psi(x). \tag{3.10}$$

With the notation of equation (3.5), it is written as

$$S_\mathrm{F}\left[U, \overline{\psi}, \psi\right] = a^4 \sum_{k,l} \overline{\psi}_k M_{kl} \psi_l. \tag{3.11}$$

where M_{kl}, an $n \times n$ matrix, is the fermion matrix.

3.3 $O(a)$ Improvement

Here we briefly review the key ingredients to $O(a)$ improvement of the theory. Following the idea of Symanzik [57, 58], one can write lattice QCD close to the continuum as an effective theory. Details can be found for example in reference [54]. In the end, we come up with a term first used for $O(a)$ improvement by Sheikholeslami and Wohlert [59],

$$\delta S\left[U,\overline{\psi},\psi\right] = a^5 \sum_x c_{\mathrm{SW}} \overline{\psi}(x) \frac{\mathrm{i}}{4} \sigma_{\mu\nu} \widehat{F}_{\mu\nu}(x) \psi(x). \tag{3.12}$$

The field strength tensor is

$$\widehat{F}_{\mu\nu}(x) = \frac{1}{8a^2}\left\{Q_{\mu\nu}(x) - Q_{\nu\mu}(x)\right\}, \tag{3.13}$$

where

$$\begin{aligned} Q_{\mu\nu}(x) = {} & U(x,\mu)U(x+a\hat{\mu},\nu)U(x+a\hat{\nu},\mu)^{-1}U(x,\nu)^{-1} \\ & + U(x,\nu)U(x-a\hat{\mu}+a\hat{\nu},\mu)^{-1}U(x-a\hat{\mu},\nu)^{-1}U(x-a\hat{\mu},\mu) \\ & + U(x-a\hat{\mu},\mu)^{-1}U(x-a\hat{\mu}-a\hat{\nu},\nu)^{-1}U(x-a\hat{\mu}-a\hat{\nu},\mu)U(x-a\hat{\nu},\nu) \\ & + U(x-a\hat{\nu},\nu)^{-1}U(x-a\hat{\nu},\mu)U(x+a\hat{\mu}-a\hat{\nu},\nu)U(x,\mu)^{-1}. \end{aligned} \tag{3.14}$$

c_{SW} has been determined non-perturbatively for $N_{\mathrm{f}} = 2$ in reference [56],

$$c_{\mathrm{SW}} = \frac{1 - 0.454 g_0^2 - 0.175 g_0^4 + 0.012 g_0^6 + 0.045 g_0^8}{1 - 0.720 g_0^2}. \tag{3.15}$$

Now we can write our improved action as

$$S_{\mathrm{impr}}\left[U,\overline{\psi},\psi\right] = S\left[U,\overline{\psi},\psi\right] + \delta S\left[U,\overline{\psi},\psi\right]. \tag{3.16}$$

3.4 Path integral

The expectation value of a field $\mathcal{O}$ is given by

$$\langle \mathcal{O} \rangle = \frac{1}{\mathcal{Z}} \int \mathrm{D}[U]\mathrm{D}[\psi]\mathrm{D}[\overline{\psi}]\mathcal{O}\, \mathrm{e}^{-S[U,\overline{\psi},\psi]}, \tag{3.17}$$

with the partition function

$$\mathcal{Z} = \int \mathrm{D}[U]\mathrm{D}[\psi]\mathrm{D}[\overline{\psi}]\, \mathrm{e}^{-S[U,\overline{\psi},\psi]}, \tag{3.18}$$

and

$$\mathrm{D}[U] = \prod_{x,\mu} \mathrm{d}U(x,\mu), \quad \mathrm{D}[\overline{\psi}] = \prod_x \mathrm{d}\overline{\psi}(x), \quad \mathrm{D}[\psi] = \prod_x \mathrm{d}\psi(x). \tag{3.19}$$

Here, $\mathrm{d}U(x,\mu)$ is the Haar measure of SU(3) and $\mathrm{d}\overline{\psi}(x)$, $\mathrm{d}\psi(x)$ are Graßmann algebra integration measures.

Suppose now we want to compute the expectation value of a field or combination of fields with an action as in equation (3.6). We have

$$\langle\mathcal{O}\rangle = \frac{1}{\mathcal{Z}}\int \mathrm{D}[U]\mathrm{D}[\psi]\mathrm{D}[\overline{\psi}]\,\mathcal{O}\,\mathrm{e}^{-S_\mathrm{F}[U,\overline{\psi},\psi]-S_\mathrm{G}[U]}, \tag{3.20}$$

with

$$\mathcal{Z} = \int \mathrm{D}[U]\mathrm{D}[\psi]\mathrm{D}[\overline{\psi}]\,\mathrm{e}^{-S_\mathrm{F}[U,\overline{\psi},\psi]-S_\mathrm{G}[u]}\,. \tag{3.21}$$

Let us separate the expectation value in equation (3.20) in its fermion and gauge parts,

$$\langle\mathcal{O}\rangle = \langle\langle\mathcal{O}\rangle_\mathrm{F}\rangle_\mathrm{G}, \tag{3.22}$$

where the fermion part is now

$$\langle\mathcal{O}\rangle_\mathrm{F} = \frac{1}{\mathcal{Z}_\mathrm{F}[U]}\int \mathrm{D}[\psi]\mathrm{D}[\overline{\psi}]\,\mathrm{e}^{-S_\mathrm{F}[U,\overline{\psi},\psi]}\,\mathcal{O}[U,\overline{\psi},\psi]. \tag{3.23}$$

The fermion partition function is given by

$$\mathcal{Z}_\mathrm{F}[U] = \int \mathrm{D}[\psi]\mathrm{D}[\overline{\psi}]\,\mathrm{e}^{-S_\mathrm{F}[U,\overline{\psi},\psi]} = \det M, \tag{3.24}$$

with the fermion determinant $\det M$. Now we are able to define the fermion propagator as

$$\langle\psi(x)\overline{\psi}(y)\rangle_\mathrm{F} = D^{-1}(x,y) \equiv S(x,y). \tag{3.25}$$

Considering equation (3.23), let us now rewrite equation (3.22):

$$\langle\mathcal{O}\rangle = \frac{1}{\mathcal{Z}}\int \mathrm{D}[U]\mathcal{O}\,\mathrm{e}^{-S_\mathrm{eff}[U]}, \tag{3.26}$$

where we have introduced the effective gauge action

$$S_\mathrm{eff}[U] = S_\mathrm{G}[U] - \log\det M = S_\mathrm{G}[U] - \mathrm{tr}\log M. \tag{3.27}$$

3.5 Computing a two-point function

Before we continue our discussion, let us consider an example. Suppose we want to compute a two-point function

$$\mathcal{C}^\mathrm{2pt}(t) = \langle\mathcal{O}_2(t)\mathcal{O}_1(0)\rangle = \frac{1}{\mathcal{Z}}\,\mathrm{tr}\{\mathrm{e}^{-(T-t)\hat{H}}\,\hat{\mathcal{O}}_2\,\mathrm{e}^{-t\hat{H}}\,\hat{\mathcal{O}}_1\}, \tag{3.28}$$

where $\hat{H}$ is the lattice Hamilton operator. It is defined as

$$\mathbb{T} = \mathrm{e}^{-a\hat{H}}, \tag{3.29}$$

where $\mathbb{T}$ is the transfer matrix [60]. It describes the evolution of a state $|\phi(\vec{x},t)\rangle$ by one lattice spacing in time direction to $|\phi(\vec{x},t+a)\rangle$. $\hat{H}$ of equation (3.28) has eigenvalues

$$\hat{H}\,|n\rangle = E_n\,|n\rangle \tag{3.30}$$

and we have introduced

$$\mathcal{Z} = \operatorname{tr} \mathrm{e}^{-T\hat{H}}\,. \tag{3.31}$$

In chapter 5, when we turn to the computation of the form factor, we will identify $\mathcal{O}$ with pseudoscalar densities, equation (5.5a), but here we keep our discussion very general. We also point out that on the right-hand side of equation (3.28), we have written physical Hilbert space operators as $\hat{\mathcal{O}}$, while on the left-hand side, we denote the corresponding lattice fields by $\mathcal{O}$. Now we insert

$$\mathbb{1} = \sum_n |n\rangle\,\langle n| \tag{3.32}$$

and use

$$\operatorname{tr}\hat{\mathcal{O}} = \sum_n \langle n|\hat{O}|n\rangle \tag{3.33}$$

to write equation (3.28) as

$$\begin{aligned}\mathcal{C}^{\mathrm{2pt}}(t) &= \frac{1}{\mathcal{Z}}\sum_{m,n}\langle m|\,\mathrm{e}^{-(T-t)\hat{H}}\,\hat{\mathcal{O}}_2|n\rangle\,\langle n|\,\mathrm{e}^{-t\hat{H}}\,\hat{\mathcal{O}}_1|m\rangle \\ &= \frac{1}{\mathcal{Z}}\sum_{m,n}\mathrm{e}^{-(T-t)E_m}\,\langle m|\hat{\mathcal{O}}_2|n\rangle\,\mathrm{e}^{-tE_n}\,\langle n|\hat{\mathcal{O}}_1|m\rangle\end{aligned} \tag{3.34}$$

and

$$\mathcal{Z} = \sum_n \langle n|\,\mathrm{e}^{-T\hat{H}}\,|n\rangle = \sum_n \mathrm{e}^{-TE_n}, \tag{3.35}$$

where we have made use of equation (3.30). We note here that the lowest state of the sums over m,n corresponds to the vacuum energy which we can set to 0. Further, let us now consider the infinite T limit in equation (3.34), which in particular means that only terms where $|m\rangle = |0\rangle$ survive:

$$\mathcal{C}^{\mathrm{2pt}}(t) \overset{T\to\infty}{=} \sum_n \langle 0|\hat{\mathcal{O}}_2|n\rangle\,\langle n|\hat{\mathcal{O}}_1|0\rangle\,\mathrm{e}^{-E_n t}\,. \tag{3.36}$$

Finally, we look at the special case where $\mathcal{O}\equiv\mathcal{O}_2 = \mathcal{O}_1^\dagger$. Then, equation (3.36) becomes

$$\mathcal{C}^{\mathrm{2pt}}(t) \overset{T\to\infty}{=} \sum_n |\langle n|\hat{\mathcal{O}}|0\rangle|^2\,\mathrm{e}^{-E_n t}\,. \tag{3.37}$$

From equation (3.37) we see that a two-point correlator can be written as a sum of amplitudes and exponentials of energies. All amplitudes and energies are real numbers. The ground state of the correlator is at $n=0$, and naturally, we have $E_0 < E_1 < \ldots < E_n$. This means in particular that at large times t, excited states $n>1$ are exponentially suppressed.

We will get back to addressing how good an approximation this is for the heavy-light and light-light two-point functions in chapter 6, when we discuss different fits to these.

3.6 Gauge field smearing

In equation (3.37) we have seen that in order to extract the ground energy (and amplitude) of a correlator, in principle it suffices to consider it at large enough times t such that all excited states have decayed. However, in practice, we are limited by finite lattice sizes and a deteriorating signal-to-noise ratio. Thus, strategies to improve the overlap of a given correlator with its ground state have been invented. In this section, we discuss gauge field smearing techniques, while in section 5.1.1, when we discuss the explicit computation of correlator, we also consider fermion smearing. First, we review the APE smearing procedure [61]. The gauge links are replaced by a given combination of surrounding links. This makes for better overlap with the physical ground state and unphysical short distance fluctuations are removed.

The gauge field at smearing step n is denoted by $U^{(n)}$. We iteratively build

$$U^{(n)}(x,\mu) = \mathrm{P}_{\mathrm{SU(3)}}\Big\{(1-\alpha)U^{(n-1)}(x,\mu) + \frac{\alpha}{6}S^{(n-1)}(x,\mu)\Big\}, \tag{3.38}$$

where by $\mathrm{P}_{\mathrm{SU(3)}}$ we indicate that we project the result back to SU(3) and $S^{(n)}(x,\mu)$ is the set of staples

$$S^{(n)}(x,\mu) = \sum_{\pm\nu\neq\mu} U(x,\nu)U(x+\hat{\nu},\mu)U^{\dagger}(x+\hat{\mu},\nu) \tag{3.39}$$

built on the gauge field $U^{(n)}$. In the following, we will use the choices $n = 3$ and $\alpha = 0.4$.

Static-light correlation functions suffer from an exponentially decreasing signal-to-noise ratio R_{SN} [62–64]. In fact, it has been shown in the given references that, for the static quark action which we will introduce in the next chapter,

$$R_{\mathrm{SN}} = \frac{\text{signal}}{\text{noise}} \propto \exp(-\Delta t), \quad \Delta = E_{\mathrm{stat}} - m_{\pi}. \tag{3.40}$$

So, in order that R_{SN} is reasonable, we require that t is of order Δ^{-1}. But, since

$$E_{\mathrm{stat}} \sim e_1 \times g_0^2/a \tag{3.41}$$

with some parameter e_1, as $a \to 0$, this is increasingly difficult to maintain. To improve on R_{SN}, we employ a smearing technique which makes use of hypercubic blocking, HYP smearing [65–68], a series of modified APE smearing steps. We here briefly review the basic ingredients as outlined in reference [65]. We replace the gauge link $U(x,\mu)$ by a combination of surrounding gauge link staples in a three step process:

1.
$$\overline{V}^{\nu\rho}(x,\mu) = \mathrm{P}_{\mathrm{SU(3)}}\Big\{(1-\alpha_3)U(x,\mu) + \frac{\alpha_3}{2}\sum_{\pm\eta\neq\rho,\nu,\mu} U(x,\eta)U(x+\hat{\eta},\mu)U^{\dagger}(x+\hat{\mu},\eta)\Big\}, \tag{3.42}$$
where superscript indices indicate that there is no staple attached in that direction(s).

2. Then, we construct
$$\overline{V}^{\nu}(x,\mu) = \mathrm{P}_{\mathrm{SU(3)}}\Big\{(1-\alpha_2)U(x,\mu) + \frac{\alpha_2}{4}\sum_{\pm\rho\neq\nu,\mu} \overline{V}^{\nu\mu}(x,\rho)\overline{V}^{\rho\nu}(x+\hat{\rho},\mu)\overline{V}^{\dagger\nu\mu}(x+\hat{\mu},\rho)\Big\}. \tag{3.43}$$

3. Finally,
$$V(x,\mu) = \mathrm{P}_{\mathrm{SU(3)}}\Big\{(1-\alpha_1)U(x,\mu) + \frac{\alpha_1}{6}\sum_{\pm\nu\neq\mu} \overline{V}^{\mu}(x,\nu)\overline{V}^{\nu}(x+\hat{\nu},\mu)\overline{V}^{\dagger\mu}(x+\hat{\mu},\nu)\Big\}. \tag{3.44}$$

For the vector $\vec{\alpha} = (\alpha_1, \alpha_2, \alpha_3)$, we adapt two different choices motivated in the literature, $\vec{\alpha} = (0.75, 0.6, 0.3)$, to which we refer as HYP1 in the following, and $\vec{\alpha} = (1.0, 1.0, 0.5)$, HYP2.

4 Heavy Quark Effective Theory

4.1 Basics

As already mentioned in the introduction, performing b physics on the lattice, one faces the challenge that the b quark can at present not be simulated dynamically. The solution to this challenge we follow here is to employ an effective theory, namely Heavy Quark Effective Theory (HQET) [45–48]. While we keep the light quarks dynamic, at leading order in HQET, we consider the heavy quark as being static, that is, fixed to a point in space and only propagating in time, and then expand in $1/m_{\mathrm{h}}$.

The static theory is (believed to be) renormalisable. A key feature of HQET is that it is renormalisable to all orders, order by order in $1/m_{\mathrm{h}}$, that is, at a given order $(1/m_{\mathrm{h}})^n$ there are a finite number of terms to render the theory finite. This is important because only then is the theory well-defined and a continuum limit exists. In order to avoid power divergences in a^{-1}, non-perturbative renormalisation is needed [69]. Non-perturbative matching of lattice HQET to QCD was first discussed in reference [70].

In order that HQET is well defined, all momentum and energy scales need to be small compared to m_{h}. In practice, with $m_{\mathrm{h}} = m_{\mathrm{b}}$, we need to make sure in particular that $p_{\mathrm{K}} \lesssim 1\,\mathrm{GeV}$.

It has been observed recently in the computation of the b quark mass [71] and the $\mathrm{B}_{(\mathrm{s})}$ meson decay constants [72], which were also done in HQET, that $O(1/m_{\mathrm{h}})$ corrections are very small and that thus HQET truncated at order $1/m_{\mathrm{h}}$ appears to be a very precise approximation.

In this chapter, we first introduce HQET in its continuum formulation, discussing the main properties. Then we focus on how it can be discretised on the lattice. Finally, we discuss the renormalisation of HQET at order $1/m_{\mathrm{h}}$.

4.2 HQET in the continuum

Here, we will not present the full derivation of HQET, which can be found in references [73, 74] and is explained in a concise manner in references [49, 75]. Let us rather focus on gathering the main formulae which we will need later on. The HQET Lagrangian is given by

$$\mathcal{L} = \mathcal{L}_{\mathrm{h}}^{\mathrm{stat}} + \frac{1}{2m}\mathcal{L}_{\mathrm{h}}^{(1)} + \mathcal{L}_{\bar{\mathrm{h}}}^{\mathrm{stat}} + \frac{1}{2m}\mathcal{L}_{\bar{\mathrm{h}}}^{(1)} + O(1/m^2), \tag{4.1}$$

where

$$\mathcal{L}_{\mathrm{h}}^{\mathrm{stat}} = \overline{\psi}_{\mathrm{h}}(\quad D_0 + m)\psi_{\mathrm{h}}, \tag{4.2}$$
$$\mathcal{L}_{\bar{\mathrm{h}}}^{\mathrm{stat}} = \overline{\psi}_{\bar{\mathrm{h}}}(-D_0 + m)\psi_{\bar{\mathrm{h}}}, \tag{4.3}$$
$$\mathcal{L}_{\mathrm{h}}^{(1)} = \overline{\psi}_{\mathrm{h}}(-D^2 - \tfrac{1}{2\mathrm{i}}F_{kl}\sigma_{kl})\psi_{\mathrm{h}}, \tag{4.4}$$
$$\mathcal{L}_{\bar{\mathrm{h}}}^{(1)} = \overline{\psi}_{\bar{\mathrm{h}}}(-D^2 - \tfrac{1}{2\mathrm{i}}F_{kl}\sigma_{kl})\psi_{\bar{\mathrm{h}}}, \tag{4.5}$$

and

$$\begin{aligned} P_+\psi_{\mathrm{h}} &= \psi_{\mathrm{h}}, \qquad & \overline{\psi}\ P_+ &= \overline{\psi}_{\mathrm{h}} \\ P_-\psi_{\bar{\mathrm{h}}} &= \psi_{\bar{\mathrm{h}}}, \qquad & \overline{\psi}_{\bar{\mathrm{h}}}P_- &= \overline{\psi}_{\bar{\mathrm{h}}}, \end{aligned} \tag{4.6}$$

with projectors P_+, P_- of equation (A.3), $\sigma_{ij} = -\epsilon_{ijk}\sigma_k$ and σ_k given in appendix A.1. Let us note at this point that the HQET Lagrangian of equation (4.1) has a quark and an antiquark part. In our project, however, there is only a single heavy quark. Let us therefore restrict the following discussion without further notice to this case and neglect all terms corresponding to a heavy antiquark. For the full expressions, we point to the cited references.

We can write equations (4.4) and (4.5) as

$$\mathcal{L}_{\mathrm{h}}^{(1)} = -\left(\mathcal{O}_{\mathrm{kin}} + \mathcal{O}_{\mathrm{spin}}\right) \tag{4.7}$$

with

$$\mathcal{O}_{\mathrm{kin}}(x) = \overline{\psi}_{\mathrm{h}}(x)\vec{D}^2\psi_{\mathrm{h}}(x), \tag{4.8}$$
$$\mathcal{O}_{\mathrm{spin}}(x) = \overline{\psi}_{\mathrm{h}}(x)\vec{\sigma}\cdot\vec{B}\psi_{\mathrm{h}}(x), \tag{4.9}$$

where

$$B_k = \mathrm{i}\,\tfrac{1}{2}\epsilon_{ijk}F_{ij}. \tag{4.10}$$

Expanding to leading order in $1/m_{\mathrm{h}}$ only, we work in the *static approximation*. We here have spin and flavour symmetry and local flavour number conservation. One obtains the heavy quark propagator

$$S_{\mathrm{h}}(x,y) = \Theta(x_0 - y_0)\delta(\vec{x} - \vec{y})\exp\{-m(x_0 - y_0)\}\mathcal{P}\exp\Big\{-\int_{y_0}^{x_0}\mathrm{d}t A_0(t,\vec{x})\Big\}P_+, \tag{4.11}$$

with $\mathcal{P}$ indicating path ordering. Note here that the $\delta(\vec{x} - \vec{y})$ ensures that the heavy quark cannot propagate in space and the $\Theta(x_0 - y_0)$ ensures that it can only propagate forward in time. In equations (4.2), (4.3), we have introduced a mass term m. This is a counterterm required due to the fact that a Lagrangian without it would lead to a divergence [46]. The same term appears in the static propagator, equation (4.11). Constructing an n-point function with such a heavy quark propagator, one observes that all correlation functions are shifted by the common factor $\exp\{-m(x_0 - y_0)\}$. Thus, one can remove this term from the Lagrangian and add it to the energies. This then leads to a redefinition of the energies

in HQET compared to QCD:

$$E_{\mathrm{h}}^{\mathrm{QCD}} = E_{\mathrm{h}}^{\mathrm{stat}}\big|_{m=0} + m. \tag{4.12}$$

Let us make a note on symmetries. The HQET heavy quark propagator has different symmetries than the QCD lattice action. Formulated in Euclidean spacetime, to which we will come in section 4.3, it is not invariant under four dimensional rotations, but instead under three dimensional spatial rotations only. Additionally, it obeys the following symmetries:

- Heavy quark spin symmetry. Action and integration measure are invariant under SU(2) spin rotations

$$\psi_{\mathrm{h}} \to \mathrm{e}^{\mathrm{i}\,\alpha_k \sigma_k}\,\psi_{\mathrm{h}}, \quad \overline{\psi}_{\mathrm{h}} \to \overline{\psi}_{\mathrm{h}}\,\mathrm{e}^{-\mathrm{i}\,\alpha_k \sigma_k}, \tag{4.13}$$

  where α_k are real parameters and σ_k as defined in appendix A.1.

- Local flavour number. In the static Lagrangian there is no spatial derivative. That is, there is an invariance under U(1) transformations

$$\psi_{\mathrm{h}} \to \mathrm{e}^{\mathrm{i}\,\eta(\vec{x})}\,\psi_{\mathrm{h}}, \quad \overline{\psi}_{\mathrm{h}} \to \mathrm{e}^{-\mathrm{i}\,\eta(\vec{x})}\,\overline{\psi}_{\mathrm{h}}, \tag{4.14}$$

  with some phase $\eta(\vec{x})$ a function of three-dimensional space $\vec{x}$ only.

4.3 Lattice HQET

The lattice static quark Lagrangian is [45]

$$\mathcal{L}_{\mathrm{h}} = \frac{1}{1 + a\delta m}\overline{\psi}_{\mathrm{h}}(x)[\nabla_0^* + \delta m]\psi_{\mathrm{h}}(x). \tag{4.15}$$

It has the same symmetries as the continuum static propagator discussed in section 4.2.

The lattice heavy propagator is given as

$$S_{\mathrm{h}}(x,y) = \Theta(x_0 - y_0)\delta(\vec{x} - \vec{y}) \exp\{-\widehat{\delta m}(x_0 - y_0)\}\mathcal{P}^{\dagger}(y,x;0)P_+, \tag{4.16}$$

where

$$\widehat{\delta m} = \tfrac{1}{a}\ln(1 + a\delta m), \tag{4.17}$$

and

$$\mathcal{P}(x, y + a\hat{0}; 0) = \mathcal{P}(x,y;0)U(y,0), \quad \mathcal{P}(x,x;0) = 1 \tag{4.18}$$

is the product of gauge links in time direction only, reflecting the fact that the heavy quark can propagate in time only and will thus pick up gauge links along the time direction. Just as in section 4.2, we here encounter a mass counter term δm which will cause a shift to the energies; we have

$$E_{\mathrm{h}}^{\mathrm{QCD}} = E_{\mathrm{h}}^{\mathrm{stat}}\big|_{\delta m=0} + m_{\mathrm{bare}}, \quad m_{\mathrm{bare}} = \widehat{\delta m} + m. \tag{4.19}$$

$\mathcal{O}_{\text{kin}}$ and $\mathcal{O}_{\text{spin}}$ of equations (4.8) and (4.9) are straightforwardly discretised by setting

$$\vec{D}^2 \to \vec{\nabla}^* \vec{\nabla} \tag{4.20}$$

and

$$F_{kl} \to \widehat{F}_{kl}, \tag{4.21}$$

with $\widehat{F}_{kl}$ as in equation (3.14).

As already noted above, the effective theory is (expected to be) renormalisable and the continuum limit can be taken order by order in $1/m_{\text{h}}$ if the path integral weight is defined in the following way [70]:

$$\begin{aligned}\exp\left\{ -a^4 \sum_x \left[\mathcal{L}_{\text{HQET}}(x) + \mathcal{L}_{\text{light}}(x)\right] \right\} &= \exp\left\{ -a^4 \sum_x \left[\mathcal{L}_{\text{stat}}(x) + \mathcal{L}_{\text{light}}(x)\right] \right\} \\ &\quad \times \left(1 + a^4 \sum_x \left[\omega_{\text{spin}} \mathcal{O}_{\text{spin}}(x) + \omega_{\text{kin}} \mathcal{O}_{\text{kin}}(x)\right] \right),\end{aligned} \tag{4.22}$$

where

$$\langle \mathcal{O}_{\text{stat}} \rangle = \frac{1}{\mathcal{Z}} \int_{\text{fields}} \mathcal{O} \exp\left\{ -a^4 \sum_x \left[\mathcal{L}_{\text{light}}(x) + \mathcal{L}_{\text{h}}^{\text{stat}}(x)\right] \right\}. \tag{4.23}$$

4.4 $O(1/m_{\text{h}})$ insertions

Operator expectation values in HQET are given as

$$\langle \mathcal{O} \rangle = \langle \mathcal{O} \rangle_{\text{stat}} + \omega_{\text{kin}} a^4 \sum_x \langle \mathcal{O} \mathcal{O}_{\text{kin}}(x) \rangle_{\text{stat}} + \omega_{\text{spin}} a^4 \sum_x \langle \mathcal{O} \mathcal{O}_{\text{spin}}(x) \rangle_{\text{stat}} \tag{4.24}$$

$$\equiv \langle \mathcal{O} \rangle_{\text{stat}} + \omega_{\text{kin}} \langle \mathcal{O} \rangle_{\text{kin}} + \omega_{\text{spin}} \langle \mathcal{O} \rangle_{\text{spin}} . \tag{4.25}$$

Choosing to work in HQET, we also need effective versions of the currents. For our purposes, we need to consider the effective vector current:

$$V_0^{\text{HQET}}(x) = Z_{V_0}^{\text{HQET}} \left[V_0^{\text{stat}}(x) + \sum_{j=1}^{2} c_{\text{V}_{0,j}} V_{0,j}(x) \right], \tag{4.26a}$$

$$V_k^{\text{HQET}}(x) = Z_{V_k}^{\text{HQET}} \left[V_k^{\text{stat}}(x) + \sum_{j=1}^{4} c_{\text{V}_{k,j}} V_{k,j}(x) \right], \tag{4.26b}$$

with Z^{HQET} renormalisation factors and $c_{\text{V}_{\mu,j}}$ matching coefficients to be determined. The current insertions $V_{\mu,j}$ are tabulated in table 4.1. We give a short explanation of the matching procedure in section 4.5.

V_μ^{HQET}	$c_{\mathrm{V}j}$	$K_{\mu j}$
V_0^{stat}	1	γ_0
$V_{0,1}$	$1/(2m_{\mathrm{h}})$	$\sum_l \gamma_l (1/2)(\nabla_l^{\mathrm{S}} - \overleftarrow{\nabla}_l^{\mathrm{S}})$
$V_{0,2}$	$1/(2m_{\mathrm{h}})$	$\sum_l \gamma_l (1/2)(\nabla_l^{\mathrm{S}} + \overleftarrow{\nabla}_l^{\mathrm{S}})$
V_k^{stat}	1	γ_k
$V_{k,1}$	$1/(2m_{\mathrm{h}})$	$\sum_l (1/2)(\nabla_l^{\mathrm{S}} - \overleftarrow{\nabla}_l^{\mathrm{S}})\gamma_l\gamma_k$
$V_{k,2}$	$-1/m_{\mathrm{h}}$	$(1/2)(\nabla_k^{\mathrm{S}} - \overleftarrow{\nabla}_k^{\mathrm{S}})$
$V_{k,3}$	$1/(2m_{\mathrm{h}})$	$\sum_l (1/2)(\nabla_l^{\mathrm{S}} + \overleftarrow{\nabla}_l^{\mathrm{S}})\gamma_l\gamma_k$
$V_{k,4}$	$-1/m_{\mathrm{h}}$	$(1/2)(\nabla_k^{\mathrm{S}} + \overleftarrow{\nabla}_k^{\mathrm{S}})$

Table 4.1: Overview of coefficients $c_{\mathrm{V}j}$ at tree level and K_j for V_μ

4.5 Renormalisation and matching

In this section, we sketch the idea of the matching between HQET and QCD. An observable computed along the lines of the previous sections is an HQET observable for which to have a physical meaning, one needs to connect it to QCD. Details on the matching procedure and the latest progress can be found in references [76, 77]. Let us emphasise at this point that the matching can be performed fully non-perturbatively, that is, completely without the use of perturbation theory.

One imposes the equation

$$\Phi_i^{\mathrm{QCD}}(L, m_{\mathrm{h}}, 0) = \Phi_i^{\mathrm{HQET}}(L, m_{\mathrm{h}}, a), \tag{4.27}$$

where Φ_i are the above-mentioned observables one is interested in. In reference [77], a total of 19 such observables are computed, but they include eight observables related to the axial current which is not needed in the project discussed here, so that we need eleven such coefficients. In fact, we have already introduced these in the previous sections. They are $\omega_{\mathrm{kin}}, \omega_{\mathrm{spin}}$ of equation (4.24), two renormalisation factors $Z_{V_{0,k}}^{\mathrm{HQET}}$, six coefficients $c_{\mathrm{V}_{\{0,k\},j}}$ of equations (4.26), and $m_{\mathrm{b,bare}}$ of equation (4.19). Here, we will not go into further detail and refer to the cited publications.

Anticipating the definitions of correlators in the next chapter, let us now see how we will expand them in HQET. For this, we need to expand in $1/m_{\mathrm{h}}$ equation (5.10), while for the operators we make insertions according to (4.24) with

$$\mathcal{O} = P_{\mathrm{ll}} V^\mu P_{\mathrm{hl}} \text{ or } P_{\mathrm{lh}} P_{\mathrm{hl}}, \tag{4.28}$$

where P, V^μ are the pseudoscalar and vector current, respectively, defined in equations (5.5), and V_μ^{HQET} is given in equation (4.26). The light-light correlator obviously has no $1/m_{\mathrm{h}}$ corrections.

Since we are interested only in terms of $O(1/m_{\mathrm{h}})$, from now on, we will drop all terms

of order $1/m_{\mathrm{h}}^2$ and higher. For notational simplicity, we here present the calculation in a schematic way, dropping all prefactors and an overall $\sum_{\{\vec{x}\}}$, and suppressing all arguments of correlators. In the next chapter, we dedicate some care to defining the correlators correctly. For the three-point function, we need

$$\begin{aligned}
&\mathcal{C}_\mu^{\mathrm{B_s}\to\mathrm{K}} \equiv \langle P_{\mathrm{ll}}|V_\mu|P_{\mathrm{hl}}\rangle \sim \\
&\sim Z_{\mathrm{V}}^{\mathrm{HQET}} Z_{\mathrm{P_{hl}}}^{\mathrm{HQET}} Z_{\mathrm{P_{ll}}} \Bigg\{ \left\langle P_{\mathrm{ll}} \left[V_\mu^{\mathrm{stat}} + \sum_j c_{\mathrm{V}}^{(j)} V_\mu^{(j)} \right] P_{\mathrm{hl}} \right\rangle_{\mathrm{stat}} + \\
&\quad + \omega_{\mathrm{kin}} \left\langle P_{\mathrm{ll}} V_\mu^{\mathrm{stat}} P_{\mathrm{hl}}^{\mathrm{stat}} \mathcal{O}_{\mathrm{kin}} \right\rangle_{\mathrm{stat}} + \omega_{\mathrm{spin}} \left\langle P_{\mathrm{ll}} V_\mu^{\mathrm{stat}} P_{\mathrm{hl}}^{\mathrm{stat}} \mathcal{O}_{\mathrm{spin}} \right\rangle_{\mathrm{stat}} \Bigg\} \\
&= Z_{\mathrm{V}}^{\mathrm{HQET}} Z_{\mathrm{P_{hl}}}^{\mathrm{HQET}} Z_{\mathrm{P_{ll}}} \left\langle P_{\mathrm{ll}} V_\mu^{\mathrm{stat}} P_{\mathrm{hl}}^{\mathrm{stat}} \right\rangle_{\mathrm{stat}} \Bigg\{ 1 + \frac{\left\langle P_{\mathrm{ll}} \sum_j c_{\mathrm{V}}^{(j)} V_\mu^{(j)} P_{\mathrm{hl}} \right\rangle_{\mathrm{stat}}}{\left\langle P_{\mathrm{ll}} V_\mu^{\mathrm{stat}} P_{\mathrm{hl}}^{\mathrm{stat}} \right\rangle_{\mathrm{stat}}} + \\
&\quad + \omega_{\mathrm{kin}} \frac{\left\langle P_{\mathrm{ll}} V_\mu^{\mathrm{stat}} P_{\mathrm{hl}}^{\mathrm{stat}} \mathcal{O}_{\mathrm{kin}} \right\rangle_{\mathrm{stat}}}{\left\langle P_{\mathrm{ll}} V_\mu^{\mathrm{stat}} P_{\mathrm{hl}}^{\mathrm{stat}} \right\rangle_{\mathrm{stat}}} + \omega_{\mathrm{spin}} \frac{\left\langle P_{\mathrm{ll}} V_\mu^{\mathrm{stat}} P_{\mathrm{hl}}^{\mathrm{stat}} \mathcal{O}_{\mathrm{spin}} \right\rangle_{\mathrm{stat}}}{\left\langle P_{\mathrm{ll}} V_\mu^{\mathrm{stat}} P_{\mathrm{hl}}^{\mathrm{stat}} \right\rangle_{\mathrm{stat}}} \Bigg\} \\
&\equiv Z_{\mathrm{V}}^{\mathrm{HQET}} Z_{\mathrm{P_{hl}}}^{\mathrm{HQET}} Z_{\mathrm{P_{ll}}} \mathcal{C}_\mu^{\mathrm{B_s}\to\mathrm{K,stat}} \left\{ 1 + \sum_j c_{\mathrm{V}}^{(j)} R_\mu^{\delta(\mathrm{B_s}\to\mathrm{K}),(j)} + \omega_{\mathrm{kin}} R_\mu^{\mathrm{B_s}\to\mathrm{K,kin}} + \omega_{\mathrm{spin}} R_\mu^{\mathrm{B_s}\to\mathrm{K,spin}} \right\}.
\end{aligned} \tag{4.29}$$

For the heavy-light two-point function, we have

$$\begin{aligned}
&\mathcal{C}^{\mathrm{B_s}} \equiv \langle P_{\mathrm{lh}} P_{\mathrm{hl}} \rangle \sim \\
&\sim \left(Z_{\mathrm{P_{hl}}}^{\mathrm{HQET}}\right)^2 \left\{ \left\langle P_{\mathrm{lh}}^{\mathrm{stat}} P_{\mathrm{hl}}^{\mathrm{stat}} \right\rangle_{\mathrm{stat}} + \omega_{\mathrm{kin}} \left\langle P_{\mathrm{lh}}^{\mathrm{stat}} P_{\mathrm{hl}}^{\mathrm{stat}} \mathcal{O}_{\mathrm{kin}} \right\rangle_{\mathrm{stat}} + \omega_{\mathrm{spin}} \left\langle P_{\mathrm{lh}}^{\mathrm{stat}} P_{\mathrm{hl}}^{\mathrm{stat}} \mathcal{O}_{\mathrm{spin}} \right\rangle_{\mathrm{stat}} \right\} \\
&\equiv \left(Z_{\mathrm{P_{hl}}}^{\mathrm{HQET}}\right)^2 \mathcal{C}^{\mathrm{B_s,stat}} \left\{ 1 + \omega_{\mathrm{kin}} R^{\mathrm{B_s,kin}} + \omega_{\mathrm{spin}} R^{\mathrm{B_s,spin}} \right\}.
\end{aligned} \tag{4.30}$$

Let us now further anticipate that in equation (5.10), we will define the ratio R_μ, and here study how it is expanded and renormalised in HQET. For this, we combine equations (4.29) and (4.30) and the two-point light-light function $\mathcal{C}^{\mathrm{K}} \equiv \langle P_{\mathrm{ll}} P_{\mathrm{ll}} \rangle$ to arrive at

$$\begin{aligned}
R_\mu &\sim Z_{\mathrm{V}}^{\mathrm{HQET}} \frac{\mathcal{C}_\mu^{\mathrm{B_s}\to\mathrm{K,stat}}}{\sqrt{\mathcal{C}^{\mathrm{B_s,stat}} \mathcal{C}^{\mathrm{K}}}} \Bigg\{ 1 + \sum_j c_{\mathrm{V}}^{(j)} R_\mu^{\delta(\mathrm{B_s}\to\mathrm{K}),(j)} + \\
&\quad + \omega_{\mathrm{kin}} R_\mu^{\mathrm{B_s}\to\mathrm{K,kin}} + \omega_{\mathrm{spin}} R_\mu^{\mathrm{B_s}\to\mathrm{K,spin}} - \frac{1}{2} \left(\omega_{\mathrm{kin}} R^{\mathrm{B_s,kin}} + \omega_{\mathrm{spin}} R^{\mathrm{B_s,spin}} \right) \Bigg\} \\
&= Z_{\mathrm{V}}^{\mathrm{HQET}} \frac{\mathcal{C}_\mu^{\mathrm{B_s}\to\mathrm{K,stat}}}{\sqrt{\mathcal{C}^{\mathrm{B_s,stat}} \mathcal{C}^{\mathrm{K}}}} \Bigg\{ 1 + \sum_j c_{\mathrm{V}}^{(j)} R_\mu^{\delta(\mathrm{B_s}\to\mathrm{K}),(j)} + \\
&\quad + \omega_{\mathrm{kin}} \left(R_\mu^{\mathrm{B_s}\to\mathrm{K,kin}} - \frac{1}{2} R^{\mathrm{B_s,kin}} \right) + \omega_{\mathrm{spin}} \left(R_\mu^{\mathrm{B_s}\to\mathrm{K,spin}} - \frac{1}{2} R^{\mathrm{B_s,spin}} \right) \Bigg\}.
\end{aligned} \tag{4.31}$$

Note in particular that renormalisation factors of the two-point functions, $Z_{\mathrm{P_{hl}}}^{\mathrm{HQET}}$ and $Z_{\mathrm{P_{ll}}}$,

cancel, and thus, the only remaining renormalisation factor needed here is the one of the vector current, $Z_{\mathrm{V}}^{\mathrm{HQET}}$.

4.6 Renormalisation and matching at static order

We detailed the renormalisation and matching programme we want to follow in section 4.5. While the needed coefficients are not yet available, at this point, we discuss also the strategy outlined in references [49, 78–80], in which the renormalisation factors are determined non-perturbatively, while the matching coefficients rely on a three-loop expression from perturbation theory. Here, we review briefly the computation performed in the given references. Let us start in general by computing a quantity Φ,

$$\Phi = C_{\mathrm{X}}(M_{\mathrm{h}}/\Lambda_{\overline{\mathrm{MS}}})\Phi_{\mathrm{RGI}} + O(1/m_{\mathrm{h}}), \tag{4.32}$$

where C_{X} is the correct matching parameter that links the renormalisation group invariant Φ_{RGI} to the physical one, M_{h} is the RGI mass of the heavy quark and $\Lambda_{\overline{\mathrm{MS}}}$ the QCD Λ parameter in the $\overline{\mathrm{MS}}$ scheme. The RGI quantities

$$\Phi_{\mathrm{RGI}} = \Phi(\mu)(2b_0\bar{g}^2)^{-\gamma_0/(2b_0)}\exp\left\{-\int_0^{\bar{g}}\mathrm{d}g\left[\frac{\gamma(g)}{\beta(g)} - \frac{\gamma_0}{b_0 g}\right]\right\}, \tag{4.33}$$

$$\Lambda = \mu(b_0\bar{g}^2)^{-b_1/(2b_0^2)}\exp\left\{-\frac{1}{2b_0\bar{g}^2}\right\}\exp\left\{-\int_0^{\bar{g}}\mathrm{d}g\left[\frac{1}{\beta(g)} + \frac{1}{b_0 g^3} - \frac{b_1}{b_0^2 g}\right]\right\} \tag{4.34}$$

are obtained from solving the renormalisation group equations

$$\mu\frac{\mathrm{d}\Phi}{\mathrm{d}\mu} = \gamma(\bar{g})\Phi, \tag{4.35}$$

$$\mu\frac{\mathrm{d}\bar{g}}{\mathrm{d}\mu} = \beta(\bar{g}) \tag{4.36}$$

and are independent of the renormalisation scale μ. Φ_{RGI} is further independent of the renormalisation scheme. The renormalisation group functions $\beta(g)$ and $\gamma(g)$ of equations (4.35), (4.36) are perturbatively expanded as

$$\beta(\bar{g}) \overset{\bar{g}\to 0}{\sim} -\bar{g}^3\{b_0 + b_1\bar{g}^2 + b_2\bar{g}^4 + O(\bar{g}^6)\}, \tag{4.37}$$

$$\gamma(\bar{g}) \overset{\bar{g}\to 0}{\sim} -\bar{g}^2\{\gamma_0 + \gamma_1\bar{g}^2 + \gamma_2\bar{g}^4 + O(\bar{g}^6)\}, \tag{4.38}$$

where [81, 82]

$$\gamma_0 = -\frac{1}{4\pi^2}, \quad b_0 = \frac{1}{(4\pi)^2}\left(\frac{11}{3}N - \frac{2}{3}N_{\mathrm{f}}\right), \quad b_1 = \frac{1}{(4\pi)^4}\left(\frac{34}{3}N^2 - \left(\frac{13}{3}N - N^{-1}\right)N_{\mathrm{f}}\right) \tag{4.39}$$

are universal coefficients, $N = N_{\mathrm{colour}} = 3$.

	{HYPn, $O(a)$ current improvement?}			
β	{1, no}	{2, no}	{1, yes}	{2, yes}
5.2	0.7104(5)(57)	0.7920(5)(63)	0.7007(5)(56)	0.7432(5)(59)
5.3	0.7057(27)(57)	0.7839(26)(63)	0.6965(27)(56)	0.7376(25)(59)
5.5	0.6901(27)(56)	0.7597(26)(62)	0.6820(26)(55)	0.7218(24)(58)

Table 4.2: Values for $Z_{\mathrm{A,RGI}}$. Values at $\beta = 5.2$ are taken directly from table 4 of reference [78], values at $\beta = 5.3$ are obtained using the interpolating polynomial of equation (B.3) and table 9 of that reference and values at $\beta = 5.5$ are obtained from a linear extrapolation of the ones at $\beta = 5.29$ and $\beta = 5.4$.

An RGI quantity is related to the bare one via

$$\Phi_{\mathrm{RGI}} = Z_{\mathrm{RGI}} \Phi_{\mathrm{bare}}, \tag{4.40}$$

with a renormalisation factor Z_{RGI},

$$Z_{\mathrm{X,RGI}}(g_0) \equiv \left[\frac{\Phi_{\mathrm{RGI}}}{\Phi(\mu)} \times Z_{\mathrm{X}}^{\mathrm{stat}}(\mu, g_0) \right]_{\mu = 1/L_{\max}} . \tag{4.41}$$

Note here that the first factor in equation (4.41) is universal, that is, it does not depend on the chosen lattice setup, while the second factor is non-universal[1]. $\Phi_{\mathrm{RGI}}/\Phi(\mu)$ is computed in a recursive series of non-perturbative scale evolution steps, known as step scaling [83–85].

In our case, Φ is the matrix element $\langle \mathrm{K}|V^\mu|\mathrm{B_s}\rangle$. That is, the operator we need to renormalise is the vector current V^μ. Equation (4.32) then becomes [49, 80]

$$V_0^{\mathrm{HQET}} = C_{\mathrm{PS}}(M_{\mathrm{h}}/\Lambda_{\overline{\mathrm{MS}}}) Z_{\mathrm{A,RGI}}^{\mathrm{stat}}(g_0) Z_{\mathrm{V/A}}^{\mathrm{stat}}(g_0) V_0^{\mathrm{stat}}, \tag{4.42a}$$

$$V_k^{\mathrm{HQET}} = C_{\mathrm{V}}(M_{\mathrm{h}}/\Lambda_{\overline{\mathrm{MS}}}) Z_{\mathrm{A,RGI}}^{\mathrm{stat}}(g_0) V_k^{\mathrm{stat}}. \tag{4.42b}$$

Interpolating polynomials for $Z_{\mathrm{A,RGI}}$ are given in equation (B.3) and table 9 of reference [78]. Since they span a range of $5.2 \leq \beta \leq 5.4$, but we need $Z_{\mathrm{A,RGI}}$ at $\beta = 5.5$, we have to proceed carefully. We get the value at $\beta = 5.5$ best as a linear extrapolation of the ones at $\beta = 5.29$ and $\beta = 5.4$. As errors for the inter- and extrapolated values, we take the same error as that of the point closest to the one in question. We show the values in table 4.2.

References [78, 79] provide approximations[2] of $C_{\mathrm{PS}}, C_{\mathrm{V}}$ that rely on a three-loop pertur-

[1] In particular, the given values are correct for $N_{\mathrm{f}} = 2$ non-perturbatively $O(a)$ improved Wilson fermions with plaquette gauge action and c_{SW} of equation (3.15). The value depends on the static action used and whether or not we use $O(a)$ improvement of the current. We discuss this in section 5.1.8.

[2] The precision of these approximations is estimated in the given references as at least 0.2% for $x \leq 0.6$, while for our purposes, $x \approx 0.3$.

bative expansion in the renormalisation group function γ [86]:

$$C_{\mathrm{PS}}(x) = x^{\gamma_0/(2b_0)}\{1 - 0.118x - 0.010x^2 + 0.043x^3\}, \tag{4.43}$$

$$C_{\mathrm{V}}(x) = x^{\gamma_0/(2b_0)}\{1 - 0.266x - 0.178x^2 + 0.193x^3\}, \tag{4.44}$$

where

$$x = \frac{1}{\ln(M/\Lambda_{\overline{\mathrm{MS}}})}. \tag{4.45}$$

$M = M_{\mathrm{b}}$ and $\Lambda_{\overline{\mathrm{MS}}}$ are provided in references [71, 87]. We then obtain, for $N_{\mathrm{f}} = 2$,

$$C_{\mathrm{PS}} = 1.2111(59), \tag{4.46}$$

$$C_{\mathrm{V}} = 1.1338(73). \tag{4.47}$$

Note that in equation (4.42a) we also need $Z^{\mathrm{stat}}_{\mathrm{V/A}} = Z^{\mathrm{stat}}_{\mathrm{V}}/Z^{\mathrm{stat}}_{\mathrm{A}}$. While this has been computed in the quenched approximation [88], it is not available for the $N_{\mathrm{f}} = 2$ theory. Since, in perturbation theory, it is expected to be a small variation around 1 and it multiplies $f_{\parallel}$ which is $O(1/m_{\mathrm{h}})$ suppressed, compare equations (2.8), its effects on the final result will be very small. To be able to give a preliminary result, estimating the effect of including or not the $f_{\parallel}$ term, we therefore assume

$$Z^{\mathrm{stat}}_{\mathrm{A}}/Z^{\mathrm{stat}}_{\mathrm{V}} = 0.97(3). \tag{4.48}$$

5 Computation of the form factor

In this chapter we discuss the correlators and the two- and three-point functions we construct out of these, and how we build a ratio which will have a physical meaning. First, we show how the two- and three-point functions are constructed in principle. Then we explain how we calculate them explicitly. In this chapter, for the technical parts of the computation, let us set the lattice spacing $a = 1$ for notational simplicity. We will reintroduce it in section 5.2 when we turn to the computation of quantities in physical units.

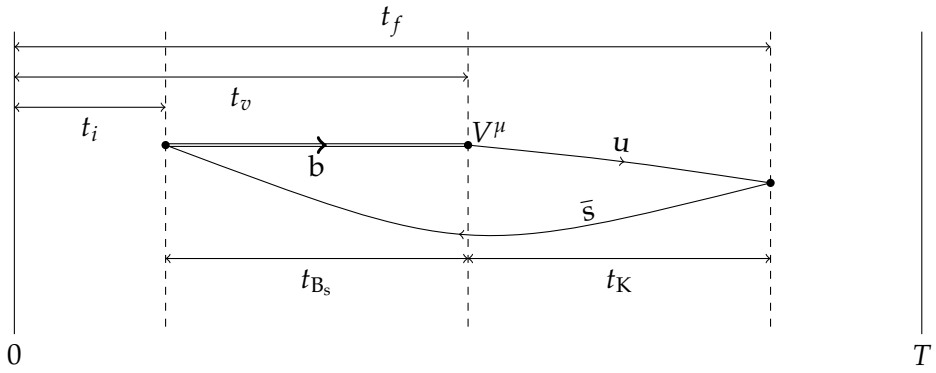

Figure 5.1: Schematic representation of $B_s \to K$

In figure 5.1, we schematically show the three-point function which we compute and set some notation. In particular, we define:

$$t_K \equiv t_f - t_v, \tag{5.1a}$$

$$t_{B_s} \equiv t_v - t_i. \tag{5.1b}$$

5.1 Correlators

We start by constructing two- and three-point functions:

$$\mathcal{C}^{\mathrm{K}}(t;\vec{p}) = \sum_{\vec{x}_f,\vec{x}_i} \mathrm{e}^{-\mathrm{i}\,\vec{p}\cdot(\vec{x}_f-\vec{x}_i)} \langle P_{\mathrm{su}}(x_f) P_{\mathrm{us}}(x_i)\rangle, \tag{5.2}$$

$$\mathcal{C}^{\mathrm{B_s}}(t;\vec{0}) = \sum_{\vec{x}_f,\vec{x}_i} \langle P_{\mathrm{sb}}(x_f) P_{\mathrm{bs}}(x_i)\rangle, \tag{5.3}$$

$$\mathcal{C}_\mu^{\mathrm{B_s}\to\mathrm{K}}(t_{\mathrm{K}}, t_{\mathrm{B_s}};\vec{p}) = \sum_{\vec{x}_f,\vec{x}_v,\vec{x}_i} \mathrm{e}^{-\mathrm{i}\,\vec{p}\cdot(\vec{x}_f-\vec{x}_v)} \langle P_{\mathrm{su}}(x_f) V^\mu(x_v) P_{\mathrm{bs}}(x_i)\rangle, \tag{5.4}$$

where

$$P_{\mathrm{q_1q_2}}(x) = \big(\overline{\psi}_{\mathrm{q_1}}\gamma_5\psi_{\mathrm{q_2}}\big)(x) = \overline{\psi}_{\mathrm{q_1}}(x)\gamma_5\psi_{\mathrm{q_2}}(x), \tag{5.5a}$$

$$V^\mu(x) = \big(\overline{\psi}_{\mathrm{u}}\gamma_\mu\psi_{\mathrm{b}}\big)(x) \;\; = \overline{\psi}_{\mathrm{u}}(x)\gamma_\mu\psi_{\mathrm{b}}(x). \tag{5.5b}$$

Note that in the light-light two-point function and in the three-point function we inject a relativistic three-momentum $\vec{p}$. For the heavy-light two-point function we choose to set the momentum to $\vec{p}_{\mathrm{B_s}} = 0$, since we work in HQET and want to treat the $\mathrm{B_s}$ meson as static up to $1/m_{\mathrm{h}}$ corrections. The heavy-light two-point function can be decomposed as

$$\mathcal{C}^{\mathrm{B_s}}(t_{\mathrm{B_s}}) = \sum_n \big(\beta^{(n)}\big)^2 \mathrm{e}^{-E^{(n)}_{\mathrm{B_s}} t_{\mathrm{B_s}}}, \tag{5.6}$$

compare section 3.5, equation (3.37). Here we have now denoted amplitudes $\beta^{(n)}$ and energies $E^{(n)}_{\mathrm{B_s}}$. In the limit of large time, only the ground state, that is, the state with the lowest energy, will remain, while all excited states with higher energies will have decayed:

$$\mathcal{C}^{\mathrm{B_s}}(t_{\mathrm{B_s}}) \overset{t_{\mathrm{B_s}}\to\infty}{=} \big(\beta^{(0)}\big)^2 \mathrm{e}^{-E^{(0)}_{\mathrm{B_s}} t_{\mathrm{B_s}}}. \tag{5.7}$$

Similarly, the light-light two-point function is, for a given momentum $\vec{p}$,

$$\mathcal{C}^{\mathrm{K}}(t_{\mathrm{K}}) = \sum_n \big(\kappa^{(n)}\big)^2 \mathrm{e}^{-E^{(n)}_{\mathrm{K}} t_{\mathrm{K}}} \overset{t_{\mathrm{K}}\to\infty}{=} \big(\kappa^{(0)}\big)^2 \mathrm{e}^{-E^{(0)}_{\mathrm{K}} t_{\mathrm{K}}}. \tag{5.8}$$

Finally, for the three-point function, we have, for a given momentum $\vec{p}$,

$$\begin{aligned} \mathcal{C}_\mu^{\mathrm{B_s}\to\mathrm{K}}(t_{\mathrm{K}}, t_{\mathrm{B_s}}) \quad &= \quad \sum_m \sum_n \kappa^{(m)} \varphi_\mu^{(m,n)} \beta^{(n)} \mathrm{e}^{-E^{(m)}_{\mathrm{K}} t_{\mathrm{K}}} \mathrm{e}^{-E^{(n)}_{\mathrm{B_s}} t_{\mathrm{B_s}}} \\ &\overset{t_{\mathrm{K}},t_{\mathrm{B_s}}\to\infty}{=} \kappa^{(0)} \varphi_\mu^{(0,0)} \beta^{(0)} \mathrm{e}^{-E^{(0)}_{\mathrm{K}} t_{\mathrm{K}}} \mathrm{e}^{-E^{(0)}_{\mathrm{B_s}} t_{\mathrm{B_s}}}. \end{aligned} \tag{5.9}$$

We use the correlators defined in equations (5.2), (5.3), (5.4) to construct the following ratio:

$$R_\mu(t_{\mathrm{K}}, t_{\mathrm{B_s}}) = \frac{\mathcal{C}_\mu^{\mathrm{B_s}\to\mathrm{K}}(t_{\mathrm{K}}, t_{\mathrm{B_s}})}{\sqrt{\mathcal{C}^{\mathrm{K}}(t_{\mathrm{K}})\mathcal{C}^{\mathrm{B_s}}(t_{\mathrm{B_s}})}}. \tag{5.10}$$

Then, in the limit of all time separations large, we obtain the matrix element of physical interest to us as

$$\varphi_\mu^{(0,0)} = \langle \mathrm{K}(p_\mathrm{K})|V^\mu|\mathrm{B_s}(0)\rangle = \lim_{T,t_\mathrm{K},t_{\mathrm{B_s}}\to\infty} R_\mu(t_\mathrm{K},t_{\mathrm{B_s}})\,\mathrm{e}^{E_\mathrm{K}^{(0)}t_\mathrm{K}/2}\,\mathrm{e}^{E_{\mathrm{B_s}}^{(0)}t_{\mathrm{B_s}}/2}, \tag{5.11}$$

where $E_\mathrm{K}^{(0)}$, $E_{\mathrm{B_s}}^{(0)}$ are the ground state energies of the K and $\mathrm{B_s}$, respectively, that can be determined independently from the two-point functions. In section 6.5, we discuss finite-T effects due to the fact that in practice, the limit $T \to \infty$ assumed in equation (5.11) cannot be simulated. Let us note here that the ratio defined in equation (5.10) is not unique, although it is the one that one frequently encounters in the literature [28, 29, 32, 35, 36]. For example, one could consider

$$R'_\mu(t_\mathrm{K},t_{\mathrm{B_s}}) = \frac{\mathcal{C}_\mu^{\mathrm{B_s}\to\mathrm{K}}(t_\mathrm{K},t_{\mathrm{B_s}})}{\mathcal{C}^\mathrm{K}(t_\mathrm{K})\mathcal{C}^{\mathrm{B_s}}(t_{\mathrm{B_s}})}, \tag{5.12}$$

and, similar to equation (5.11), one would obtain the physical matrix element as

$$\varphi_\mu^{(0,0)} = \langle \mathrm{K}(p_\mathrm{K})|V^\mu|\mathrm{B_s}(0)\rangle = \lim_{T,t_\mathrm{K},t_{\mathrm{B_s}}\to\infty} R'_\mu(t_\mathrm{K},t_{\mathrm{B_s}})\kappa^{(0)}\beta^{(0)}, \tag{5.13}$$

where now $\kappa^{(0)}$, $\beta^{(0)}$ are the ground state amplitudes of the K and $\mathrm{B_s}$, respectively, determined independently from the two-point functions. In sections 6.1 and 6.3, we discuss how to determine $E_\mathrm{K}^{(0)}$, $\kappa^{(0)}$ and $E_{\mathrm{B_s}}^{(0)}$, $\beta^{(0)}$, respectively, as fitting parameters in fits to the corresponding correlators.

We will come back to the discussion of energies and amplitudes of the two- and three-point functions in section 6.4 where we discuss a combined fit to these in order to obtain the form factors $\varphi_\mu^{(0,0)}$ as fit parameters.

In the following sections, we discuss the ingredients needed to compute the correlators of equations (5.2), (5.3) and (5.4).

5.1.1 Light quark smearing

A (light) fermion on the lattice, ψ, as introduced in section 3.2, is a field that lives on a single lattice point x in spacetime. Contracted with an antiquark field $\overline{\psi}$ located at y, we obtain a quark propagator $S(x,y)$ which propagates the quark from x to y. A meson propagator is the product of such a quark propagator with an antiquark propagator from y to x. It is a δ_x function at the source and a δ_y function at the sink. As already addressed in section 3.6, it is desirable to improve the overlap of a lattice correlator with the physical ground state. Although the light-light correlator does not suffer from an exponentially worsening signal-to-noise ratio as the heavy-light correlator does, it is still favourable to improve on its overlap with the ground state which we want to determine. To achieve better overlap with a physical meson, which has a finite extension, we employ Wuppertal (Gaussian) fermion smearing [89–91]. In this procedure, the fermion field gets iteratively

smeared and thus broadened, making for a better representation of the physical meson we want to simulate. We define

$$W \equiv (1 + \kappa \nabla^* \nabla)^N, \tag{5.14}$$

where

$$\kappa = \sigma^2/(4N), \tag{5.15}$$

with a parameter σ and N the number of smearing iterations. In this thesis, all light quark fields that we encounter will be smeared, that is

$$\psi^{\mathrm{sm}}_{\{\mathrm{u,s}\}}(x) = W\psi_{\{\mathrm{u,s}\}}(x), \tag{5.16}$$

while heavy quarks will not be smeared. The corresponding propagator obtained from the contraction of two such quarks fields is

$$\left\langle \psi^{\mathrm{sm}}_{\{\mathrm{u,s}\}}(x)\overline{\psi}^{\mathrm{sm}}_{\{\mathrm{u,s}\}}(y)\right\rangle_{\mathrm{F}} = W_x S_{\{\mathrm{u,s}\}}(x,y)\overleftarrow{W}_y \equiv S^{\mathrm{sm}}_{\{\mathrm{u,s}\}}(x,y), \tag{5.17}$$

where the subscript to the smearing operator indicates at which point the smearing is performed. We note that although we will not smear a b quark, the heavy-light two-point function, that is, a meson made up of heavy and a light quark, can be smeared when we smear the light quark.

In this thesis, we will work with smeared light quark fields and propagators everywhere, that is, they are of the form of equation (5.16) and (5.17), while all heavy quark fields and propagators will not be smeared. In particular, a light quark propagator will be smeared at both source and sink. Keeping this in mind, for notational simplicity, from now on we will suppress the superscript "sm" everywhere.

5.1.2 Random sources method

To achieve better statistical precision and less noise, we compute all-to-all light quark propagators with U(1) random sources $\eta_r(x)$ [92, 93] on a time slice t. For this, we make use of the fact that the correlators of equations (5.2), (5.3), (5.4), when averaged over gauge configurations, are invariant under translations of the source point $\vec{x}$. Instead of computing a single propagator, we want to compute a number of propagators from different source points and then take the average of the resulting propagators which stochastically reduces the variance. The cost of this is, naturally, that we have to compute a set of propagators instead of a single one. Let us define

$$\phi_r(x) \equiv S(x,y)\eta_r(y) \tag{5.18a}$$

$$\phi_{r,\vec{p}}(x) \equiv S(x,y)\eta_{r,\vec{p}}(y), \qquad \eta_{r,\vec{p}}(y) = \eta_r(y)\,\mathrm{e}^{\mathrm{i}\,\vec{p}\cdot\vec{y}}, \tag{5.18b}$$

where we imply a sum $\sum_y$ over all spacetime and understand that

$$\left\langle \eta_r(x)\eta_r^\dagger(y)\right\rangle_\eta = \delta(x-y) = \frac{1}{N_r}\sum_r \left\langle \eta_r(x)\eta_r^\dagger(y)\right\rangle_\eta , \tag{5.19}$$

with $\langle . \rangle_\eta$ the average over all η and N_r the number of sources. We will use sources that reside on a single time slice t_{source}, that is,

$$\eta_r(x) = \delta(t - t_{\text{source}})\eta_r(\vec{x}). \tag{5.20}$$

We use full time dilution, that is, we work with T random sources, placed on all time slices, and averaged over.

5.1.3 Light quark twisting

In the setup considered so far, we are only able to assign discrete momenta to the two- and three-point correlators of equation (5.2) and (5.4),

$$\vec{p} = (2\pi/L)\vec{n}, \quad n_i \in \mathbb{Z}, \tag{5.21}$$

so that we compute the form factor at certain values of $q^2 = (p_{\text{B}_\text{s}} - p_\text{K})^2$ only, which differ depending on the ensemble of gauge configurations we choose.

Once we have simulated the correlators, we will have to extrapolate the results to the continuum and to the physical sea pion mass. We will discuss these extrapolations in section 7.2. We would, however, like to avoid a third extrapolation in q^2 due to the fact that our data from different ensembles do not have the same physical light meson momentum and thus are not at the same values of q^2. Thus we would like to have values of the form factor at (nearly) the same q^2 for different ensembles.

By applying flavour twisted boundary conditions to the quark fields [94–97], we are able to tune the momentum of the light meson freely. To this end, instead of imposing periodic boundary conditions, we impose the boundary condition

$$\psi(x + L\hat{k}) = \mathrm{e}^{\mathrm{i}\,\theta_k}\,\psi(x), \tag{5.22}$$

where $\vec{\theta}$ is a three-vector in space, but more generally, $\theta = (0, \vec{\theta})$ can be written as a four-vector. In order to be able to Fourier transform these twisted fields in a well-defined fashion, that is, obeying

$$\sum_{\vec{p}} \mathrm{e}^{\mathrm{i}\,\vec{p}\cdot(\vec{x}+L\hat{k})}\,\tilde{\psi}(\vec{p}) = \mathrm{e}^{\mathrm{i}\,\vec{\theta}}\sum_{\vec{p}} \mathrm{e}^{\mathrm{i}\,\vec{p}\cdot\vec{x}}\,\tilde{\psi}(\vec{p}), \tag{5.23}$$

we have to redefine our momentum of equation (5.21) to

$$\vec{p}^{\,\theta} = \frac{2\pi}{L}(\vec{n} + \vec{\theta}/(2\pi)). \tag{5.24}$$

Following the cited references, for convenience we then define

$$\psi_\theta(x) = \mathrm{e}^{-\mathrm{i}\, x\cdot\theta/L}\, \psi(x), \tag{5.25}$$

noting that $\psi_\theta(x)$ has periodic boundary conditions. This causes a transformation of the Dirac operator for the field ψ_θ, D^θ, in the action, according to

$$\overline{\psi}(x)D(x,y)\psi(y) \to \overline{\psi}_\theta(x)D^\theta(x,y)\psi_\theta(y) = \overline{\psi}_\theta(x)\,\mathrm{e}^{-\mathrm{i}\,\theta\cdot x/L}\,D(x,y)\,\mathrm{e}^{\mathrm{i}\,\theta\cdot y/L}\,\psi_\theta(y). \tag{5.26}$$

This can be achieved using the derivatives as written in equations (A.6) instead of ordinary lattice derivatives of equation (A.5), which amounts to a phase multiplication of the gauge fields,

$$U_\mu(x) \to U^\theta_\mu(x) = \mathrm{e}^{\mathrm{i}\,\theta_k/L}\, U_\mu(x). \tag{5.27}$$

In our program we choose to include this phase multiplication into the gauge field through which the quark which we want to twist is propagating. In equation (5.27), we divide the total twist per direction, θ_k, to L shares with each gauge link receiving a contribution of θ_k/L.

When considering a function of more than one quark, the most general case is that we allow for each of the quarks q_{f_i} to be twisted by $\vec{\theta}_{\mathrm{f}_i}$. For example, for the kaon two-point function, we can twist the u by $\vec{\theta}_{\mathrm{u}}$ and the s by $\vec{\theta}_{\mathrm{s}}$. Then, we have

$$\begin{aligned}
\mathcal{C}^{\mathrm{K}}(t;\vec{p},\vec{\theta}_{\mathrm{u}},\vec{\theta}_{\mathrm{s}}) &= \sum_{\vec{x}} \mathrm{e}^{\mathrm{i}\,\vec{p}^{\,\theta}_{\mathrm{K}}\cdot\vec{x}}\,\langle P_{\mathrm{su}}(x)P_{\mathrm{us}}(0)\rangle \\
&= \sum_{\vec{x}} \mathrm{e}^{\mathrm{i}\,\vec{p}^{\,\theta}_{\mathrm{K}}\cdot\vec{x} - \mathrm{i}\,\frac{\vec{\theta}_{\mathrm{u}}-\vec{\theta}_{\mathrm{s}}}{L}\cdot\vec{x}} \left\langle P^\theta_{\mathrm{su}}(x)P^\theta_{\mathrm{us}}(0)\right\rangle_\theta \\
&= \sum_{\vec{x}} \mathrm{e}^{\mathrm{i}\,\vec{p}_{\mathrm{K}}\cdot\vec{x}} \left\langle P^\theta_{\mathrm{su}}(x)P^\theta_{\mathrm{us}}(0)\right\rangle_\theta,
\end{aligned} \tag{5.28}$$

where by $\langle . \rangle_\theta$ we indicate that in the action we use the Dirac operator D^θ of equation (5.26). The kaon will then receive the resulting momentum

$$\vec{p}^{\,\theta}_{\mathrm{K}} = \frac{2\pi}{L}(\vec{n} + (\vec{\theta}_{\mathrm{u}} - \vec{\theta}_{\mathrm{s}})/(2\pi)). \tag{5.29}$$

In our project we choose not to twist the up quark. The ensembles we will simulate on have two dynamical light quarks in the sea. When we set up our measurements, we will set the mass of the valence light quarks to that of the sea light quarks, that is, $m_{\mathrm{light}} = m_{\mathrm{sea}}$. Now a twist on the up quark would correspond to a partial quenching of that quark which is undesirable, because we would lose unitarity. The valence strange quark, on the other hand, is already quenched, since it is not dynamic in the sea. So, by twisting it, we cannot cause any more harm than we did by quenching it in the first place[1].

Note that as depicted in the sketch in figure 5.1, the b and u are quarks and the s is an

[1] This reasoning will no longer hold when simulating $\mathrm{B} \to \pi$ decays since then, both light quarks are unquenched.

antiquark. Let us consider for now only twisting the $\bar{s}$ (thus setting $\theta_u = 0$). In the next subsection we will then also discuss twisting the b. Twisting the $\bar{s}$, we vary the momenta of both the K and the B_s,

$$\vec{p}^{\,\theta}_{K} = \frac{2\pi}{L}(\vec{n} + \vec{\theta}_s/(2\pi)) \tag{5.30a}$$

$$\vec{p}^{\,\theta}_{B_s} = \vec{0} + \vec{\theta}_s/L. \tag{5.30b}$$

As we twist the antiquark, a phase shift as in equation (5.27) will pick up an extra minus sign, so that in order to get a positive shift in momentum, we need to set the components of $\vec{\theta}_s$ to a negative value. Note here that the B_s receives a momentum $\vec{p}_{B_s}$, which enters in the relativistic energy-momentum relation $E = m_{B_s}(1 + \vec{p}^{\,2}/(2m_{B_s}^2) + \ldots)$ at order $1/m_{B_s}$. Since we treat the B_s in HQET, the quantities $m_{b,\,\text{bare}}$ and E_{stat} are independent of $\vec{p}_{B_s}$ and therefore of $\vec{\theta}_s$. Once we turn to $O(1/m_h)$, however, we will encounter effects due to the fact the B_s has a non-vanishing momentum. The form factor decomposition we discussed in section 2.1 is based on being in the B_s rest frame. So in order to restore our considering the B_s in the rest frame, we will also twist the b quark. We discuss this in the next subsection. In appendix C.2, we also discuss in more detail some implications of quark twisting.

5.1.4 Heavy quark twisting

As we have seen in equation (5.30b), when we twist the s quark, the B_s meson will receive a momentum, which we would like to avoid. Thus we discuss twisting the b quark by $\vec{\theta}_b$, the idea being that when we set $\vec{\theta}_b = \vec{\theta}_s$, the effects of the two twists will cancel, compare equation (5.29), and the B_s will be in its rest frame. As we noted previously, for our purposes, this is convenient, so we adapt this choice, but we note that in principle it is possible to have $\vec{\theta}_b \neq \vec{\theta}_s$, thus leaving the B_s with a non-vanishing momentum. Hence, from now on, we will assume $\vec{\theta}_b = \vec{\theta}_s \equiv \vec{\theta}$. Note that also in the measurement code, only $\vec{\theta}_b = \vec{\theta}_s$ or, as a relic, $\vec{\theta}_b = 0$ are implemented.

Hence, the s and b quarks will be twisted by $\vec{\theta}$, thus propagating through gauge fields of equation (5.27), while the u quark has $\vec{\theta}_u = \vec{0}$. As we noted already, in the static approximation, the b quark propagates in time-direction only, consequently, it will not feel any effect of the quark twist, since the twist is in spatial directions only. At order $1/m_h$, it will feel an effect when spatial derivatives act on the heavy quark propagator, introducing a dependence on spatial gauge links, compare equation (5.27). We discuss this in sections 5.1.6 and 5.1.7.

In the following, we will work with periodic fields ψ_θ everywhere. Thus, to keep notation simple, from now on, we drop the subscript θ everywhere.

5.1.5 Computation of correlators

Now that we are equipped with the necessary tools, let us see how to compute the correlators introduced in section 5.1 explicitly. Since it is the most intricate case, we present the

computation of the three-point function in some detail.

For the three-point function, with $\{\vec{x}\} = \vec{x}_f, \vec{x}_v, \vec{x}_i$, we compute

$$\mathcal{C}_\mu^{\mathrm{B_s}\to\mathrm{K}}(t_\mathrm{K}, t_{\mathrm{B_s}}; \vec{p}, \theta) = \frac{-1}{V_3} \sum_{\{\vec{x}\}} \mathrm{e}^{-\mathrm{i}\,\vec{p}\cdot(\vec{x}_f - \vec{x}_v)} \left\langle \left\langle P_\mathrm{su}(x_f) V^\mu(x_v) P_\mathrm{bs}(x_i) \right\rangle_\mathrm{F} \right\rangle \tag{5.31}$$

$$= \frac{-1}{V_3} \sum_{\{\vec{x}\}} \mathrm{e}^{-\mathrm{i}\,\vec{p}\cdot(\vec{x}_f - \vec{x}_v)} \left\langle \left\langle \overline{\psi}_\mathrm{s}(x_f)\gamma_5\psi_\mathrm{u}(x_f)\overline{\psi}_\mathrm{u}(x_v)\gamma_\mu\psi_\mathrm{b}(x_v)\overline{\psi}_\mathrm{b}(x_i)\gamma_5\psi_\mathrm{s}(x_i) \right\rangle_\mathrm{F} \right\rangle ,$$

where $V_3 = L^3$ is the three-volume of the lattice. Remembering equation (3.25), we now perform Wick contractions:

$$= \frac{1}{V_3} \sum_{\{\vec{x}\}} \mathrm{e}^{-\mathrm{i}\,\vec{p}\cdot(\vec{x}_f - \vec{x}_v)} \left\langle \mathrm{tr}\left\{ S_\mathrm{u}(x_f, x_v)\gamma^\mu S_\mathrm{b}(x_v, x_i)\gamma_5 S_\mathrm{s}(x_i, x_f)\gamma_5 \right\} \right\rangle$$

Next, we move the γ_5 at the end of the trace to the front; commuting the other γ_5 to the left with S_b, we get $P_+ \to P_-$ in the propagator which we denote by $\mathrm{b} \to \tilde{\mathrm{b}}$, and commuting it further with γ_μ causes a factor -1. Then, we insert $\eta_r, \eta^\dagger_{r,\vec{p}}$ of equations (5.18) in x_f, with the sum now running also over $x_{f'}$, and arrive at

$$= \frac{-1}{V_3 N_r} \sum_{\{\vec{x}\}} \sum_r \mathrm{e}^{\mathrm{i}\,\vec{p}\cdot\vec{x}_v} \left\langle \mathrm{tr}\left\{ \gamma_5 S_\mathrm{u}(x_f, x_v)\gamma_5\gamma^\mu S_{\tilde{\mathrm{b}}}(x_v, x_i) S_\mathrm{s}(x_i, x_f)\eta_r(x_f)\eta^\dagger_{r,\vec{p}}(x_{f'}) \right\} \right\rangle ,$$

where we now imply that the average $\langle . \rangle$ is also over η, compare equation (5.19). We now use γ_5-hermiticity, $\gamma_5 S(x,y)\gamma_5 = S^\dagger(y,x)$, on the up quark propagator and move $\eta^\dagger_{r,\vec{p}}(x_{f'})$ to the front, thus making the trace summation implicit,

$$= \frac{-1}{V_3 N_r} \sum_{\{\vec{x}\}} \sum_r \mathrm{e}^{\mathrm{i}\,\vec{p}\cdot\vec{x}_v} \left\langle \eta^\dagger_{r,\vec{p}}(x_{f'}) S^\dagger_\mathrm{u}(x_v, x_f)\gamma^\mu S_{\tilde{\mathrm{b}}}(x_v, x_i) S_\mathrm{s}(x_i, x_f)\eta_r(x_f) \right\rangle$$

$$= \frac{-1}{V_3 N_r} \sum_{\{\vec{x}\}} \sum_r \mathrm{e}^{\mathrm{i}\,\vec{p}\cdot\vec{x}_v} \left\langle \phi^\dagger_{r,\vec{p}}(x_v)\gamma^\mu S_{\tilde{\mathrm{b}}}(x_v, x_i)\phi_r(x_i) \right\rangle , \tag{5.32}$$

where finally, we substituted ϕ_r, $\phi^\dagger_{r,\vec{p}}$ of equations (5.18). The computation for the two-point functions is analogous to that presented in equation (5.32). We here give only the result. We get for the light-light two-point function

$$\mathcal{C}^\mathrm{K}(t_\mathrm{K}; \vec{p}, \vec{\theta}) = \frac{1}{V_3 N_r} \sum_{\vec{x}_i, \vec{x}_f} \sum_r \mathrm{e}^{\mathrm{i}\,\vec{p}\vec{x}_i} \left\langle \phi^\dagger_{r,\vec{p}}(x_i)\phi_r(x_i) \right\rangle , \tag{5.33}$$

and for the heavy-light two-point function[2]

$$\begin{aligned}\mathcal{C}^{\mathrm{B_s}}(t_{\mathrm{B_s}};\vec{\theta}) &= \frac{1}{V_3 N_r}\sum_{\vec{x}_i,\vec{x}_f}\sum_r \left\langle \eta_r^\dagger(x_f)\gamma_5 S_{\mathrm{b}}(x_f,x_i)\gamma_5\phi_r(x_i)\right\rangle \\ &= \frac{1}{V_3 N_r}\sum_{\vec{x}_i,\vec{x}_f}\sum_r \left\langle \eta_r^\dagger(x_f) S_{\tilde{\mathrm{b}}}(x_f,x_i)\phi_r(x_i)\right\rangle . \end{aligned} \tag{5.34}$$

5.1.6 $O(1/m_{\mathrm{h}})$ Lagrangian insertions

Here we discuss the computation of the Lagrangian insertions, defined in section 4.2. Let us insert equations (4.8) and (4.9) into equation (4.24), where $\mathcal{O}$ is our static three-point function of equation (5.31). For the kinetic insertions, we then have

$$\begin{aligned}\mathcal{C}_\mu^{\mathrm{B_s}\to\mathrm{K,kin}}(t_{\mathrm{K}},t_{\mathrm{B_s}};\vec{p},\vec{\theta}) &= \frac{-1}{V_3}\sum_{\{\vec{x}\},z}\mathrm{e}^{-\mathrm{i}\,\vec{p}\cdot(\vec{x}_f-\vec{x}_v)}\left\langle\left\langle P_{\mathrm{su}}(x_f)V^\mu(x_v)\mathcal{O}_{\mathrm{kin}}(z)P_{\mathrm{bs}}(x_i)\right\rangle_{\mathrm{F}}\right\rangle \\ &= \frac{-1}{V_3}\sum_{\{\vec{x}\},z}\mathrm{e}^{-\mathrm{i}\,\vec{p}\cdot(\vec{x}_f-\vec{x}_v)}\left\langle\left\langle (\overline{\psi}_{\mathrm{s}}\gamma_5\psi_{\mathrm{u}})(x_f)(\overline{\psi}_{\mathrm{u}}\gamma_\mu\psi_{\mathrm{b}})(x_v)\left[\overline{\psi}_{\mathrm{b}}(z)\vec{D}^2\psi_{\mathrm{b}}(z)\right](\overline{\psi}_{\mathrm{b}}\gamma_5\psi_{\mathrm{s}})(x_i)\right\rangle_{\mathrm{F}}\right\rangle .\end{aligned} \tag{5.35}$$

Now we evaluate the derivative and contract:

$$\begin{aligned}\mathcal{C}_\mu^{\mathrm{B_s}\to\mathrm{K,kin}}(t_{\mathrm{K}},t_{\mathrm{B_s}};\vec{p},\vec{\theta}) &= \frac{-1}{V_3}\sum_{\{\vec{x}\},l,z}\mathrm{e}^{-\mathrm{i}\,\vec{p}\cdot(\vec{x}_f-\vec{x}_v)}\left\langle\left\langle (\overline{\psi}_{\mathrm{s}}\gamma_5\psi_{\mathrm{u}})(x_f)(\overline{\psi}_{\mathrm{u}}\gamma_\mu\psi_{\mathrm{b}})(x_v)\times\right.\right. \\ &\left.\left.\times\,\overline{\psi}_{\mathrm{b}}(z)\left[U_l(z)\,\mathrm{e}^{\mathrm{i}\,\theta_l/L}\,\psi_{\mathrm{b}}(z+\hat{l}) + U_l^\dagger(z-\hat{l})\,\mathrm{e}^{-\mathrm{i}\,\theta_l/L}\,\psi_{\mathrm{b}}(z-\hat{l}) - 2\psi_{\mathrm{b}}(z)\right](\overline{\psi}_{\mathrm{b}}\gamma_5\psi_{\mathrm{s}})(x_i)\right\rangle_{\mathrm{F}}\right\rangle \\ &= \frac{1}{V_3}\sum_{\{\vec{x}\},l,z}\mathrm{e}^{-\mathrm{i}\,\vec{p}\cdot(\vec{x}_f-\vec{x}_v)}\left\langle \mathrm{tr}\left\{\gamma_5 S_{\mathrm{u}}(x_f,x_v)\gamma_\mu S_{\mathrm{b}}(x_v,z)\times\right.\right. \\ &\left.\left.\left[U_l^\theta(z)S_{\mathrm{b}}(z+\hat{l},x_i) + (U_l^\theta)^\dagger(z-\hat{l})S_{\mathrm{b}}(z-\hat{l},x_i) - 2S_{\mathrm{b}}(z,x_i)\right]\gamma_5 S_{\mathrm{s}}(x_f,x_i)\right\}\right\rangle .\end{aligned} \tag{5.36}$$

Now, analogous to equation (5.32), we insert sources $\eta_r, \eta_{r,\vec{p}}^\dagger$ in x_f, commute the γ_5 through the b quark propagators and past the γ_μ, accounting for $P_+ \to P_-$ and an overall sign change, use γ_5-hermiticity and the notation of equations (5.18) to arrive at

$$\begin{aligned}\mathcal{C}_\mu^{\mathrm{B_s}\to\mathrm{K,kin}}(t_{\mathrm{K}},t_{\mathrm{B_s}};\vec{p},\vec{\theta}) &= \frac{1}{V_3 N_r}\sum_{\{\vec{x}\},r,l,z}\mathrm{e}^{-\mathrm{i}\,\vec{p}\cdot(\vec{x}_f-\vec{x}_v)}\left\langle \mathrm{tr}\left\{\phi_{r,\vec{p}}^\dagger(x_v)\gamma_\mu S_{\tilde{\mathrm{b}}}(x_v,z)\times\right.\right. \\ &\left.\left.\left[U_l^\theta(z)S_{\tilde{\mathrm{b}}}(z+\hat{l},x_i) + (U_l^\theta)^\dagger(z-\hat{l})S_{\tilde{\mathrm{b}}}(z-\hat{l},x_i) - 2S_{\tilde{\mathrm{b}}}(z,x_i)\right]\phi_r(x_i)\right\}\right\rangle \\ &\equiv \frac{1}{V_3 N_r}\sum_{\{\vec{x}\},r}\mathrm{e}^{-\mathrm{i}\,\vec{p}\cdot(\vec{x}_f-\vec{x}_v)}\left\langle \mathrm{tr}\left\{\phi_{r,\vec{p}}^\dagger(x_v)\gamma_\mu S_{\tilde{\mathrm{b}}}^{\mathrm{kin}}(x_v,x_i)\phi_r(x_i)\right\}\right\rangle ,\end{aligned} \tag{5.37}$$

[2] In our program code, we compute $\mathcal{C}^{\mathrm{B_s}}$ as in the first line of equation (5.34), that is, with both γ_5s explicit and the projector P_+.

where we have defined

$$S^{\text{kin}}_{\tilde{\mathrm{b}}}(x_v, x_i) \equiv \sum_{l,z} S_{\tilde{\mathrm{b}}}(x_v, z)\left[U^{\theta}_l(z) S_{\tilde{\mathrm{b}}}(z+\hat{l}, x_i) + (U^{\theta}_l)^{\dagger}(z-\hat{l}) S_{\tilde{\mathrm{b}}}(z-\hat{l}, x_i) - 2S_{\tilde{\mathrm{b}}}(z, x_i)\right]. \tag{5.38}$$

For the spin insertions, we have, following the same steps of computation,

$$\begin{aligned}
\mathcal{C}^{\mathrm{B_s}\to\mathrm{K},\text{spin}}_{\mu}(t_{\mathrm{K}}, t_{\mathrm{B_s}}; \vec{p}, \vec{\theta}) &= \frac{-1}{V_3} \sum_{\{\vec{x}\},z} \mathrm{e}^{-\mathrm{i}\,\vec{p}\cdot(\vec{x}_f - \vec{x}_v)} \left\langle \left\langle P_{\mathrm{su}}(x_f) V^{\mu}(x_v) \mathcal{O}_{\mathrm{kin}}(z) P_{\mathrm{bs}}(x_i) \right\rangle_{\mathrm{F}} \right\rangle \\
&= \frac{-1}{V_3} \sum_{\{\vec{x}\},z} \mathrm{e}^{-\mathrm{i}\,\vec{p}\cdot(\vec{x}_f - \vec{x}_v)} \left\langle \left\langle (\overline{\psi}_{\mathrm{s}}\gamma_5\psi_{\mathrm{u}})(x_f) (\overline{\psi}_{\mathrm{u}}\gamma_{\mu}\psi_{\mathrm{b}})(x_v) \left[\overline{\psi}_{\mathrm{b}}(z)\vec{\sigma}\cdot\vec{B}\psi_{\mathrm{b}}(z)\right] (\overline{\psi}_{\mathrm{b}}\gamma_5\psi_{\mathrm{s}})(x_i) \right\rangle_{\mathrm{F}} \right\rangle \\
&= \frac{-1}{V_3 N_r} \sum_{\{\vec{x}\},r,z} \mathrm{e}^{-\mathrm{i}\,\vec{p}\cdot(\vec{x}_f - \vec{x}_v)} \left\langle \mathrm{tr}\left\{ \phi^{\dagger}_{r,\vec{p}}(x_v)\gamma_{\mu} S_{\tilde{\mathrm{b}}}(x_v, z)\left[\vec{\sigma}\cdot\vec{B}\right] S_{\tilde{\mathrm{b}}}(z, x_i)\phi_r(x_i) \right\} \right\rangle \\
&\equiv \frac{-1}{V_3 N_r} \sum_{\{\vec{x}\},r} \mathrm{e}^{-\mathrm{i}\,\vec{p}\cdot(\vec{x}_f - \vec{x}_v)} \left\langle \mathrm{tr}\left\{ \phi^{\dagger}_{r,\vec{p}}(x_v)\gamma_{\mu} S^{\text{spin}}_{\tilde{\mathrm{b}}}(x_v, x_i)\phi_r(x_i) \right\} \right\rangle,
\end{aligned} \tag{5.39}$$

where now

$$S^{\text{spin}}_{\tilde{\mathrm{b}}}(x_v, x_i) \equiv \sum_{z} S_{\tilde{\mathrm{b}}}(x_v, z)\left[\vec{\sigma}\cdot\vec{B}\right] S_{\tilde{\mathrm{b}}}(z, x_i). \tag{5.40}$$

Finally, we give the expressions for the kinetic and spin insertions for the two-point heavy-light function, obtained in a very similar computation:

$$\mathcal{C}^{\mathrm{B_s},\text{kin}}_{\mu}(t_{\mathrm{B_s}}; \vec{\theta}) = \frac{1}{V_3 N_r} \sum_{\{\vec{x}\},r} \left\langle \eta^{\dagger}_r(x_f) S^{\text{kin}}_{\tilde{\mathrm{b}}}(x_v, x_i)\phi_r(x_i) \right\rangle \tag{5.41}$$

and

$$\mathcal{C}^{\mathrm{B_s},\text{spin}}_{\mu}(t_{\mathrm{B_s}}) = \frac{1}{V_3 N_r} \sum_{\{\vec{x}\},r} \left\langle \eta^{\dagger}_r(x_f) S^{\text{spin}}_{\tilde{\mathrm{b}}}(x_v, x_i)\phi_r(x_i) \right\rangle. \tag{5.42}$$

5.1.7 $O(1/m_{\mathrm{h}})$ current insertions

We now turn to the computation of the $O(1/m_{\mathrm{h}})$ current insertions introduced in section 4.4 and tabulated in table 4.1. To this end, let us first see symbolically how a kernel $K_{\mu j}$

μ	j	$s_{\mu j}$	Γ^{μ}_{jl}
0	1	1	$\sum_l \gamma_l$
	2	-1	$\sum_l \gamma_l$
k	1	1	$\sum_l \gamma_l\gamma_k$
	2	1	$\mathbb{1}$
	3	-1	$\sum_l \gamma_l\gamma_k$
	4	-1	$\mathbb{1}$

Table 5.1: Overview of coefficients to be inserted in equation (5.44).

containing derivatives and some gamma structure Γ^{μ} acts on functions $f(x), g(x)$:

$$\begin{aligned}
&\sum_{\vec{x}}[f^{\dagger}(x)K_{\mu j}g(x)]\,\mathrm{e}^{\mathrm{i}\,\vec{p}\cdot\vec{x}} = \sum_{\vec{x}}[f^{\dagger}(x)(\nabla^{\mathrm{S}}_l \pm \overleftarrow{\nabla}^{\mathrm{S}}_l)\Gamma^{\mu}g(x)]\,\mathrm{e}^{\mathrm{i}\,\vec{p}\cdot\vec{x}}\\
&= \sum_{\vec{x}}\Big\{[\pm f^{\dagger}(x+\hat{l})U^{\dagger}_l(x) \mp f^{\dagger}(x-\hat{l})U_l(x-\hat{l})]\Gamma^{\mu}g(x)\\
&\quad + f^{\dagger}(x)\Gamma^{\mu}[U_l(x)\,\mathrm{e}^{\mathrm{i}\,\theta_l/L}\,g(x+\hat{l}) - U^{\dagger}_l(x-\hat{l})\,\mathrm{e}^{-\mathrm{i}\,\theta_l/L}\,g(x-\hat{l})]\Big\}\,\mathrm{e}^{\mathrm{i}\,\vec{p}\cdot\vec{x}}\\
&= \sum_{\vec{x}}\big\{[\pm f^{\dagger}(x+\hat{l})U^{\dagger}_l(x) \mp f^{\dagger}(x-\hat{l})U_l(x-\hat{l})]\Gamma^{\mu}g(x)\\
&\quad + f^{\dagger}(x-\hat{l})U_l(x-\hat{l})\,\mathrm{e}^{\mathrm{i}\,\theta_l/L}\,\Gamma^{\mu}g(x)\,\mathrm{e}^{-\mathrm{i}\,p_l} - f^{\dagger}(x+\hat{l})U^{\dagger}_l(x)\,\mathrm{e}^{-\mathrm{i}\,\theta_l/L}\,\Gamma^{\mu}g(x)\,\mathrm{e}^{\mathrm{i}\,p_l}\Big\}\,\mathrm{e}^{\mathrm{i}\,\vec{p}\cdot\vec{x}}\\
&= \sum_{\vec{x}}\Big\{ - f^{\dagger}(x+\hat{l})U^{\dagger}_l(x)\left[\mp 1 + \mathrm{e}^{\mathrm{i}(p_l-\theta_l/L)}\right] +\\
&\quad + f^{\dagger}(x-\hat{l})U_l(x-\hat{l})\left[\mp 1 + \mathrm{e}^{-\mathrm{i}(p_l-\theta_l/L)}\right]\Big\}\Gamma^{\mu}g(x)\,\mathrm{e}^{\mathrm{i}\,\vec{p}\cdot\vec{x}},
\end{aligned} \tag{5.43}$$

where, since summing over all $\vec{x}$, we shifted summation variables $\vec{x} \to \vec{x} \pm \hat{l}$ where needed so as to get our final result in terms of $g(x)$. Now, we apply the same steps of computation of equation (5.43) to our three-point correlator of equation (5.32), inserting $K_{\mu j}$ in the place of γ_{μ}, to arrive at:

$$\begin{aligned}
\mathcal{C}^{\mathrm{B_s}\to\mathrm{K},1/m}_{\mu,j}(t_{\mathrm{K}}, t_{\mathrm{B_s}}; \vec{p}, \vec{\theta}) = \frac{-1}{V_3 N_r}\sum_{\{\vec{x}\}}\sum_{r,l,j} c_{\mathrm{V}_{\mu j}}\,\mathrm{e}^{\mathrm{i}\,\vec{p}\cdot\vec{x}_v}\Big\{\Big\langle\Big[-\phi^{\dagger}_{r,\vec{p}}(x_v+\hat{l})(d^{\mu}_{jl})^{*}U^{\dagger}_l(x_v) +\\
+\ \phi^{\dagger}_{r,\vec{p}}(x_v-\hat{l})d^{\mu}_{jl}U_l(x_v-\hat{l})\Big]\,\Gamma^{\mu}_{jl}S_{\tilde{\mathfrak{b}}}(x_v,x_i)\phi_r(x_i)\Big\rangle\Big\},
\end{aligned} \tag{5.44}$$

where

$$d^{\mu}_{jl} = \tfrac{1}{4}\left(s_{\mu j} + \mathrm{e}^{-\mathrm{i}(p_l-\theta_l/L)}\right). \tag{5.45}$$

Expressions of Γ^{μ}_{jl} and $s_{\mu j}$ are shown in table 5.1. The $c_{\mathrm{V}_{\mu j}}$ are the matching coefficients introduced in section 4.4. They need to be determined non-perturbatively; an effort to achieve this is currently underway [76, 77].

5.1.8 $O(a)$ current improvement in the static case

We want to $O(a)$ improve the vector current at static order. Once we fully include $O(1/m_\mathrm{h})$ terms, we automatically have $O(a)$ improvement. At static order, we have [49]

$$(V_\mathrm{I}^\mathrm{stat})_\mu = V_\mu^\mathrm{stat} + c_{\mathrm{V}_\mu}^\mathrm{stat}\delta V_\mu^\mathrm{stat}. \tag{5.46}$$

For this, we need the following terms:

$$\delta V_0^\mathrm{stat} = \overline{\psi}_\mathrm{l}\sum_l \overleftarrow{\nabla}_l^\mathrm{S}\gamma_l\psi_\mathrm{h}, \tag{5.47a}$$

$$\delta V_k^\mathrm{stat} = -\overline{\psi}_\mathrm{l}\sum_l \overleftarrow{\nabla}_l^\mathrm{S}\gamma_l\gamma_k\psi_\mathrm{h}, \tag{5.47b}$$

with ∇^S as in equation (A.7). We can obtain them as linear combinations of the $O(1/m_\mathrm{h})$ terms listed in table 4.1. In fact,

$$\delta V_0^\mathrm{stat} = (V_{0,2} - V_{0,1}), \tag{5.48a}$$

$$\delta V_k^\mathrm{stat} = (V_{k,1} - V_{k,3}). \tag{5.48b}$$

From reference [67], $c_\mathrm{A}^\mathrm{stat}$ is known perturbatively:

$$c_\mathrm{A}^\mathrm{stat}(g_0) = c_\mathrm{A}^{\mathrm{stat},(1)} \times g_0^2 + O(g_0^4), \quad c_\mathrm{A}^{\mathrm{stat},(1)} = \begin{cases} 0.039(4) & \text{HYP1} \\ 0.220(14) & \text{HYP2.} \end{cases} \tag{5.49}$$

From spin symmetry, we know that [49]

$$V_0^\mathrm{stat} \to [V_0^\mathrm{stat}]' = A_k^\mathrm{stat}, \quad [A_0^\mathrm{stat}]' = V_k^\mathrm{stat} \tag{5.50}$$

and

$$[\delta V_0^\mathrm{stat}]' = \delta A_k^\mathrm{stat}, \quad [\delta A_0^\mathrm{stat}]' = \delta V_k^\mathrm{stat}. \tag{5.51}$$

Note that this applies also to $c_\mathrm{V}^\mathrm{stat}$, $c_\mathrm{A}^\mathrm{stat}$, that is, equation (5.46) becomes

$$(V_\mathrm{I}^\mathrm{stat})_0 = V_0^\mathrm{stat} + c_\mathrm{V}^\mathrm{stat}\delta V_0^\mathrm{stat}, \tag{5.52a}$$

$$(V_\mathrm{I}^\mathrm{stat})_k = V_k^\mathrm{stat} + c_\mathrm{A}^\mathrm{stat}\delta V_k^\mathrm{stat}. \tag{5.52b}$$

The coefficient $c_\mathrm{V}^\mathrm{stat}$ is again only known to one loop in perturbation theory [98]:

$$c_\mathrm{V}^\mathrm{stat}(g_0) = c_\mathrm{V}^{\mathrm{stat},(1)} \times g_0^2 + O(g_0^4), \quad c_\mathrm{V}^{\mathrm{stat},(1)} = \begin{cases} 0.0223(6) & \text{HYP1} \\ 0.0380(6) & \text{HYP2.} \end{cases} \tag{5.53}$$

Here, again, the coefficients are small at one-loop order of perturbation theory, and multiply $f_\parallel$ which is $O(1/m_\mathrm{h})$ suppressed. Hence their effect on the final result will be very small. At this stage of the work, where $O(1/m_\mathrm{h})$ effects are not yet included, to be able

to give a preliminary result and to estimate the effect of including or not the $f_\parallel$ term, we assume that these values can be used.

5.2 Simulation details

The expressions derived in the previous sections for the two- and three-point functions, as well as the $O(1/m_\mathrm{h})$ insertions to these, have been implemented in the `c`-code `hqet_btopi_all`, located in `~/main/`. It is based on the `DD-HMC` (Domain Decomposition Hybrid Monte Carlo) program package [99] and employs a deflated `sap-gcr` solver [100–103] for the inversions of the Dirac operator. Modules specifically written for the measurements of the $\mathrm{B_s} \to \mathrm{K}$ project are collected in `~/modules/meas/`. Setting all gauge links to unit matrices, the computations of correlators presented in section 5.1 can be performed analytically. Comparing the results of analytic computations with the output of the measurement code is a valuable tool for checking the correctness of both. In appendix B, we discuss in detail how we perform these analytic computations. In appendix C, we further discuss some underlying properties of the project.

Upon execution, `hqet_btopi_all` produces output files `hit`*hit*`2pt` for the two-point light-light function, `hit`*hit*`_3pt-`*tag*`-hyp`*hyp* for the three-point function and `hit`*hit*`-`*tag*`-hyp`*hyp* for the two-point heavy-light function, where *hit* is an integer indicating the replicum of the measurement, *tag* $\in$ {`stat, kin, spin, v1om`} specifies whether the static correlator, the kinetic, spin or $1/m$ current insertions were computed and *hyp* $\in$ {`1, 2`} indicates the HYP-smearing used, see section 3.6.

Simulations were performed on CLS gauge configurations[3] with $N_\mathrm{f} = 2$ dynamical sea quark flavours. An overview of the ensembles used is given in table 5.2. We perform measurements on the three ensembles A5, F6 and N6, which have roughly the same pion mass, allowing us to perform a continuum extrapolation. Measuring on ensemble F7, which has a different pion mass, we can estimate chiral effects. For the future, measurements on O7 and B6 are planned, so that a continuum limit can be taken at a second value of the pion mass. All measurements, the results of which are presented in this thesis, were performed on the SuperMUC Petascale System[4] at the Leibniz-Rechenzentrum.

Let us now discuss which κ_s we use, that is, which mass of the strange quark. While the simulations run on ensembles with $N_\mathrm{f} = 2$ light dynamical sea quark flavours, when considering a $\mathrm{B_s} \to \mathrm{K}$ decay, we have a valence $\bar{\mathrm{s}}$ quark. Its mass is an input parameter to the measurements. To choose it, we follow what is referred to as "strategy 1" in reference [87]. Following this strategy, we keep constant at its physical value the quantity

$$R_\mathrm{K} = \frac{m_\mathrm{K}^2}{f_\mathrm{K}^2}, \tag{5.54}$$

where f_K is the kaon decay constant. In a lattice simulation, R_K will be a function of the

[3] `https://twiki.cern.ch/twiki/bin/view/CLS/`
[4] `http://www.lrz.de/services/compute/supermuc/`

light quark masses ($\kappa_1 = \kappa_2$) and the strange quark mass κ_3. We use the physical kaon mass and decay constant in the isospin limit [16, 104],

$$m_{\mathrm{K}} = 494.2\ \mathrm{MeV}, \quad f_{\mathrm{K}} = 155\ \mathrm{MeV}. \tag{5.55}$$

Thus, once we fix κ_1 and m_{K}, κ_3 will be given as some function $\kappa_3 = h(\kappa_1)$. Then

$$R_{\mathrm{K}}(\kappa_1, \kappa_3) = R_{\mathrm{K}}(\kappa_1, h(\kappa_1)) = \frac{(a m_{\mathrm{PS}}(\kappa_1, h(\kappa_1)))^2}{(Z_{\mathrm{A}} a f_{\mathrm{PS}}^{\mathrm{bare}}(\kappa_1, h(\kappa_1)))^2} \stackrel{!}{=} R_{\mathrm{K}}^{\mathrm{phys}}. \tag{5.56}$$

As light quark mass κ_1, we use the one that was used in the generation of the ensembles, that is, $m_{\mathrm{light}} = m_{\mathrm{sea}}$. In tables 16 to 18 of reference [87], for that choice of κ_1, we find tabulated for some values of κ_3 the corresponding values of masses and decay constants of a pseudoscalar meson made up of two quarks with these masses. In section 5.4 of reference [87], a strategy to determine the strange quark mass, that is, to approximate the function $\kappa_3 = h(\kappa_1)$, is proposed. It fits the four points closed to the physical point in terms of distance $d = |R_{\mathrm{K}}(\kappa_1, \kappa_3) - R_{\mathrm{K}}^{\mathrm{phys}}|$ to a polynomial $P_2(\kappa_3 - \kappa_1) = \sum_{n=0}^{2} c_n (\kappa_3 - \kappa_1)^n$. The points are weighted with $(d^2 + \epsilon^2)^{-1}$, with a regulator $\epsilon = \frac{1}{100}\big(\max_{\kappa_3}\{R_{\mathrm{K}}(\kappa_1, \kappa_3)\} - \min_{\kappa_3}\{R_{\mathrm{K}}(\kappa_1, \kappa_3)\}\big)$. We tabulate the resulting values for κ_{s} in table 5.2.

While we smear the quarks of the light meson with 50 iterations and $\kappa = 0.1$ everywhere (see section 5.1.1, equations (5.14) and (5.15)), the light quark that is part of the heavy meson is smeared with various numbers smearing iterations R_k, thus creating different trial wave functions. For the choice of iterations we adopt the values used for example in reference [71], motivated by keeping roughly constant in physical units the smearing radii $r_k = 2a\sqrt{\kappa R_k}$, with κ of equation (5.15) kept at 0.1 throughout. We tabulate the values for R_k in table 5.2.

In the $\mathrm{B_s}$ rest frame, $p_{\mathrm{B_s}} = (m_{\mathrm{B_s}}, \vec{0}), p_{\mathrm{K}} = (E_{\mathrm{K}}, \vec{p}_{\mathrm{K}})$. We require the continuum energy-momentum relation to hold, $E_{\mathrm{K}} = \sqrt{\vec{p}_{\mathrm{K}}^2 + m_{\mathrm{K}}^2}$. We use the PDG [3] value for the $\mathrm{B_s}$ mass, $m_{\mathrm{B_s}} = 5.3667(4)$ GeV, and the conversion constant $\hbar c = 0.1973269718(44)$ GeV fm. We have

$$\begin{aligned} q^2 &= (p_{\mathrm{B_s}} - p_{\mathrm{K}})^2 \\ &= m_{\mathrm{B_s}}^2 - 2 m_{\mathrm{B_s}} \sqrt{\vec{p}_{\mathrm{K}}^2 + m_{\mathrm{K}}^2} + m_{\mathrm{K}}^2. \end{aligned} \tag{5.57}$$

To convert the lattice momentum to physical units, we use

$$\sqrt{(\vec{p}_{\mathrm{K}}^{\mathrm{phys}})^2}\,[\mathrm{GeV}] = \Big((\vec{p}_{\mathrm{K}}^{\mathrm{lat}} / (a\,[\mathrm{fm}]))^2 \times (\hbar c\,[\mathrm{Gev\ fm}])^2 \Big)^{1/2}, \tag{5.58}$$

where $\vec{p}_{\mathrm{K}}^{\mathrm{lat}}$ is given in equation (5.30a) and lattice spacings a in fm, obtained via scale setting using f_{K}, as in reference [87]. Their values have been updated in reference [105], tabulated in table 5.2. Now we can use equations (5.58) and (5.57) to compute the physical momenta and the momentum transfer given a lattice momentum. As pointed out in the introduction, in this thesis, we focus on the computation of the form factor at one value

id	β	L/a	a [fm]	m_π [MeV]	$m_\pi L$	N_{cfg}	κ_s	$\{R_1, R_2, R_3, R_4\}$
A5	5.2	32	0.0749(8)	330	4.0	500	0.13535(2)	$\{0, 15, 60, 155\}$
B6		48		280	5.1		0.13530(2)	
F6	5.3	48	0.0652(6)	310	5.0	300	0.13579(2)	$\{0, 22, 90, 225\}$
F7		48		270	4.3	635	0.13578(2)	
N6	5.5	48	0.0483(4)	340	4.0	1200	0.13631(1)	$\{0, 33, 135, 338\}$
O7		64		270	4.2		0.13627(1)	

Table 5.2: Overview of the subset of $N_f = 2$ CLS ensembles on which we performed our measurements. Lattice spacings are taken from reference [87], updated in reference [105]. m_π is the mass of a pion in the sea. We observe that $m_\pi L \geq 4$ on all ensembles. N_{cfg} is the number of configurations on which we measured. κ_s is the κ of the valence strange quark we use, determined as described in the text. R_k are the numbers of light quark smearing iterations we use for the heavy-light meson, obtaining different trial wave functions.

A5	F6, F7	N6	$\sqrt{\vec{p}_K^{\,2}}$	q^2
$\vec{n} + \vec{\theta}/(2\pi)$	$\vec{n} + \vec{\theta}/(2\pi)$	$\vec{n}$	[GeV]	[GeV^2]
$(0,0,0)$	$(0,0,0)$	$(0,0,0)$	0	23.74
$(1.034,0,0)$	$(1.350,0,0)$	$(1,0,0)$	0.535	21.23
		$(1,1,0)$	0.757	19.35
		$(1,1,1)$	0.927	17.77
		$(2,0,0)$	1.070	16.39

Table 5.3: Overview of momenta.

of q^2, $q^2 = 21.23$ GeV^2, the second row of table 5.3. For completeness, in table 5.3 we also tabulate other values of q^2 and their corresponding lattice momenta. We here restrict ourselves to leaving lattice N6 untwisted, while in principle, there is no reason to do so. In particular, any value of q^2 can be reached by twisting all lattices accordingly. We also restrict ourselves here to showing only those q^2 satisfying $p_K \lesssim 1\,\text{GeV}$, which is necessary for HQET to be well-defined. We note here that distributing the twist to components of $\vec{p}_K$ in order to reach a given value in GeV is not unambiguous. In table 5.4, we show for lattice A5 some of the possible combinations. To pick a combination that we use in our measurement, we choose the following rule. Any vanishing momentum component on an untwisted lattice is zero also for a twisted lattice. The twist is distributed equally among all non-zero components.

$\vec{n} + \vec{\theta}/(2\pi)$	$\sqrt{\vec{p}_{\mathrm{K}}^2}$ [GeV]	q^2 [GeV^2]
$(0.597, 0.597, 0.597)$	0.535	21.23
$(0.731, 0.733, 0)$	0.535	21.23
$(1, 0.263, 0)$	0.535	21.23
$(1.034, 0, 0)$	0.535	21.23

Table 5.4: Overview of different twisting combinations to reach the same physical kaon momenta $\vec{p}_{\mathrm{K}}$ and hence q^2 for lattice A5.

6 Analysis

Now that we ran our measurements as detailed in section 5.2, we have acquired a set of raw output data for the quantities motivated in section 5.1. In this chapter, we discuss how to extract physical quantities from these raw data, in particular, of course, the form factor as introduced in section 2.1. In the following, we focus our discussion on HYP1, as discussed in section 3.6.

6.1 Effective masses

The effective mass is defined as [52]

$$m_{\text{eff, naive}}(t+1/2) = \log \frac{\mathcal{C}(t)}{\mathcal{C}(t+1)} = -\partial_t \log(\mathcal{C}(t)). \tag{6.1}$$

For a symmetric correlator, like the light-light correlator, we can consider

$$\frac{\mathcal{C}(t)}{\mathcal{C}(t+1)} = \frac{\cosh(m_{\text{eff,symm}}(t - T/2))}{\cosh(m_{\text{eff,symm}}(t+1-T/2))} \tag{6.2}$$

and solve this equation for $m_{\text{eff,symm}}$.

Taking two surrounding points into account, equation (6.2) becomes

$$\frac{\mathcal{C}(t+2)}{\mathcal{C}(t+1)} = \frac{\mathrm{e}^{-m_{\text{eff}}(T-(t+1))} + \mathrm{e}^{-m_{\text{eff}}(t+1)}}{\mathrm{e}^{-m_{\text{eff}}(T-t)} + \mathrm{e}^{-m_{\text{eff}}t}}. \tag{6.3}$$

We solve equation (6.3) to obtain $m_{\text{eff}}(t+1)$.

When considering an effective mass plot of a two-point function, we identify the ground state, reached at sufficiently large t, as a plateau. That is, all excited states have decayed and only the ground state remains. To determine its energy, one now could perform a fit to a constant, that is, a weighted average, in the plateau region. Here, however, for the light-light two-point function, we choose to follow the strategy presented in section 3.2 of reference [87]. Let us briefly recapitulate it here. A two-point correlator can be written in its spectral decomposition, compare equation (3.37), according to

$$\begin{aligned} \mathcal{C}(t) &= \sum_{n=0}^{\infty} A^{(n)} \, \mathrm{e}^{-E^{(n)}t} \\ &\approx \sum_{n=0}^{1} A^{(n)} \, \mathrm{e}^{-E^{(n)}t} = A^{(0)} \, \mathrm{e}^{-E^{(0)}t} + A^{(1)} \, \mathrm{e}^{-E^{(1)}t}, \end{aligned} \tag{6.4}$$

	from eq. (6.8)		from eq. (6.6)			
ens	$\left(\kappa^{(0)}\right)^2 \times 10^5$	$E_{\mathrm{K}}^{(0)}$	$\left(\kappa^{(0)}\right)^2 \times 10^5$	$E_{\mathrm{K}}^{(0)}$	$\left(\kappa^{(1)}\right)^2 \times 10^5$	$E_{\mathrm{K}}^{(1)}$
A5	9.83(16)	0.28401(88)	9.80(14)	0.2839(15)	5.8(1.0)	0.693(57)
F6	10.37(22)	0.24850(92)	10.27(13)	0.24816(77)	9.5(1.7)	0.618(42)
N6	8.57(29)	0.18358(115)	8.55(16)	0.18356(62)	11.1(1.4)	0.449(21)
F7	10.01(22)	0.24569(89)	9.95(9)	0.24550(52)	9.0(9)	0.595(25)

Table 6.1: Fit results for $\kappa^{(n)}$ and $E_{\mathrm{K}}^{(n)}$ for the ensembles on which we measured. Shown are both the fit results of the one-exponential fit, equation (6.8), and of the two-exponential fit, equation (6.6).

assuming that we restrict ourselves to considering large enough t that only two states, ground and first excited state, contribute. For the two-point light-light correlator, making use of its symmetry property, we have

$$\mathcal{C}^{\mathrm{K}}(t) = \left(\kappa^{(0)}\right)^2 \left(\mathrm{e}^{-E_{\mathrm{K}}^{(0)} t} + \mathrm{e}^{-E_{\mathrm{K}}^{(0)} (T-t)} \right) + \left(\kappa^{(1)}\right)^2 \left(\mathrm{e}^{-E_{\mathrm{K}}^{(1)} t} + \mathrm{e}^{-E_{\mathrm{K}}^{(1)} (T-t)} \right). \tag{6.5}$$

Now we perform a two-exponential fit to equation (6.5) in a region where this assumption is assumed to be valid. Using the fit results, we then reconstruct the fitted correlator,

$$\mathcal{C}_{\mathrm{fit}}^{\mathrm{K}} = \left(\kappa_{\mathrm{fit}}^{(0)}\right)^2 \left[\mathrm{e}^{-E_{\mathrm{fit}}^{(0)} t} + \mathrm{e}^{-E_{\mathrm{fit}}^{(0)} (T-t)} \right] + \left(\kappa_{\mathrm{fit}}^{(1)}\right)^2 \left[\mathrm{e}^{-E_{\mathrm{fit}}^{(1)} t} + \mathrm{e}^{-E_{\mathrm{fit}}^{(1)} (T-t)} \right]. \tag{6.6}$$

Now, we compute the effective mass of the fitted correlator, $m_{\mathrm{eff}}^{\mathrm{fit}}(t)$, using equation (6.3). Then we impose

$$\frac{m_{\mathrm{eff}}^{\mathrm{fit}}(t)}{E_{\mathrm{fit}}^{(0)}} - 1 < \tilde{c} \times \frac{\delta m_{\mathrm{eff}}(t)}{m_{\mathrm{eff}}(t)}, \tag{6.7}$$

with a constant $\tilde{c}$. That is, we look for the t where the excited state contribution to the effective mass as given by the fit is less than $\tilde{c}$ times the relative statistical error of $m_{\mathrm{eff}}(t)$ at that t. In other words, we demand that the systematic error be negligible compared to the statistical one. We here choose $\tilde{c} = 1/4$. The first t for which this is satisfied will be the t_{min} for a second fit, in a region $[t_{\mathrm{min}}, T - t_{\mathrm{min}}]$, this time to the ground state of the correlator only:

$$\mathcal{C}^{\mathrm{K}}(t) = \left(\kappa^{(0)}\right)^2 \left(\mathrm{e}^{-E_{\mathrm{K}}^{(0)} t} + \mathrm{e}^{-E_{\mathrm{K}}^{(0)} (T-t)} \right). \tag{6.8}$$

From this fit, we obtain the values for $\kappa^{(0)}$, $E_{\mathrm{K}}^{(0)}$ that we use in the following sections. Having performed this procedure, we show the result graphically in figure 6.1 for the ensemble N6, similar to figure 2 of reference [87]. While if in the following, we need values for $\kappa^{(0)}$, $E_{\mathrm{K}}^{(0)}$, we take them from the fit to equation (6.8), note that from the first fit, equation (6.5), we also have $\kappa^{(1)}$, $E_{\mathrm{K}}^{(1)}$. In table 6.1, we tabulate our results for the various ensembles on which we measured.

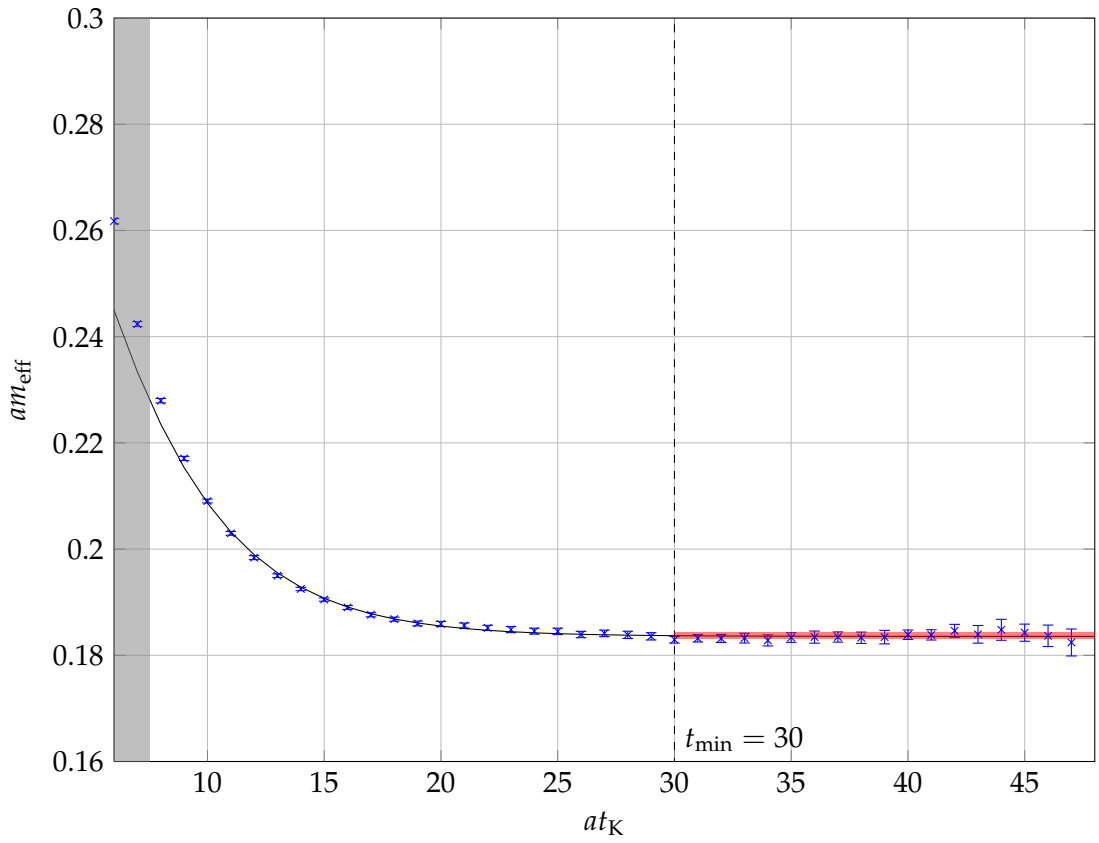

Figure 6.1: Effective mass plot for the light-light correlator on ensemble N6. The shown curve is the result of the fit to equation (6.5) to data points outside the shaded area. The red band is the result of the one-exponential fit as in equation (6.8).

6.2 Generalised Eigenvalue Problem

When considering matrix elements involving a heavy quark, employing solutions to the Generalized Eigenvalue Problem (GEVP) has been suggested [106, 107] in order to obtain plateau values for effective masses of the ground and excited states of these quantities. In this section, we discuss how we apply the GEVP to our problem. Let us first review very briefly the key points of the cited references, while a detailed derivation can be found therein. In this section, we deviate from the notation of the literature in that we denote the ground state by $n = 0$ instead of $n = 1$.

The GEVP is defined by

$$\mathcal{C}(t)v_n(t,t_0) = \lambda_n(t,t_0)\mathcal{C}(t_0)v_n(t,t_0), \quad n = 0,\ldots,N-1, \quad t_0 < t < 2t_0, \tag{6.9}$$

where $\mathcal{C}_{ij}$ is a matrix of correlation functions involving a heavy quark field. In practice, we construct this matrix by choosing different light quark smearing levels, see section 5.1.1, tabulated in table 5.2. For our purposes, we will use the heavy-light correlators defined in equation (5.3). The key feature of the GEVP is that it allows the determination of the

effective energy of the n-th state

$$E_{\text{eff}}^{(n)}(t,t_0) = -\partial_t \log(\lambda_n(t,t_0)) \tag{6.10}$$

as [108]

$$E_{\text{eff}}^{(n)}(t,t_0) = E^{(n)} + O(\mathrm{e}^{-\Delta_{N+1,n}t}), \quad \Delta_{N+1,n} = E^{(N+1)} - E^{(n)}. \tag{6.11}$$

This means in particular that if we are interested in the ground state energy and use, for example, $N = 3$ correlators, we obtain it up to corrections of order $\exp\{-\Delta_{3,0}t\}$, compared to $\exp\{-\Delta_{1,0}t\}$ without the use of GEVP. The energy of the n-th state can now be determined by performing a plateau fit, that is, a weighted average, to $E_{\text{eff}}^{(n)}(t,t_0)$ of equation (6.11).

Let us point out here that for our purposes, what we need is only a rough estimate of the energies of the first three states, since they serve as initial values for our final fit. We discuss this in some detail in the following sections.

6.3 Fitting the heavy-light correlators

In this section, we discuss a strategy to extract energies and amplitudes of the heavy-light two-point function. Having simulated $N_{\text{wvfn}} = 4$ light-quark smearing levels as discussed in section 5.1.1, for the heavy-light two-point function, we obtain a correlator matrix $\mathcal{C}_{ij}^{\text{B}_\text{s}}(t_{\text{B}_\text{s}})$ in smearing-level space, $i,j = 0,\ldots,N_{\text{wvfn}}-1$, where $i,j = 0$ corresponds to the unsmeared wave function which we omit in our analysis because of its poor overlap with the physical ground state. That is, $\mathcal{C}_{ij}^{\text{B}_\text{s}}$ is a 3×3 matrix. We symmetrise $\mathcal{C}_{ij}^{\text{B}_\text{s}} = (\mathcal{C}_{ij}^{\text{B}_\text{s}} + \mathcal{C}_{ji}^{\text{B}_\text{s}})/2$ so that we deal with six different correlators. We restrict ourselves to considering the first three energy states, $N = 3$, that is, the ground, first and second excited state.

Let us remember equation (5.6) and write the heavy-light two-point function as

$$\mathcal{C}_{ij}^{\text{B}_\text{s}}(t_{\text{B}_\text{s}}) = \sum_n \beta_i^{(n)}\beta_j^{(n)}\,\mathrm{e}^{-E_{\text{B}_\text{s}}^{(n)}t_{\text{B}_\text{s}}} \approx \sum_{n=0}^{2} \beta_i^{(n)}\beta_j^{(n)}\,\mathrm{e}^{-E_{\text{B}_\text{s}}^{(n)}t_{\text{B}_\text{s}}}\,. \tag{6.12}$$

In particular, for the diagonal entries $\mathcal{C}_{ii}^{\text{B}_\text{s}}(t_{\text{B}_\text{s}})$ we have

$$\mathcal{C}_{ii}^{\text{B}_\text{s}}(t_{\text{B}_\text{s}}) = \sum_n \left(\beta_i^{(n)}\right)^2 \mathrm{e}^{-E_{\text{B}_\text{s}}^{(n)}t_{\text{B}_\text{s}}} \approx \sum_{n=0}^{2} \left(\beta_i^{(n)}\right)^2 \mathrm{e}^{-E_{\text{B}_\text{s}}^{(n)}t_{\text{B}_\text{s}}}\,. \tag{6.13}$$

If we now assume $(E_{\text{B}_\text{s}}^{(n)})_{\text{GEVP}}$ known as determined from the GEVP as discussed in section 6.2, we can perform a linear fit to $\mathcal{C}_{ii}^{\text{B}_\text{s}}$ to determine $\left(\beta_i^{(n)}\right)^2_{\text{lin}}$ as in equation (6.13). Now we can use these as input values, with $(E_{\text{B}_\text{s}}^{(n)})_{\text{GEVP}}$ still fixed from GEVP, to determine $(\beta_i^{(n)})_{\text{non-lin}}$ as *non-linear* fit parameters in a fit to the full matrix $\mathcal{C}_{ij}^{\text{B}_\text{s}}$, that is, including off-diagonal entries. In this way, we are sensitive to possible minus signs in any of the $\beta_i^{(n)}$, which we are unable to determine from the linear fit for $\left(\beta_i^{(n)}\right)^2$. Obviously, the absolute

values of all $\beta_i^{(n)}$ should be compatible between linear and non-linear determination, that is,

$$\left|\beta_i^{(n)}\right|_{\text{lin}} = \left|\beta_i^{(n)}\right|_{\text{non-lin}} \tag{6.14}$$

and

$$\left.\frac{\beta_i^{(n)}}{\beta_1^{(n)}}\right|_{\text{lin}} = \left.\frac{\beta_i^{(n)}}{\beta_1^{(n)}}\right|_{\text{non-lin}}. \tag{6.15}$$

6.4 Extracting the form factors

In this section, we discuss a strategy to extract energies and amplitudes of the three-point function by performing a combined fit to the three-point data together with the data of the two-point functions, sometimes referred to as a "factorising fit" [109]. We here make some assumptions about the correlators and the fits and discuss these; then we present the fit to which these assumptions lead. In appendix D, we present some possible models for the fits that are the result of different assumptions.

Unlike the heavy-light two-point function, which is a matrix in smearing-level space (see section 6.3), $\mathcal{C}_{\mu,i}^{\mathrm{B_s}\to\mathrm{K}}(t_{\mathrm{K}}, t_{\mathrm{B_s}})$ is a $1 \times N_{\text{wvfn}}$ vector[1]. Again, we restrict ourselves to omitting the unsmeared wave function and considering the first three energy states, $N = 3$, that is, the ground, first and second excited state.

Let us remember equation (5.8) and write the light-light two-point function as

$$\mathcal{C}^{\mathrm{K}}(t_{\mathrm{K}}) = \sum_n (\kappa^{(n)})^2 \, \mathrm{e}^{-E_{\mathrm{K}}^{(n)} t_{\mathrm{K}}} \approx (\kappa^{(0)})^2 \, \mathrm{e}^{-E_{\mathrm{K}}^{(0)} t_{\mathrm{K}}}, \tag{6.16}$$

where we assume that all t_{K} that we consider are large enough such that excited kaon states are negligible. Remembering equation (5.9), we write the three-point function, for a set of fixed $\vec{p}, \vec{\theta}$, as

$$\begin{aligned}\mathcal{C}_{\mu,i}^{\mathrm{B_s}\to\mathrm{K}}(t_{\mathrm{K}}, t_{\mathrm{B_s}}) &= \sum_m \sum_n \kappa^{(m)} \varphi_\mu^{(m,n)} \beta_i^{(n)} \, \mathrm{e}^{-E_{\mathrm{K}}^{(m)} t_{\mathrm{K}}} \, \mathrm{e}^{-E_{\mathrm{B_s}}^{(n)} t_{\mathrm{B_s}}} \\ &\approx \sum_{n=0}^{2} \kappa^{(0)} \varphi_\mu^{(0,n)} \beta_i^{(n)} \, \mathrm{e}^{-E_{\mathrm{K}}^{(0)} t_{\mathrm{K}}} \, \mathrm{e}^{-E_{\mathrm{B_s}}^{(n)} t_{\mathrm{B_s}}},\end{aligned} \tag{6.17}$$

also neglecting excited kaon states in the three-point functions. While in chapter 7, we discuss in detail how to obtain the physical form factors from $\varphi_\mu^{(0,0)}$, here we focus on discussing the combined fit to $\mathcal{C}_{\mu=0}^{\mathrm{B_s}\to\mathrm{K}}$ and $\mathcal{C}_{\mu=1}^{\mathrm{B_s}\to\mathrm{K}}$ for $\varphi_0^{(0,0)}$ and $\varphi_1^{(0,0)}$.

By "combined fit" we mean that we perform one fit minimising

$$\chi^2 = \sum_j \frac{(y_j - f(p, x_j))^2}{\sigma_j^2}, \tag{6.18}$$

[1] Here we only smear the heavy-light part at one point (at x_i, compare figure 5.1.). The "other end" of the three-point function is the kaon. While we also have simulated two different smearing levels for the kaon, and one could in principle also include these, no gain is expected from this. Then the light-light two-point function, naturally, is a 1×1 object in the space of usable wave functions.

with a fit function f for a set p of fit parameters and a set (x_j, y_j, σ_j) of data points that come from the different correlators entering the fit.

We observe that once we have determined $\kappa^{(n)}$, $E_{\mathrm{K}}^{(n)}$ and $\beta_i^{(n)}$, $E_{\mathrm{B_s}}^{(n)}$ independently from the two-point functions as described in sections 6.1 and 6.3, respectively, we can rewrite the three-point function of equation (6.17) as

$$\mathcal{C}_{\mu,i}^{\mathrm{B_s}\to\mathrm{K}}(t_{\mathrm{K}}, t_{\mathrm{B_s}}) \approx \sum_{n=0}^{2} A_i^{(n)}(t_{\mathrm{K}}, t_{\mathrm{B_s}})\varphi_\mu^{(0,n)}, \tag{6.19}$$

where now

$$A_i^{(n)}(t_{\mathrm{K}}, t_{\mathrm{B_s}}) = \kappa^{(0)}\beta_i^{(n)}\,\mathrm{e}^{-E_{\mathrm{K}}^{(0)}t_{\mathrm{K}}}\,\mathrm{e}^{-E_{\mathrm{B_s}}^{(n)}t_{\mathrm{B_s}}} \tag{6.20}$$

are known. Using these as input, we can now determine $\varphi_\mu^{(0,n)}$ as linear fit parameters in a fit to equation (6.19).

We remark that at this point, in principle, we could stop the discussion of our analysis: We are able to determine the form factors $\varphi_\mu^{(0,n)}$ along with all amplitudes and energies that enter the two- and three-point functions. However, we have reason to now also perform a combined fit to all correlators that we discussed. In doing so, we combine all available information on a given quantity, thus making for a better, more accurate determination less affected by both statistical and systematic errors. Consider for example the amplitudes $\beta_i^{(n)}$ of the two-point heavy-light functions. If we assumed them fixed to their final values as determined solely from the two-point heavy-light functions, we would lose all information on them coming from the three-point function, where they also enter. In addition, if we then were to determine the same $\beta_i^{(n)}$ from the three-point function data, we might get slightly different values for the same quantities. Thus, a combined, monolithic fit, as we shall discuss below, is superior to a modular fitting strategy.

Let us therefore now collect all correlators that enter the combined fit. From equations (6.12), (6.16) and (6.17), we perform a combined fit to

$$\begin{cases} \mathcal{C}_{0,i}^{\mathrm{B_s}\to\mathrm{K}}(t_{\mathrm{B_s}}, t_{\mathrm{K}}) = \displaystyle\sum_{n=0}^{2} \kappa^{(0)}\varphi_0^{(0,n)}\beta_i^{(n)}\,\mathrm{e}^{-E_{\mathrm{K}}^{(0)}t_{\mathrm{K}}}\,\mathrm{e}^{-E_{\mathrm{B_s}}^{(n)}t_{\mathrm{B_s}}} \\ \mathcal{C}_{1,i}^{\mathrm{B_s}\to\mathrm{K}}(t_{\mathrm{B_s}}, t_{\mathrm{K}}) = \displaystyle\sum_{n=0}^{2} \kappa^{(0)}\varphi_1^{(0,n)}\beta_i^{(n)}\,\mathrm{e}^{-E_{\mathrm{K}}^{(0)}t_{\mathrm{K}}}\,\mathrm{e}^{-E_{\mathrm{B_s}}^{(n)}t_{\mathrm{B_s}}} \\ \mathcal{C}_{ij}^{\mathrm{B_s}}(t_{\mathrm{B_s}}) = \displaystyle\sum_{n=0}^{2} \beta_i^{(n)}\beta_j^{(n)}\,\mathrm{e}^{-E_{\mathrm{B_s}}^{(n)}t_{\mathrm{B_s}}} \\ \mathcal{C}^{\mathrm{K}}(t_{\mathrm{K}}) = (\kappa^{(0)})^2\,\mathrm{e}^{-E_{\mathrm{K}}^{(0)}t_{\mathrm{K}}}\,. \end{cases} \tag{6.21}$$

For $i, j = 1, 2, 3$, $N = 3$, as discussed above, this fit has 20 fit parameters: nine $\beta_i^{(n)}$, three $E_{\mathrm{B_s}}^{(n)}$, one $\kappa^{(0)}$, one $E_{\mathrm{K}}^{(0)}$, three $\varphi_0^{(0,n)}$ and three $\varphi_1^{(0,n)}$. Since all of these parameters are non-linear fit parameters, care has to be taken to choose appropriate initial guesses for them in order to obtain a stable and reliable fit. In the last sections, we have discussed how this is done. At this point, let us list again our preparatory steps:

1. Perform the procedure detailed in section 6.1 to obtain $\kappa^{(0)}$, $E_{\mathrm{K}}^{(0)}$ (and $\kappa^{(1)}$, $E_{\mathrm{K}}^{(1)}$).
2. Use GEVP on $\mathcal{C}_{ij}^{\mathrm{B_s}}$ as described in section 6.2 to get $(E_{\mathrm{B_s}}^{(n)})_{\mathrm{GEVP}}$.
3. Use $(E_{\mathrm{B_s}}^{(n)})_{\mathrm{GEVP}}$ to get $(\beta_i^{(n)})_{\mathrm{lin}}^2$ from a linear fit to $\mathcal{C}_{ii}^{\mathrm{B_s}}$, equation (6.13).
4. Use $(E_{\mathrm{B_s}}^{(n)})_{\mathrm{GEVP}}$ and $(\beta_i^{(n)})_{\mathrm{lin}}^2$ as input values to get $(\beta_i^{(n)})_{\text{non-lin}}$ from a non-linear fit to $\mathcal{C}_{ij}^{\mathrm{B_s}}$, as described in section 6.3, equation (6.12).
5. Use $\kappa^{(0)}$, $E_{\mathrm{K}}^{(0)}$, $(E_{\mathrm{B}}^{(n)})_{\mathrm{GEVP}}$ and $(\beta_i^{(n)})_{\text{non-lin}}$ to get $\varphi_\mu^{(0,n)}$ from a linear fit to $\mathcal{C}_{\mu,i}^{\mathrm{B_s}\to\mathrm{K}}$, equation (6.19).

Once we have determined $\kappa^{(n)}$, $E_{\mathrm{K}}^{(n)}$, $\beta_i^{(n)}$, $E_{\mathrm{B_s}}^{(n)}$, $\varphi_\mu^{(0,n)}$ in these individual steps, we use the resulting values as input parameters for our combined fit. In section 6.6, we discuss how we choose appropriate fit ranges for the fit.

6.5 Finite-T effects

In this section, we discuss finite-size effects, that is, effects which are due to our lattice being of finite temporal extent T rather than infinitely large ($T \to \infty$), a limit which so far we have assumed to be possible to take, compare equation (5.11).

To keep notation simple, in this section, we perform our computations in a rather schematic way. In comparison with equation (5.31), for example, we drop $\sum_{\{\vec{x}\}}$, the prefactor, the momentum factor and $\langle . \rangle$. To simplify notation further, in this section, we write $E_{\{\mathrm{K,B_s}\}} \equiv E_{\{\mathrm{K,B_s}\}}^{(0)}$. Consider the three-point correlator of equation (5.4). In its spectral decomposition, analogous to equation (3.34), it is written as[2]

$$\begin{aligned}\mathcal{C}_\mu^{\mathrm{B_s}\to\mathrm{K}} &\sim \mathrm{tr}\left(\mathrm{e}^{-\hat{H}(T-t_f)} P_{\mathrm{su}}(\vec{x}_f) \mathrm{e}^{-\hat{H}(t_f-t_v)} V^\mu(\vec{x}_v) \mathrm{e}^{-\hat{H}(t_v-t_i)} P_{\mathrm{bs}}(\vec{x}_i) \mathrm{e}^{-\hat{H}t_i}\right) \\ &= \sum_{k,n,m} \left\langle k \,\middle|\, P_{\mathrm{su}}(\vec{x}_f) \,\middle|\, n \right\rangle \langle n \,|\, V^\mu(\vec{x}_v) \,|\, m \rangle \langle m \,|\, P_{\mathrm{bs}}(\vec{x}_i) \,|\, k \rangle \times \mathrm{e}^{-E_m(t_v-t_i)}\, \mathrm{e}^{-E_n(t_f-t_v)}\, \mathrm{e}^{-E_k(T-t_f+t_i)} \qquad (6.22) \\ &\approx \mathcal{A}_0^{(knm)} + \mathcal{A}_1^{(k'n'm')}, \qquad (6.23)\end{aligned}$$

where we have inserted $\mathbb{1} = \sum_n \langle n \,|\, n \rangle$ twice and made use of $\mathrm{tr}\, O = \sum_k \langle k \,|\, O \,|\, k \rangle$. Note that each of the three sums over k, n, m runs over an infinite number of states. We here make the assumption that the sums are dominated by only two terms, $\mathcal{A}_0$, $\mathcal{A}_1$, corresponding to some combination of k, n, m. Other excited states $\mathcal{A}_{j>1}$ will also contribute, for example the one similar to figure 6.2, but with a kaon and two pions propagating, but these will be exponentially suppressed and we assume their contributions to be negligible.

[2] Note that for the computation of the three-point correlator, we have to consider a normalisation factor $\mathcal{Z}$, analogous to that of the two-point correlator, discussed in section 3.5, equation (3.35). Since we here discuss the situation where the limit $T \to \infty$ does not apply, in principle, we also have to consider $\mathcal{Z}$ at finite T. These contributions are, however, exponentially suppressed, and thus, we will neglect them.

In the remainder of this section, we consider $\mathcal{A}_0$ and $\mathcal{A}_1$ and discuss the validity of our assumption. Note that since we will not include excited states in our discussion in this section, it is only valid for t_{K}, $t_{\mathrm{B_s}}$ large enough such that the contributions of these are small enough to be negligible.

The dominating case is the one in which we identify k with the vacuum, m with a $\mathrm{B_s}$ meson and n with a kaon, contribution $\mathcal{A}_0$, sketched in figure 6.2. In this case, the

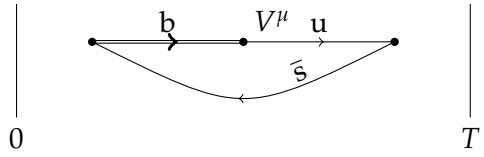

Figure 6.2: Schematic representation of $\mathrm{B_s} \to \mathrm{K}$

exponential factors of equation (6.22) read, coming back to the notation of equations (5.1),

$$\mathrm{e}^{-E_m(t_v-t_i)}\,\mathrm{e}^{-E_n(t_f-t_v)}\,\mathrm{e}^{-E_k(T-t_f+t_i)} = \mathrm{e}^{-E_{\mathrm{B_s}}t_{\mathrm{B_s}}}\,\mathrm{e}^{-E_{\mathrm{K}}t_{\mathrm{K}}}\,\mathrm{e}^{-E_0(T-t_{\mathrm{K}}-t_{\mathrm{B_s}})} \tag{6.24}$$

where E_0 is the energy of the vacuum which we can choose to be 0. Then we have

$$\mathcal{A}_0 = \langle 0 \,|\, P_{\mathrm{su}} \,|\, \mathrm{K}\rangle \,\langle \mathrm{K} \,|\, V^\mu \,|\, \mathrm{B_s}\rangle \,\langle \mathrm{B_s} \,|\, P_{\mathrm{bs}} \,|\, 0\rangle \,\mathrm{e}^{-E_{\mathrm{B_s}}t_{\mathrm{B_s}}}\mathrm{e}^{-E_{\mathrm{K}}t_{\mathrm{K}}}. \tag{6.25}$$

Now let us look at the wrap-around state $\mathcal{A}_1$, depicted in figure 6.3, where, in the language

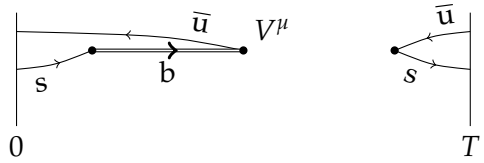

Figure 6.3: Schematic representation of $\mathrm{B_s} \to \mathrm{K}$ with a wrap-around kaon

of equation (6.22), k is a kaon, m is a B^* state and n is the vacuum. This is of course an unwanted finite-T effect. The contribution of the wrap-around case of figure 6.3 to equation (6.23) is

$$\mathcal{A}_1 = \langle \mathrm{K} \,|\, P_{\mathrm{su}} \,|\, 0\rangle \,\langle 0 \,|\, V^\mu \,|\, \mathrm{B}^*\rangle \,\langle \mathrm{B}^* \,|\, P_{\mathrm{bs}} \,|\, \mathrm{K}\rangle \,\mathrm{e}^{-E_{\mathrm{B}^*}t_{\mathrm{B_s}}}\,\mathrm{e}^{-E_{\mathrm{K}}(T-t_{\mathrm{B_s}}-t_{\mathrm{K}})}, \tag{6.26}$$

where E_{B^*} is the energy of a B^* state. Let us note at this point that a contribution of a wrap-around $\mathrm{B_s}$ is not allowed because the $\Theta(t)$ function in the b quark propagator enforces forward $\mathrm{B_s}$ propagation in time, compare equation (4.16). Now we insert equations (6.25)

and (6.26) into equation (6.23):

$$\mathcal{A}_0 + \mathcal{A}_1 = \langle 0 \,|\, P_{\mathrm{su}} \,|\, \mathrm{K} \rangle \, \langle \mathrm{K} \,|\, V^\mu \,|\, \mathrm{B_s} \rangle \, \langle \mathrm{B_s} \,|\, P_{\mathrm{bs}} \,|\, 0 \rangle \, \mathrm{e}^{-E_{\mathrm{B_s}} t_{\mathrm{B_s}}} \, \mathrm{e}^{-E_{\mathrm{K}} t_{\mathrm{K}}} + \\ + \langle \mathrm{K} \,|\, P_{\mathrm{su}} \,|\, 0 \rangle \, \langle 0 \,|\, V^\mu \,|\, \mathrm{B}^* \rangle \, \langle \mathrm{B}^* \,|\, P_{\mathrm{bs}} \,|\, \mathrm{K} \rangle \, \mathrm{e}^{-E_{\mathrm{B}^*} t_{\mathrm{B_s}}} \, \mathrm{e}^{-E_{\mathrm{K}}(T - t_{\mathrm{B_s}} - t_{\mathrm{K}})} \,. \quad (6.27)$$

Let us rewrite equation (6.27) with the notation of equations (6.12), (6.16) and (6.17):

$$\mathcal{C}_{\mu,i}^{\mathrm{B_s}\to\mathrm{K}}(t_{\mathrm{K}}, t_{\mathrm{B_s}}) \approx \mathcal{A}_0 + \mathcal{A}_1 \\ = \kappa^{(0)} \varphi_\mu^{(0,0)} \beta_i^{(0)} \mathrm{e}^{-E_{\mathrm{B_s}} t_{\mathrm{B_s}}} \, \mathrm{e}^{-E_{\mathrm{K}} t_{\mathrm{K}}} + \kappa^{(0)} \xi_{\mu,i} \, \mathrm{e}^{-E_{\mathrm{B}^*} t_{\mathrm{B_s}}} \, \mathrm{e}^{-E_{\mathrm{K}}(T - t_{\mathrm{B_s}} - t_{\mathrm{K}})} \,. \quad (6.28)$$

where

$$\xi_{\mu,i} = \left\langle 0 \,\middle|\, V_\mu \,\middle|\, \mathrm{B}^* \right\rangle \langle \mathrm{B}^* \,|\, P_{\mathrm{hl}} \,|\, \mathrm{K} \rangle \quad (6.29)$$

and E_{B^*} are to be determined.

The idea we get here is rather obvious: Can we extend the fit discussed in section 6.4 such that it includes also the wrapper contribution of equation (6.28)? The answer is yes, but the cost of doing so is that we would introduce (at least) six additional fit parameters $\xi_{\mu,i}$. We note here that at static order, $E_{\mathrm{B}^*} = E_{\mathrm{B_s}}$. Note further that when we write B^*, this does not correspond to a single physical state. Rather, like the $\mathrm{B_s}$, it has a ground and excited states. Including it as a single fit parameter in a fit, we would assume that only its ground state contributes, an assumption that *a priori* is not guaranteed to be valid, so in fact we might have to consider a second B^* state, and thus, a second set of six fit parameters.

As we already pointed out when discussing the fit in section 6.4, numerically, we observe that in t_{K} it is safe to restrict ourselves to considering the ground state only, since there is a long enough plateau region where only the ground state contributes significantly. Including the wrapper contribution of equation (6.28) in the fit would allow us to extend the fit range only in t_{K}, because in $t_{\mathrm{B_s}}$, before the wrapper contribution becomes relevant, we enter the region of large statistical noise. This said, we claim that the extension of the t_{K} range we could gain is not worth the price of introducing additional fit parameters, and thus we remain with the fit as discussed in section 6.4.

Still, one thing we can get from the above discussion and equation (6.28) is to find a suitable $t_{\mathrm{K}}^{\mathrm{max}}$ for our fits by performing a (preparatory) fit as in equation (6.28) and then checking whether the finite-T contribution is small compared to the statistical error of the correlator at that point. To this end, let us rewrite equation (6.28) for fixed $t_{\mathrm{B_s}}$:

$$\mathcal{C}_{\mu,i}^{\mathrm{B_s}\to\mathrm{K}}(t_{\mathrm{K}}) \approx B_{\mu,i} \, \mathrm{e}^{-E_{\mathrm{K}} t_{\mathrm{K}}} + C_{\mu,i} \, \mathrm{e}^{+E_{\mathrm{K}} t_{\mathrm{K}}}, \quad (6.30)$$

with linear fit parameters

$$B_{\mu,i} = \kappa^{(0)} \varphi_\mu^{(0,0)} \beta_i^{(0)} \mathrm{e}^{-E_{\mathrm{B_s}} t_{\mathrm{B_s}}}, \tag{6.31}$$

$$C_{\mu,i} = \kappa^{(0)} \xi_{\mu,i} \, \mathrm{e}^{-E_{\mathrm{B}^*} t_{\mathrm{B_s}}} \, \mathrm{e}^{-E_{\mathrm{K}}(T - t_{\mathrm{B_s}})} \, . \tag{6.32}$$

By fitting $C_{\mu,i}^{\mathrm{B_s}\to\mathrm{K}}$ to equation (6.30) for each $t_{\mathrm{B_s}}$ that we consider, we can now determine the wrapper contribution at each $t_{\mathrm{B_s}}$ and impose

$$\frac{C_{\mu,i}(t_{\mathrm{B_s}}) \, \mathrm{e}^{+E_{\mathrm{K}} t_{\mathrm{K}}}}{B_{\mu,i}(t_{\mathrm{B_s}}) \, \mathrm{e}^{-E_{\mathrm{K}} t_{\mathrm{K}}} + C_{\mu,i}(t_{\mathrm{B_s}}) \, \mathrm{e}^{+E_{\mathrm{K}} t_{\mathrm{K}}}} < c_{\mathrm{fT}} \times \frac{\delta C_{\mu,i}^{\mathrm{B_s}\to\mathrm{K}}(t_{\mathrm{K}}, t_{\mathrm{B_s}})}{C_{\mu,i}^{\mathrm{B_s}\to\mathrm{K}}(t_{\mathrm{K}}, t_{\mathrm{B_s}})}, \tag{6.33}$$

for a given constant c_{fT} which we choose to $c_{\mathrm{fT}} = 1/3$. That is, we demand that the finite-T contributions be small compared to the relative statistical error of the three-point correlator. The last t_{K} where condition (6.33) is satisfied will be our $t_{\mathrm{K}}^{\mathrm{max}}$. Note that for each $t_{\mathrm{B_s}}$ this depends on the smearing level i and on μ, so $t_{\mathrm{K}}^{\mathrm{max}}(t_{\mathrm{B_s}}, i, \mu)$. Now we can either take a different $t_{\mathrm{K}}^{\mathrm{max}}$ for each individual case or take a common $t_{\mathrm{K}}^{\mathrm{max}}$ for all cases.

We choose to take $t_{\mathrm{K}}^{\mathrm{max,\,final}} = \max_\mu(\min_{i,t_{\mathrm{B_s}}}(t_{\mathrm{K}}^{\mathrm{max}}(t_{\mathrm{B_s}}, i, \mu)))$, that is, we assume the same $t_{\mathrm{K}}^{\mathrm{max,\,final}}$ for each smearing level i, $t_{\mathrm{B_s}}$ and μ, while taking the minimum over i and $t_{\mathrm{B_s}}$ here is a conservative choice. There is only a small difference between the values for $\mu = 0$ and $\mu = 1$, so we choose the maximum over μ. We will get back to this question in section 6.6.

For completeness, we note here that from equation (6.31), we obtain

$$\varphi_\mu^{(0,0)} = \frac{B_{\mu,i}}{\kappa^{(0)} \beta_i^{(0)} \mathrm{e}^{-E_{\mathrm{B_s}} t_{\mathrm{B_s}}}}, \tag{6.34}$$

if we provide $\kappa^{(0)}$, $\beta_i^{(0)}$, $E_{\mathrm{B_s}}$ determined independently from the two-point functions as described in sections 6.1, 6.3 and 6.2, respectively. However, for the determination of $\varphi_\mu^{(0,0)}$, we use the fits as described in section 6.4, because they use a larger set of data in a combined fit and do not rely on several independent fits.

The discussion presented here is straightforwardly extended to the situation where we consider the ratio of equation (5.10). We will not use this, but for completeness, we still present the derivation in appendix E.

6.6 Fit ranges

In this section, we address the question of how to determine appropriate fit ranges for the combined fit to two- and three-point functions discussed in section 6.4. We therefore make some assumptions and discuss their implications:

- The two-point light-light correlator gets a fit range $[(t_{\mathrm{K}})_{\mathrm{min}}^{\mathrm{2pt}}, (t_{\mathrm{K}})_{\mathrm{max}}^{\mathrm{2pt}}]$. $(t_{\mathrm{K}})_{\mathrm{min}}^{\mathrm{2pt}}$ is determined as described in section 6.1. We use the symmetrised light-light correlator, so we take $(t_{\mathrm{K}})_{\mathrm{max}}^{\mathrm{2pt}} = T/2$.

- The six two-point correlators $\mathcal{C}_{ij}^{\mathrm{B_s}}(t_{\mathrm{B_s}})$ get the same fit range $[(t_{\mathrm{B_s}})_{\mathrm{min}}^{\mathrm{2pt}}, (t_{\mathrm{B_s}})_{\mathrm{max}}^{\mathrm{2pt}}]$. For a given t_{min}, we determine t_{max} by imposing

$$\delta_{\mathrm{rel}}(t_{\mathrm{max}}) < d \tag{6.35}$$

  with a constant d and the relative error of the correlator

$$\delta_{\mathrm{rel}}(t) = \frac{\delta\mathcal{C}(t)}{\mathcal{C}(t)}. \tag{6.36}$$

  The largest t at which condition (6.35) is satisfied will be t_{max}. For our analysis, we choose $d = 0.1$.

- The six three-point correlators $\mathcal{C}_{\mu,i}^{\mathrm{B_s}\to\mathrm{K}}(t_{\mathrm{K}}, t_{\mathrm{B_s}})$ get the same $t_{\mathrm{B_s}}$ fit range $[(t_{\mathrm{B_s}})_{\mathrm{min}}^{\mathrm{3pt}}, (t_{\mathrm{B_s}})_{\mathrm{max}}^{\mathrm{3pt}}]$, that can, however, be different from that of the two-point heavy-light correlators. This means that we assume that the fit range is the same for $\mu = 0, 1$ and $i = 1, 2, 3$. For a given $(t_{\mathrm{B_s}})_{\mathrm{min}}^{\mathrm{3pt}}$, we determine $(t_{\mathrm{B_s}})_{\mathrm{max}}^{\mathrm{3pt}}$ by imposing condition (6.35), again with $d = 0.1$.

- The six three-point correlators $\mathcal{C}_{\mu,i}^{\mathrm{B_s}\to\mathrm{K}}(t_{\mathrm{K}}, t_{\mathrm{B_s}})$ get the same t_{K} fit range $[(t_{\mathrm{K}})_{\mathrm{min}}^{\mathrm{3pt}}, (t_{\mathrm{K}})_{\mathrm{max}}^{\mathrm{3pt}}]$, that can, however, be different from that of the two-point light-light correlator. This means that we assume that the fit range is the same for $\mu = 0, 1$ and $i = 1, 2, 3$. For a given $(t_{\mathrm{K}})_{\mathrm{min}}^{\mathrm{3pt}}$, we determine $(t_{\mathrm{K}})_{\mathrm{max}}^{\mathrm{3pt}}$ by imposing condition (6.33), that is, imposing that finite-T effects be negligible.

- While in principle, for each $(t_{\mathrm{K}})^{\mathrm{3pt}}$ in the range $[(t_{\mathrm{K}})_{\mathrm{min}}^{\mathrm{3pt}}, (t_{\mathrm{K}})_{\mathrm{max}}^{\mathrm{3pt}}]$, there could be a different $(t_{\mathrm{B_s}})^{\mathrm{3pt}}$ range, we here assume that the $(t_{\mathrm{K}})^{\mathrm{3pt}}$ range is the same for all $(t_{\mathrm{B_s}})^{\mathrm{3pt}}$, and the $(t_{\mathrm{B_s}})^{\mathrm{3pt}}$ range is the same for all $(t_{\mathrm{K}})^{\mathrm{3pt}}$. In other words, we assume a rectangular fit region in the plane spanned by $(t_{\mathrm{K}})^{\mathrm{3pt}}$ and $(t_{\mathrm{B_s}})^{\mathrm{3pt}}$.

Applying these assumptions, we are left with three unknown quantities to be fixed: $(t_{\mathrm{B_s}})_{\mathrm{min}}^{\mathrm{2pt}}$, $(t_{\mathrm{B_s}})_{\mathrm{min}}^{\mathrm{3pt}}$ and $(t_{\mathrm{K}})_{\mathrm{min}}^{\mathrm{3pt}}$. If we choose one or more of these values too small, the model we are fitting to is not correct. For example, since we consider only the kaon ground state everywhere, we need to make sure that $(t_{\mathrm{K}})_{\mathrm{min}}^{\mathrm{3pt}}$ is large enough such that excited kaon states are sufficiently suppressed for that assumption to be valid. If $(t_{\mathrm{K}})_{\mathrm{min}}^{\mathrm{3pt}}$ is too small, this assumption is not valid because excited kaon states do contribute: Our model is not correct. If, on the other hand, we choose one or more of these values too large, our fit parameters are under-constrained, resulting in larger systematic and statistical errors. For example, we have assumed that the first three $\mathrm{B_s}$ states contribute. If we chose $(t_{\mathrm{B_s}})_{\mathrm{min}}^{\mathrm{3pt}}$ too large, we are in a region where the second excited state does no longer contribute significantly. Thus, in the fit, energy and amplitudes of that state cannot be determined reliably. Moreover, by choosing t_{min} too large, we cut away data points that otherwise serve to stabilise and constrain the fit. The fit results will thus have larger statistical errors.

These considerations suggest that we need to find the window for each of the t_{min} where they are neither too small nor too large. Within this region, we expect that the fit results

do not depend on the t_{min} we choose. Therefore, once we choose a set of t_{min} for which we perform our fit, we will also perform the fit varying each t_{min} by one or two time units and then compare the final fit results to determine whether we are in the optimal t_{min} window. If so, neither the fit results nor their errors vary significantly between the fits. Note that this statement should hold most rigorously for ground state quantities. We keep in mind that when we refer to the "second excited state", this is probably not a pure physical state, but rather an effective combination of all higher states that we neglect. Thus, fit results for the second excited state might fluctuate even when the fit range is changed only slightly. The important criterion is that ground state quantities do not fluctuate, since these, ultimately, are of physical interest to us in this thesis. Another issue to point out is that when we are in such a window of t_{min} in which fit results do not depend on the t_{min} we choose, we want to perform a final fit using a t_{min} from the lower end of that window. The reason is that in doing so, we use the most data points that fit our model. Increasing t_{min}, we discard good data points. Hence, when scanning through possible t_{min}, on the lower bound, we restrict ourselves to considering, with respect to the central t_{min} value, $t_{\text{min}} - 1$, while on the upper bound, we expect that $t_{\text{min}} + 2$ still gives a good fit. We show such a scan through the three t_{min} in the appendix in figures F.1 to F.3 for all fit parameters for ensemble N6. Further, in figure F.4, we show a scan through a larger range of $(t_{\text{B}_\text{s}})^{\text{3pt}}_{\text{min}}$ for $\varphi^{(0)}_\mu$, with the other t_{min} held fixed. In figure F.5, we show a scan through the same range of $(t_{\text{B}_\text{s}})^{\text{3pt}}_{\text{min}}$ for $\Delta\varphi^{(0)}_\mu = \varphi^{(0)}_\mu\big((t_{\text{B}_\text{s}})^{\text{3pt}}_{\text{min}} = 13\big) - \varphi^{(0)}_\mu\big((t_{\text{B}_\text{s}})^{\text{3pt}}_{\text{min}}\big)$, that is, we show the variation of $\varphi^{(0)}_\mu$ as a function of $(t_{\text{B}_\text{s}})^{\text{3pt}}_{\text{min}}$ around the values obtained from our central fit at $(t_{\text{B}_\text{s}})^{\text{3pt}}_{\text{min}} = 13$. The final fit ranges for our fits on all ensembles are shown in table 6.2. All fit results for all ensembles, using the central t_{min} values, are also tabulated in table 6.2.

6.7 Discussion of the fit results

In figure 6.4, we show a comparison of the effective energies of the first three states of the heavy-light meson. The points are obtained from the GEVP, equation (6.10). Transparent bands are the result of the combined fit described in the previous sections. The first two energies are modelled rather precisely and GEVP results agree well with the results of the final fit. As discussed above, the second excited state may not be a single, well-defined physical state, but rather some effective combination of higher states. This is reflected by the fact that its energy is determined with low precision. Keeping this in mind, our final fit results agree quite nicely with the GEVP results.

In figures 6.5 and 6.6, we show the fit result for the form factors $\varphi^{(0)}_0$ and $\varphi^{(0)}_1$, respectively, compared to the ratio method of equation (5.11), for ensemble N6 as a function of t_{B_s} at fixed t_{K}. We note here that we are not worried by the slight discrepancies we observe between the points and the fitted curve. Firstly, the fit is to the correlators, while the points are obtained from the ratio multiplied by the exponential factors containing the energies which have been determined independently from the two-point functions, see sections 6.1 and 6.2. Since these energies enter exponentially in equation (5.11), the resulting points of

figures 6.5 and 6.6 are very sensitive to slight changes in these. This motivates us to also consider the alternative ratio method of equation (5.13), where we multiply with amplitudes $\kappa^{(0)}$, $\beta^{(0)}$ instead of exponentials of energies and are thus less sensitive to changes in these. We show such plots in figure F.6. While we see that in these plots, the fitted curve agrees better with the ratio points, these also have a larger statistical uncertainty which predominantly comes from the uncertainty of $\kappa^{(0)}$, see section 6.1. Further, in figure F.7, we show the ratio method of equation (5.11) compared to our fit results, but here, we use the energies that we obtained in the final fit, table 6.2, rather than those determined independently from the two-point functions in our preparatory steps.

Another reason for a possible discrepancy between the ratio points and the fitted curves is that the fit is to a large set of data points while the points of the ratio only represent a very small subset of these data points; in particular, the ratio is shown at fixed t_K and was obtained using a single smearing level only. Thus, these comparison plots should serve only as a guide which allows for a simple way to judge graphically whether our fit is in rough agreement with the ratio.

Looking at the ratio points only, due to the rather slow plateau approach, particularly for $\varphi_1^{(0)}$, it is difficult to judge by eye where the plateau starts and which value to quote. The fit, on the other hand, includes three $\mathrm{B_s}$ states, so we describe not only the ground state, but also the plateau approach, where excited states contribute. This allows for a more robust determination of the ground state form factor, since we have excited state contaminations under control.

Let us make another observation concerning the slow plateau approach of $\varphi_1^{(0)}$. Comparing absolute values of $\varphi_1^{(0)}$ with the excited states $\varphi_1^{(1)}$ and $\varphi_1^{(2)}$ as listed in table 6.2, it stands out that $\varphi_1^{(0)}$ is roughly a factor 2 smaller than $\varphi_1^{(1)}$ and $\varphi_1^{(2)}$. For $\varphi_0^{(0)}$, this is not the case; in fact, it is significantly bigger than its first excited state $\varphi_0^{(1)}$. The fact that the ground state amplitude $\varphi_1^{(0)}$ is suppressed compared to the excited state amplitude $\varphi_1^{(1)}$ explains the slow plateau approach for $\mu = 1$. Reversely, the fact that the excited state amplitude $\varphi_0^{(1)}$ is suppressed compared to $\varphi_0^{(0)}$ explains the good plateau we see for $\mu = 0$.

Let us make a note on signs. Since for a given state n, $\beta^{(n)}, \varphi_\mu^{(n)}$ only enter as products $\beta_i^{(n)}\beta_j^{(n)}$ or $\beta_i^{(n)}\varphi_\mu^{(n)}$ in the two- and three-point functions, respectively, there is an invariance under sign change $\{\beta^{(n)}, \varphi_\mu^{(n)}\} \to \{-\beta^{(n)}, -\varphi_\mu^{(n)}\}$ where the sign corresponds to a phase of a state $|n\rangle$. In table 6.2, we have fixed the phase by the convention that $\beta_1^{(n)} > 0$.

6.8 A foretaste of the future: $O(1/m_\mathrm{h})$ insertions

As we already noted in section 4.5, for the full analysis at order $O(1/m_\mathrm{h})$ eleven matching parameters are needed. These have not yet been computed, so that the analysis we present here is limited to static order of HQET. However, let us look at equation (4.31) for just a

par	A5	F6	F7	N6
$E_{\mathrm{B_s}}^{(0)}$	0.4326(13)	0.3906(14)	0.39007(83)	0.32565(78)
$E_{\mathrm{B_s}}^{(1)}$	0.668(31)	0.586(17)	0.582(17)	0.492(14)
$E_{\mathrm{B_s}}^{(2)}$	0.842(35)	0.727(26)	0.719(21)	0.650(65)
$E_{\mathrm{K}}^{(0)}$	0.2844(14)	0.24913(84)	0.24576(63)	0.18322(78)
$\beta_1^{(0)}$	0.06566(81)	0.04628(58)	0.04603(40)	0.02772(27)
$\beta_1^{(1)}$	0.0641(95)	0.0445(50)	0.0437(46)	0.0331(34)
$\beta_1^{(2)}$	0.058(11)	0.0398(57)	0.0404(52)	0.0279(39)
$\beta_2^{(0)}$	0.02146(24)	0.01131(13)	0.011297(89)	0.005345(48)
$\beta_2^{(1)}$	0.01226(32)	0.00659(42)	0.00653(24)	0.003790(70)
$\beta_2^{(2)} \times 10^3$	0.5(2.6)	0.5(1.2)	0.7(1.1)	0.3(1.1)
$\beta_3^{(0)}$	0.003197(29)	0.0010824(99)	0.0010855(72)	$0.2995(23) \times 10^{-3}$
$\beta_3^{(1)} \times 10^3$	0.82(21)	0.317(51)	0.318(45)	0.102(12)
$\beta_3^{(2)} \times 10^3$	−0.95(17)	−0.356(78)	−0.329(61)	−0.090(37)
$\varphi_0^{(0)}$	1.152(16)	1.137(20)	1.1446(95)	1.139(12)
$\varphi_0^{(1)}$	−0.29(18)	0.00(18)	−0.11(13)	−0.31(17)
$\varphi_0^{(2)}$	0.42(45)	−0.55(35)	−0.31(18)	1.1(3.0)
$\varphi_1^{(0)}$	0.630(17)	0.614(12)	0.628(12)	0.609(11)
$\varphi_1^{(1)}$	−1.23(15)	−1.11(17)	−1.17(11)	−1.23(14)
$\varphi_1^{(2)}$	1.07(72)	0.86(45)	0.93(42)	2.5(3.2)
$\kappa^{(0)}$	0.01003(13)	0.01029(10)	0.010024(74)	0.00939(12)
χ^2/dof	836.9/945	480.4/1664	811.1/1735	1965.1/1619
$(t_{\mathrm{B_s}})^{\mathrm{2pt}}$	[3, 28]	[6, 31]	[6, 33]	[7, 38]
$(t_{\mathrm{K}})^{\mathrm{3pt}}$	[10, 20]	[11, 35]	[11, 36]	[15, 28]
$(t_{\mathrm{B_s}})^{\mathrm{3pt}}$	[7, 18]	[9, 18]	[9, 18]	[13, 29]

Table 6.2: Results of the fits discussed in section 6.4 and the fit ranges used for these fits, obtained as discussed in section 6.6, for different ensembles.

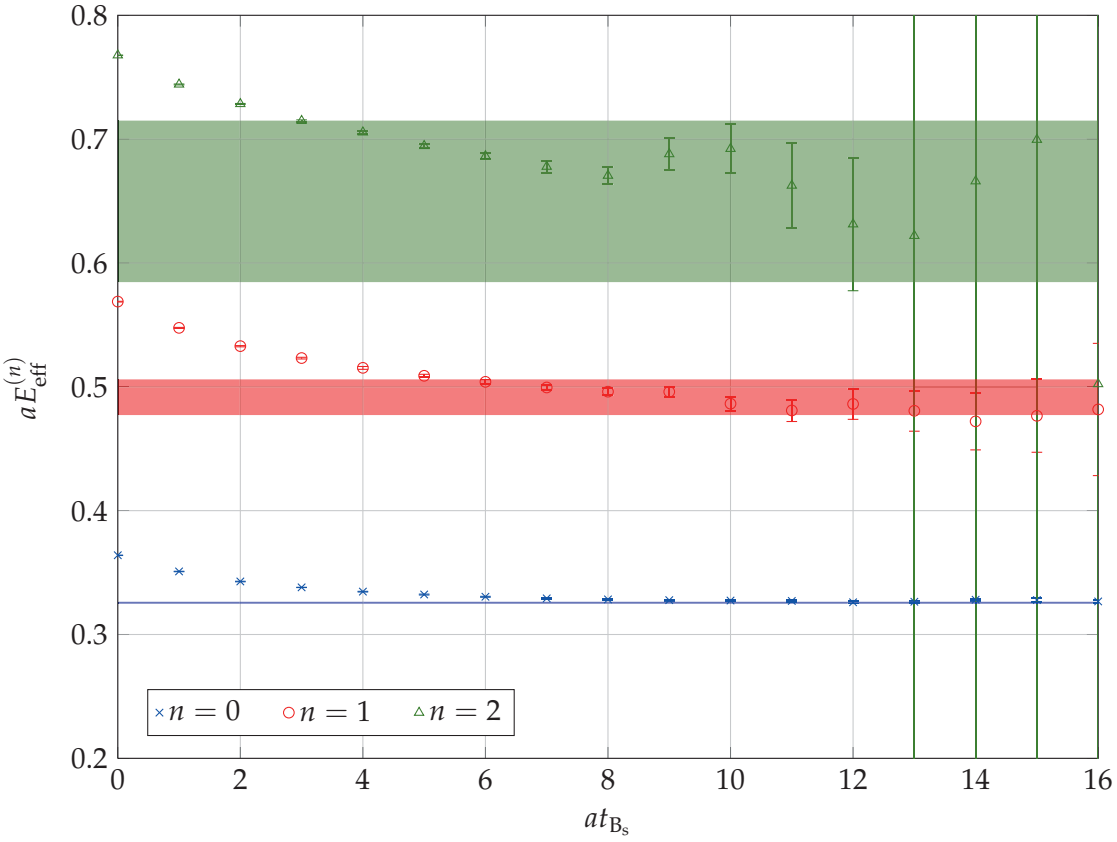

Figure 6.4: Comparison of the effective energies of the first three states of the heavy-light meson from GEVP, equation (6.10) (points), with the results of the final fit as discussed in section 6.4 (bands), for ensemble N6.

little longer and rewrite it here for illustrative purposes:

$$\begin{aligned} R_\mu &\sim Z_{\text{V}}^{\text{HQET}} \frac{\mathcal{C}_\mu^{\text{B}_\text{s}\to\text{K,stat}}}{\sqrt{\mathcal{C}^{\text{B}_\text{s},\text{stat}}\mathcal{C}^{\text{K}}}} \left\{ 1 + \sum_j c_{\text{V}}^{(j)} R_\mu^{\delta(\text{B}_\text{s}\to\text{K}),(j)} + \right. \\ &\quad \left. + \omega_{\text{kin}} R_\mu^{\text{B}_\text{s}\to\text{K,kin}} + \omega_{\text{spin}} R_\mu^{\text{B}_\text{s}\to\text{K,spin}} - \frac{1}{2}\left(\omega_{\text{kin}} R^{\text{B}_\text{s},\text{kin}} + \omega_{\text{spin}} R^{\text{B}_\text{s},\text{spin}}\right) \right\} \\ &= Z_{\text{V}}^{\text{HQET}} \left\{ \frac{\mathcal{C}_\mu^{\text{B}_\text{s}\to\text{K,stat}}}{\sqrt{\mathcal{C}^{\text{B}_\text{s},\text{stat}}\mathcal{C}^{\text{K}}}} + \sum_j c_{\text{V}}^{(j)} \frac{\mathcal{C}_{\mu,j}^{\text{B}_\text{s}\to\text{K},1/m}}{\sqrt{\mathcal{C}^{\text{B}_\text{s},\text{stat}}\mathcal{C}^{\text{K}}}} + \{\text{kin},\text{spin}\} \right\} \\ &\equiv Z_{\text{V}}^{\text{HQET}} \left\{ R_\mu^{\text{stat}} + \sum_j c_{\text{V}}^{(j)} R_{\mu,j}^{1/m} + \{\text{kin},\text{spin}\} \right\}, \end{aligned} \tag{6.37}$$

where we abbreviate the kinetic and spin insertion terms schematically as $\{\text{kin},\text{spin}\}$. In the last sections, we have discussed how to determine the first term of equation (6.37), the ratio at static order, compare also equation (5.10). Now, similar steps of discussion and computation can also be applied to the $O(1/m_{\text{h}})$ current insertions (and the kinetic

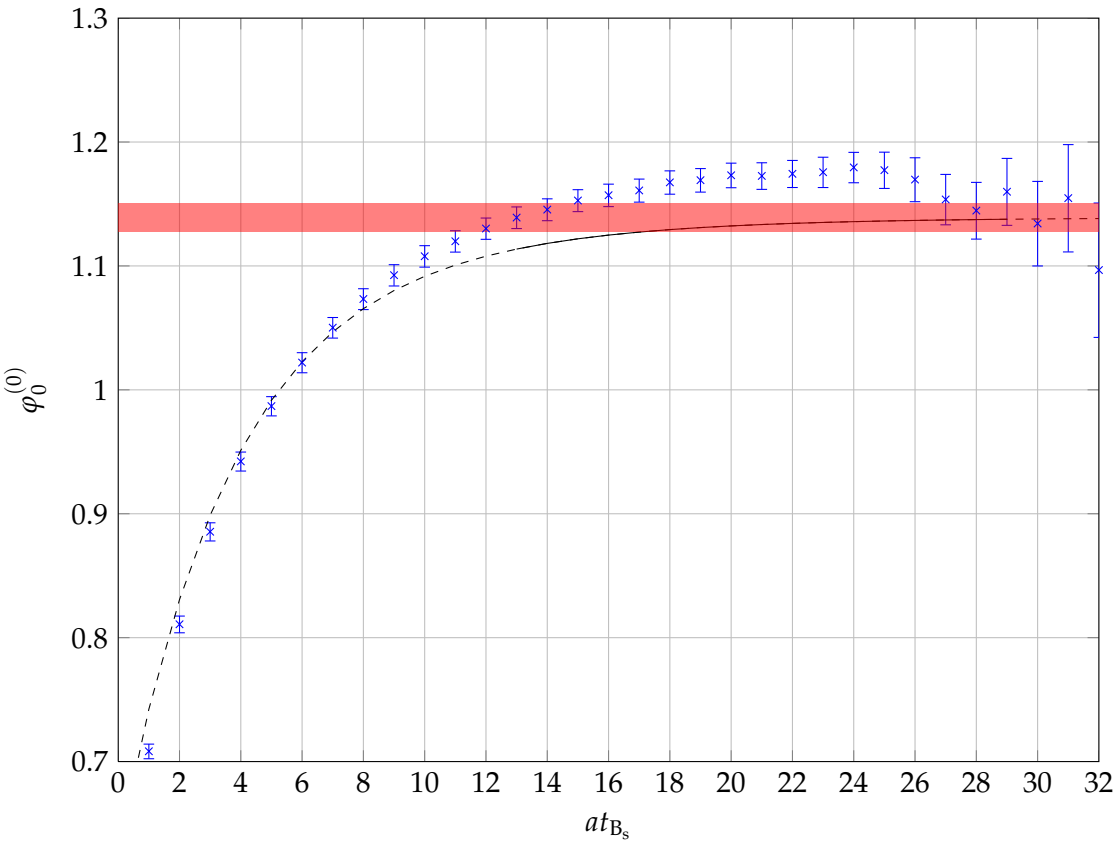

Figure 6.5: Comparison of the right hand side of equation (5.11) (blue points), and the results of the fit as described in section 6.4 shown as a black solid curve in the fit range and extended as a dashed line for illustration, for ensemble N6. The red band is the fit results for $\varphi_0^{(0)}$. On the x axis is $t_{\mathrm{B_s}}$; $t_{\mathrm{K}} = 15$ is fixed. The shown points are constructed from the correlators with the highest smearing level, $i = 3$.

and spin insertions). In particular, in analogy to equation (5.11), when multiplied with $\exp\{E_{\mathrm{K}}^{(0)} t_{\mathrm{K}}/2\} \exp\{E_{\mathrm{B_s}}^{(0)} t_{\mathrm{B_s}}/2\}$, the second term of equation (6.37), for each μ and j, gives a plateau analogous to that of the static case. In figures 6.7 and 6.8, we show such plateau plots for ensemble N6, for $\mu = 0, 1$, $j = 1$. We remark here that plateaux for different combinations of μ and j look qualitatively similar. Since in this section, we only want to illustrate that the $O(1/m_{\mathrm{h}})$ current insertions are well-behaved and actually reach a plateau, we restrict ourselves to showing plots for $j = 1$. The plateaux look promising: there seems to be a region in which the ground state dominates over the excited states and that is not yet noise-dominated, for both $\mu = 0$ and $\mu = 1$. We note that this is particularly interesting compared to the static case, where for $\mu = 1$, we do not see a clear plateau, compare figure 6.6 and the discussion on this in section 6.7.

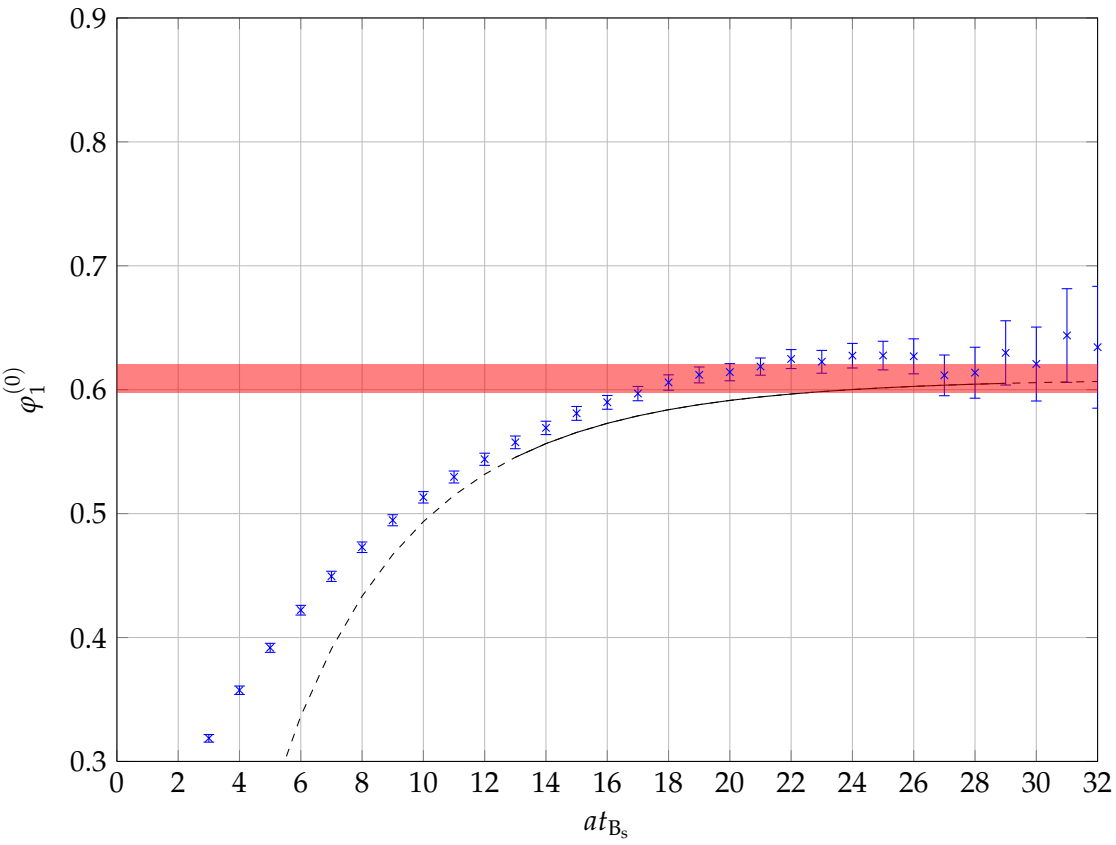

Figure 6.6: Comparison of the right hand side of equation (5.11) (blue points), and the results of the fit as described in section 6.4 shown as a black solid curve in the fit range and extended as a dashed line for illustration, for ensemble N6. The red band is the fit results for $\varphi_1^{(0)}$. On the x axis is $t_{\mathrm{B_s}}$; $t_{\mathrm{K}} = 15$ is fixed. The shown points are constructed from the correlators with the highest smearing level, $i = 3$.

6.9 Error estimation

In this thesis, we follow the error estimation and propagation techniques introduced and elaborated in references [110–112] and concisely summarised in reference [113]. Let us here very briefly recapitulate the main ideas, while for any details we refer to the cited references. We here follow the notation of reference [112].

We want to estimate the error of a function F of observables O_α, $F(\langle O_\alpha \rangle)$. The observables O_α are averaged over an ensemble,

$$\langle O_\alpha \rangle = \sum_q O_\alpha(q) P(q), \tag{6.38}$$

where $P(q)$ is the ensemble distribution defined by $\sum_q M(q' \leftarrow q) P(q) = P(q')$ for a Markov chain $M(q' \leftarrow q)$. In practice, we will consider N Monte Carlo steps, corre-

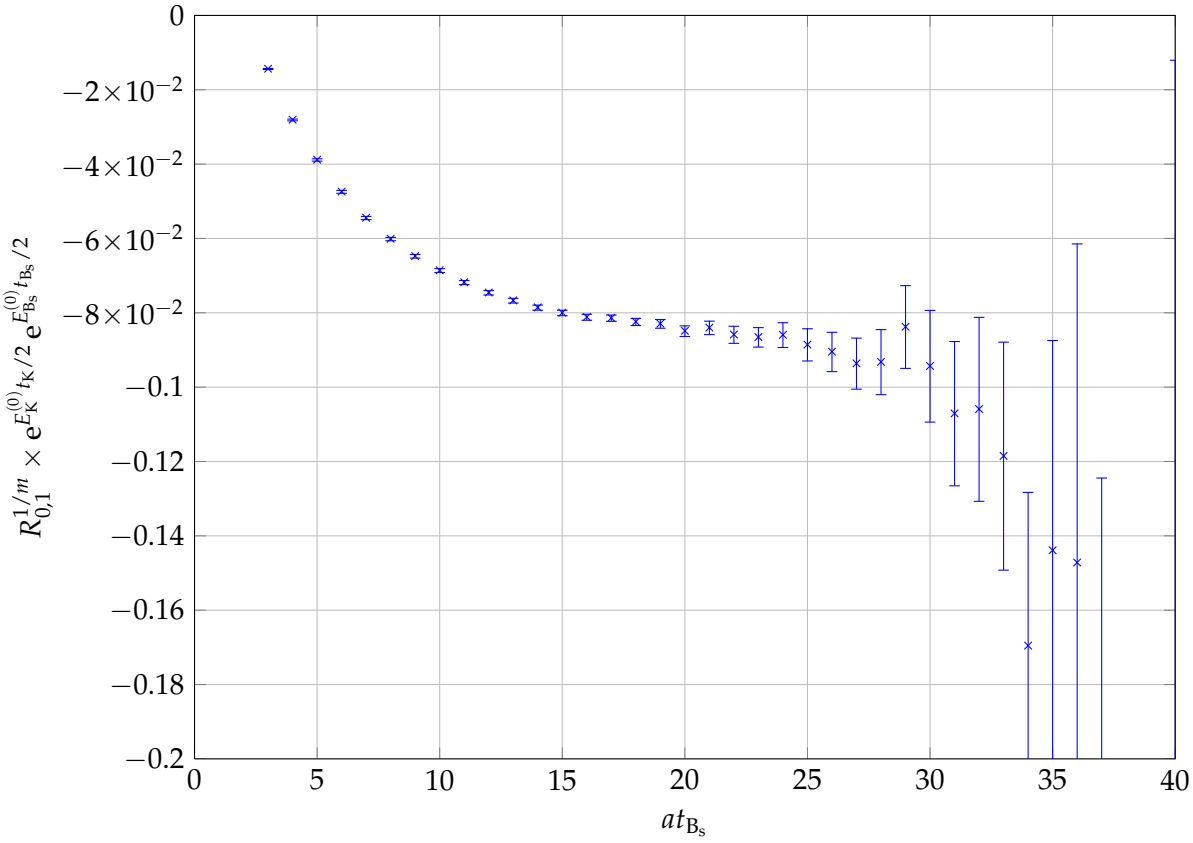

Figure 6.7: $R_{0,1}^{1/m}$ of equation (6.37) multiplied by $e^{E_K^{(0)} t_K/2} e^{E_{B_s}^{(0)} t_{B_s}/2}$ for ensemble N6. On the x axis is t_{B_s}; $t_K = 15$ is fixed. The shown points are constructed from the correlators with the highest smearing level, $i = 3$.

sponding to states $q_1, \ldots, q_N$. We then have

$$\langle O_\alpha \rangle = \overline{O}_\alpha \pm \delta\overline{O}_\alpha, \quad \overline{O}_\alpha = \frac{1}{N}\sum_{i=1}^{N} O_\alpha(q_i). \tag{6.39}$$

The auto-correlation function is defined as [114]

$$\Gamma_{\alpha\beta} = \lim_{K\to\infty} \frac{1}{K}\sum_{i=1}^{K} [O_\alpha(q_{i+t}) - \langle O_\alpha \rangle][O_\beta(q_i) - \langle O_\beta \rangle]. \tag{6.40}$$

Then, for the error of the function F, we have

$$(\delta\overline{F})^2 = \frac{\sigma_F^2}{N} 2\tau_{\text{int}}(F), \tag{6.41}$$

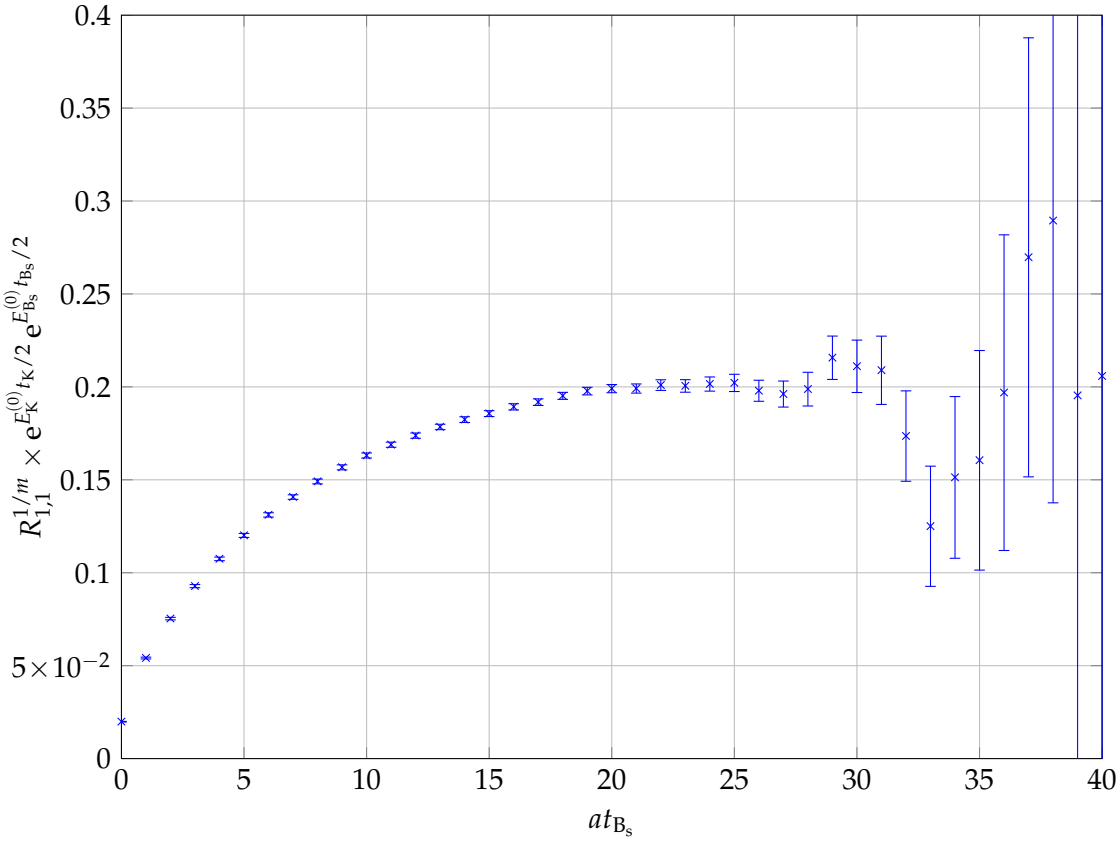

Figure 6.8: $R_{1,1}^{1/m}$ of equation (6.37) multiplied by $\mathrm{e}^{E_{\mathrm{K}}^{(0)} t_{\mathrm{K}}/2}\, \mathrm{e}^{E_{\mathrm{B_s}}^{(0)} t_{\mathrm{B_s}}/2}$ for ensemble N6. On the x axis is $t_{\mathrm{B_s}}$; $t_{\mathrm{K}} = 15$ is fixed. The shown points are constructed from the correlators with the highest smearing level, $i = 3$.

with [110, 114, 115]

$$\sigma_F^2 = \Gamma_F(0), \tag{6.42}$$

$$\tau_{\mathrm{int}}(F) = \frac{1}{2} + \sum_{t=1}^{\infty} \rho_F(t), \tag{6.43}$$

$$\rho_F(t) = \frac{\Gamma_F(t)}{\Gamma_F(0)}, \tag{6.44}$$

$$\Gamma_F(t) = \sum_{\alpha,\beta} F_\alpha \Gamma_{\alpha\beta}(t) F_\beta, \tag{6.45}$$

derived from a Taylor expansion of F in $\langle O_\alpha \rangle$. Here, F_α denotes the derivatives of the function F with respect to the observables $\langle O_\alpha \rangle$,

$$F_\alpha = \frac{\partial F}{\partial \langle O_\alpha \rangle}. \tag{6.46}$$

If they are not given analytically, they can be evaluated numerically:

$$F_i \approx \frac{1}{2h_i}[F(O_1, \ldots, O_i + h_i, \ldots) - f(O_1, \ldots, O_i - h_i, \ldots)], \tag{6.47}$$

where h_i is a step size to be chosen. For any Markov chain [64],

$$|\Gamma_F(t)| \leq \text{const.} \times \mathrm{e}^{-\tau/\tau_{\text{exp}}}, \tag{6.48}$$

where τ_{exp} is the exponential auto-correlation time.

$\tau_{\text{int}}(F)$ is the integrated auto-correlation time. Instead of evaluating the infinite sum in equation (6.43), a suitable window W is chosen along the lines of references [110, 114]. Then,

$$\tau_{\text{int}}(F, W) = \frac{1}{2} + \sum_{t=1}^{W-1} \rho_F(t). \tag{6.49}$$

The authors of references [111, 112] proposed an improvement to the above error estimation by an estimation of τ_{int} that includes attaching a tail, estimating the large-τ behaviour of the auto-correlation function. To this end, they define a window W_{u} where the auto-correlation function is still significant. Then,

$$\tau_{\text{int}}^{\text{u}}(F) = \tau_{\text{int}}(F, W_{\text{u}}) + \tau_{\text{exp}}\rho_F(W_{\text{u}}). \tag{6.50}$$

7 Towards the physical form factor

Now that in the last chapters, we described how to compute the relevant quantities and how to extract them from the raw data, in this chapter, we combine everything to get physical results.

7.1 The physical form factor at static order

Let us start by remembering equation (2.8a). At static order, that is, before we include $O(1/m_\mathrm{h})$ effects, equation (2.8a) houses an ambiguity of whether or not we include $O(1/m_\mathrm{h})$ suppressed terms. In particular, we can write $f_+(q^2)$

1. as $f_+^{(1)} = \dfrac{1}{\sqrt{2m_{\mathrm{B_s}}}} f_\parallel + \dfrac{1}{\sqrt{2m_{\mathrm{B_s}}}}(m_{\mathrm{B_s}} - E_\mathrm{K}) f_\perp$, as in equation (2.8a),
2. as $f_+^{(2)} = \dfrac{1}{\sqrt{2m_{\mathrm{B_s}}}}(m_{\mathrm{B_s}} - E_\mathrm{K}) f_\perp$, neglecting the $f_\parallel$ term,
3. as $f_+^{(3)} = \dfrac{1}{\sqrt{2m_{\mathrm{B_s}}}} m_{\mathrm{B_s}} f_\perp$, neglecting both the $f_\parallel$ and the E_K term.

We note from equation (2.8b) that $f_0(q^2)$ is inherently $O(1/m_\mathrm{h})$ suppressed. After what we discussed in the previous chapter, let us now stick to the notation

$$\left\langle \mathrm{K}(p_\mathrm{K}^\mu) | \hat{V}^\mu | \mathrm{B_s}(p_{\mathrm{B_s}}^\mu) \right\rangle = \varphi_\mu^{(0,0)} \tag{7.1}$$

and rewrite equations (2.9) in terms of it:

$$f_\parallel = \frac{\varphi_0^{(0,0)}}{\sqrt{2m_{\mathrm{B_s}}}}\,, \tag{7.2a}$$

$$f_\perp = \frac{\varphi_k^{(0,0)}}{\sqrt{2m_{\mathrm{B_s}}}\, p_\mathrm{K}^k}\,. \tag{7.2b}$$

We remember the factor $2\sqrt{E_\mathrm{K} m_{\mathrm{B_s}}}$ introduced in section 2.1 and the renormalisation and matching factors of section 4.6. Now we have collected everything and can give the

expression for the physical form factor:

$$\begin{aligned} f_+^{(1)} &= \frac{1}{\sqrt{2m_{\mathrm{B_s}}}}(m_{\mathrm{B_s}} - E_{\mathrm{K}}) \times \frac{\varphi_k^{(0,0)}}{\sqrt{2m_{\mathrm{B_s}}}p_{\mathrm{K}}^k} \times C_{\mathrm{V}} \times Z_{\mathrm{A,RGI}}^{\mathrm{stat}} \times 2\sqrt{E_{\mathrm{K}}m_{\mathrm{B_s}}} \\ &\quad + \frac{1}{\sqrt{2m_{\mathrm{B_s}}}}\frac{\varphi_0^{(0,0)}}{\sqrt{2m_{\mathrm{B_s}}}} \times C_{\mathrm{PS}} \times Z_{\mathrm{A,RGI}}^{\mathrm{stat}} \times Z_{\mathrm{V/A,RGI}}^{\mathrm{stat}} \times 2\sqrt{E_{\mathrm{K}}m_{\mathrm{B_s}}} \\ &= Z_{\mathrm{A,RGI}}^{\mathrm{stat}} \times \sqrt{\frac{E_{\mathrm{K}}}{m_{\mathrm{B_s}}}} \times \left[\frac{(m_{\mathrm{B_s}} - E_{\mathrm{K}})}{p_{\mathrm{K}}^k} \times \varphi_k^{(0,0)} \times C_{\mathrm{V}} + \varphi_0^{(0,0)} \times C_{\mathrm{PS}} \times Z_{\mathrm{V/A,RGI}}^{\mathrm{stat}}\right]. \end{aligned} \tag{7.3}$$

Similarly,

$$f_+^{(2)} = Z_{\mathrm{A,RGI}}^{\mathrm{stat}} \times \sqrt{\frac{E_{\mathrm{K}}}{m_{\mathrm{B_s}}}} \times \left[\frac{(m_{\mathrm{B_s}} - E_{\mathrm{K}})}{p_{\mathrm{K}}^k} \times \varphi_k^{(0,0)} \times C_{\mathrm{V}}\right] \tag{7.4}$$

and

$$f_+^{(3)} = Z_{\mathrm{A,RGI}}^{\mathrm{stat}} \times \sqrt{\frac{E_{\mathrm{K}}}{m_{\mathrm{B_s}}}} \times \left[\frac{m_{\mathrm{B_s}}}{p_{\mathrm{K}}^k} \times \varphi_k^{(0,0)} \times C_{\mathrm{V}}\right]. \tag{7.5}$$

In the next section, we focus our discussion on $f_+^{(1)}$ and $f_+^{(3)}$.

7.2 Continuum extrapolation

We extrapolate both $f_+^{(1)}$ and $f_+^{(3)}$ to the continuum, using the points from ensembles A5, F6 and N6, that have roughly the same pion mass, compare table 5.2. For comparison, we also show the points of ensemble F7, which has a different pion mass. For both $f_+^{(1)}$ and $f_+^{(3)}$, we perform a linear extrapolation in a^2 using the points from ensembles A5, F6 and N6 as well as a constant extrapolation in a^2 using only the points from F6 and N6.[1] The results of the extrapolations are shown in figure 7.1 and tabulated in table 7.1. Since both extrapolations appear reasonable, as our final values, we take that of the linear extrapolations, because they have the larger and thus more conservative error. In figure 7.2, we compare our results with those recently published by HPQCD [31] and RBC/UKQCD [28] collaborations. Note that this figure should only serve as a rough guide, since HPQCD points are at finite lattice spacing $a = 0.09\,\mathrm{fm}$ and unphysical pion mass $m_\pi \approx 320\,\mathrm{MeV}$, approximately the same as those of the ensembles used in this thesis, while RBC/UKQCD points are chiral and continuum extrapolated. The results of this thesis are extrapolated to the continuum but not extrapolated to the physical pion mass.

[1] Note that as shown in table 5.2, the lattice spacings have an uncertainty. For the extrapolations we perform here, however, these enter only on the x axis. Since the functions we consider are rather flat, compare figure 7.1, we can safely neglect these errors here and only take into account the errors of the form factors. Further, uncertainties in a enter in the determination of p_{K}, equation (5.58) and thus of q^2, the x axis of figure 7.2. These effects, however, are small compared to the uncertainties of $f_+(q^2)$, and thus, we can also safely neglect them here.

ens	a^2/fm^2	$f_+^{(1)}$	$f_+^{(3)}$
A5	0.005607	1.970(48)	1.599(46)
F6	0.004247	1.913(37)	1.548(35)
F7	0.004247	1.950(37)	1.584(35)
N6	0.002330	1.861(34)	1.504(32)
const	0	1.885(25)	1.524(23)
lin	0	1.785(68)	1.437(63)

Table 7.1: Results of the form factors $f_+^{(1)}$ and $f_+^{(3)}$ of equations (7.3) and (7.5), respectively, for different ensembles and the corresponding constant and linear continuum extrapolations. All values are plotted in figure 7.1.

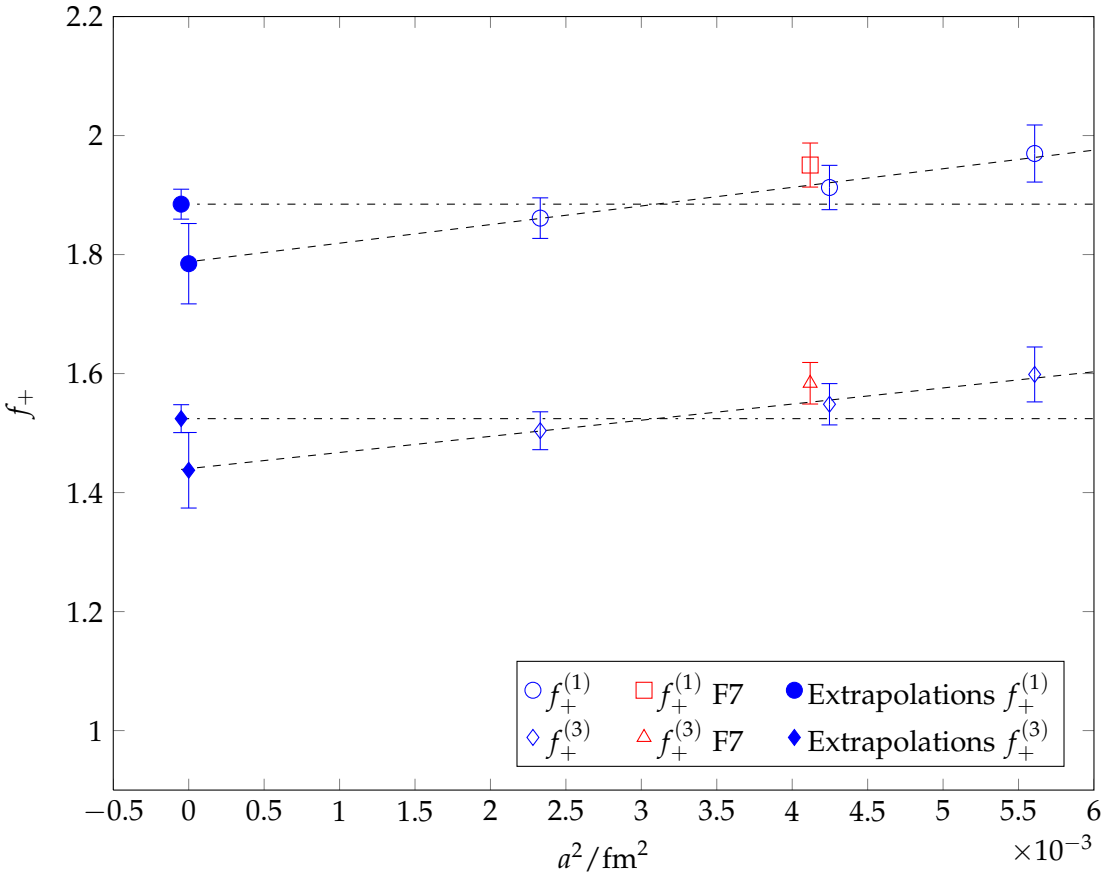

Figure 7.1: Continuum extrapolations. For both $f_+^{(1)}$ and $f_+^{(3)}$, we show a constant (dash-dotted) and linear (dashed) extrapolation in a^2. Ensembles A5, F6, N6 (blue circles and diamonds) enter the linear extrapolations; ensembles F6 and N6 enter the constant extrapolations; ensemble F7 (red square and triangle) does not enter the extrapolations and is shown for comparison only. F7 points are slightly shifted horizontally for better visibility. All values are tabulated in table 7.1.

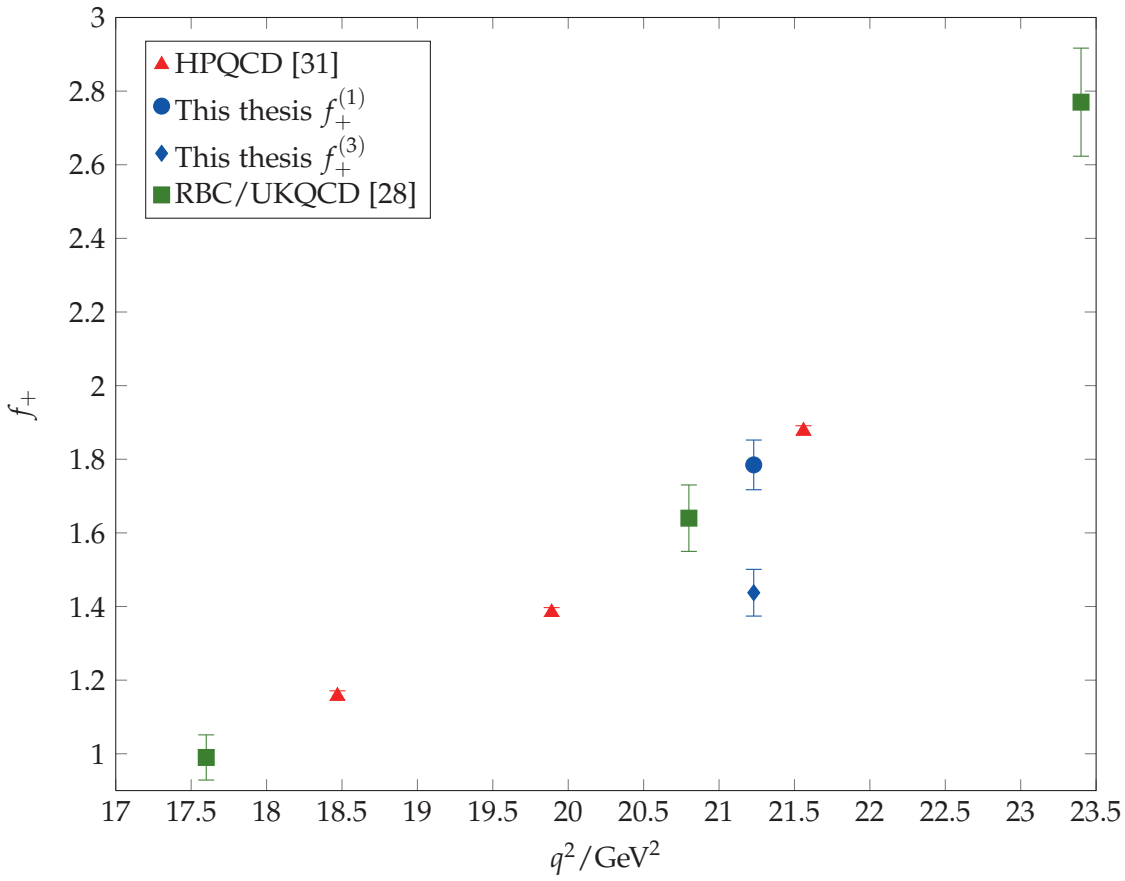

Figure 7.2: Comparison of the form factor $f_+(q^2)$ computed in this thesis with recent results from HPQCD and RBC/UKQCD collaborations. This should only serve as a rough comparison, for note that HPQCD results are at finite lattice spacing and unphysical pion mass, while RBC/UKQCD results are chiral and continuum extrapolated. As the results of this thesis, we show both $f_+^{(1)}$ and $f_+^{(3)}$, extrapolated to the continuum, compare figure 7.1, at unphysical pion mass.

8 Summary and Outlook

In this thesis, we have discussed the computation of the form factors $f_+(q^2)$ and $f_0(q^2)$ for the semileptonic decay $B_s \to K\ell\nu$ in lattice QCD. Simulations were performed on CLS gauge configurations that have $N_f = 2$ dynamical sea quarks. We work at one fixed value of momentum transfer, $q^2 = 21.23\ \text{GeV}^2$. The heavy quark is treated in HQET. We presented the derivation and computation of the form factors at leading (static) order in HQET, while all needed large volume measurements of the $1/m_h$ insertions have also been performed. To tune kaon momenta to the needed value such that it corresponds to the same q^2 on all ensembles, we employ light quark twisting: We impose twisted boundary conditions for the s quark fields, meaning that the quark fields are multiplied by a freely tunable phase factor, the twist parameter. This acts on the quark like a change in momentum which thus becomes freely tunable as well. To keep the B_s meson at rest, we also twist the heavy quark by the same amount such that the effects cancel within the heavy-light meson.

Due to the fact that the results given here are still at static order, there is an ambiguity of whether or not to include terms that are suppressed with $1/m_h$. We discussed two possible choices to compute the form factor within this ambiguity. Once $1/m_h$ effects are included, this ambiguity will disappear. We extrapolated the form factors from the lattice calculations to the continuum. Performing both a constant and a linear extrapolation in the lattice spacing squared, we encountered small discretisation errors. We point out that this is a noteworthy observation, since *a priori* there is no reason to expect this to be the case. Our measurements were done on three ensembles with roughly the same pion mass. Measuring on another ensemble with different pion mass, we do not see any significant change. This indicates that also the chiral extrapolation will be rather flat. We remark that in the strategy we have outlined, we perform successively and separately a continuum extrapolation, a chiral extrapolation and, when eventually combined with experimental data, employing the BCL parameterisation, an extrapolation over the range of q^2.

We have discussed complementary methods to extract the form factors. For the ratio method, we construct a suitable ratio of two- and three-point functions, such that the form factors can be extracted as plateaux values in the limit of large times. The second method we used is to perform combined fits to the data of the two- and three-point correlators that have amplitudes, energies and the form factors as fit parameters. The ratio and the fit results are in reasonable agreement. Our result for the form factor is in rough agreement with recently published results by HPQCD and RBC/UKQCD collaborations.

We gave a brief outlook on the analysis of the $O(1/m_h)$ current insertions and obtained a promising impression.

The next two steps to be done in the project are, firstly, the full inclusion of $O(1/m_{\mathrm{h}})$ effects in the analysis, once the matching coefficients will be available. The large volume measurements have been done as discussed in this thesis. Secondly, a chiral extrapolation needs to be performed, such that the form factors can be quoted at the physical point.

Once future experimental measurements of $\mathrm{B_s} \to \mathrm{K}$ become available, a possibility worth its effort can be to compute the form factor at additional values of the momentum transfer q^2, such that when combined with experiment, the uncertainty from theory is reduced. For the nearer future, however, it may be more interesting to first turn to simulating $\mathrm{B} \to \pi$. Since for this decay, experimental data are already available, this would allow for the determination of $|V_{\mathrm{ub}}|$. For this, all tools devised in the context of this work can readily be used. In fact, the only difference to $\mathrm{B_s} \to \mathrm{K}$ is the mass of the light spectator quark which is an input parameter to the measurement code.

A future step will also be to perform simulations for $\mathrm{B_s} \to \mathrm{K}$, $\mathrm{B} \to \pi$ or both with $N_{\mathrm{f}} = 2 + 1$ dynamical sea quark flavours; such gauge configurations are currently being generated [116].

Appendix

A Notation and conventions

Lorentz indices of spacetime $\mu, \nu, \ldots$ run from 0 to 3, indices $k, l, \ldots$ are spatial indices over directions 1 to 3. Indices $a, b, \ldots$ of symmetry groups run over the extension of that group.

A.1 Dirac matrices

Dirac matrices are used in the chiral basis,

$$\begin{aligned} \gamma_0 &= \begin{pmatrix} 0 & -\mathbb{1} \\ -\mathbb{1} & 0 \end{pmatrix}, \qquad \gamma_1 = \begin{pmatrix} 0 & -\mathrm{i}\sigma_1 \\ \mathrm{i}\sigma_1 & 0 \end{pmatrix}, \qquad \gamma_2 = \begin{pmatrix} 0 & -\mathrm{i}\sigma_2 \\ \mathrm{i}\sigma_2 & 0 \end{pmatrix}, \\ \gamma_3 &= \begin{pmatrix} 0 & -\mathrm{i}\sigma_3 \\ \mathrm{i}\sigma_3 & 0 \end{pmatrix}, \qquad \gamma_5 = \gamma_0\gamma_1\gamma_2\gamma_3 = \begin{pmatrix} \mathbb{1} & 0 \\ 0 & -\mathbb{1} \end{pmatrix}, \end{aligned} \tag{A.1}$$

with Pauli matrices σ_k:

$$\sigma_1 = \begin{pmatrix} 0 & 1 \\ 1 & 0 \end{pmatrix}, \qquad \sigma_2 = \begin{pmatrix} 0 & -\mathrm{i} \\ \mathrm{i} & 0 \end{pmatrix}, \qquad \sigma_3 = \begin{pmatrix} 1 & 0 \\ 0 & -1 \end{pmatrix}. \tag{A.2}$$

Projectors are given as

$$P_+ = \frac{1+\gamma_0}{2}, \quad P_- = \frac{1-\gamma_0}{2}. \tag{A.3}$$

A.2 Lattice derivatives

Ordinary lattice derivatives are defined as

$$\nabla_\mu \psi(x) = \tfrac{1}{a}[\psi(x + a\hat{\mu}) - \psi(x)], \quad \nabla^*_\mu \psi(x) = \tfrac{1}{a}[\psi(x) - \psi(x - a\hat{\mu})]. \tag{A.4}$$

Gauge covariant lattice derivatives are defined as

$$\nabla_\mu \psi(x) = \tfrac{1}{a}[U(x,\mu)\psi(x + a\hat{\mu}) - \psi(x)], \quad \nabla^*_\mu \psi(x) = \tfrac{1}{a}[\psi(x) - U^\dagger(x - a\hat{\mu}, \mu)\psi(x - a\hat{\mu})]. \tag{A.5}$$

In this thesis, we need lattice derivatives that act on quark propagators $S(x, y)$ and that include a phase factor $\vec{\theta}$ as discussed in section 5.1.3. We here give the corresponding

expressions:

$$\nabla_k(\theta)S(x,y) = \tfrac{1}{a}[\mathrm{e}^{\mathrm{i}a\theta_k/L}\,U_k(x)S(x+\hat{k},y) - S(x,y)], \tag{A.6a}$$
$$\nabla_k^*(\theta)S(x,y) = \tfrac{1}{a}[S(x,y) - \mathrm{e}^{-\mathrm{i}a\theta_k/L}\,U^\dagger(x-\hat{k})S(x-\hat{k},y)]. \tag{A.6b}$$

Symmetric lattice derivatives are given as

$$\nabla_k^{\mathrm{S}} = \frac{1}{2}(\nabla_k + \nabla_k^*), \quad \overleftrightarrow{\nabla}_k^{\mathrm{S}} = \frac{1}{2}(\overleftrightarrow{\nabla}_k + \overleftrightarrow{\nabla}_k^*). \tag{A.7}$$

A.3 Lattice Fourier transform

We here follow the conventions of reference [49]. We use the lattice δ-function

$$\delta(x_\mu) = a^{-1}\delta_{x_\mu 0}, \quad \delta(\vec{x}) = \prod_{k=1}^{3}\delta(x_k), \quad \delta(x) = \prod_{\mu=0}^{3}\delta(x_\mu). \tag{A.8}$$

The lattice Fourier transform is given as

$$\tilde{f}(p) = a^4\sum_x \mathrm{e}^{-\mathrm{i}px} f(x), \quad f(x) = \frac{1}{V}\sum_p \mathrm{e}^{\mathrm{i}px}\tilde{f}(p). \tag{A.9}$$

A.4 SU(3)

Vector fields $A_\mu(x)$ have values in the Lie algebra su(3) and can be written as

$$A_\mu(x) = A_\mu^a(x)T^a, \tag{A.10}$$

with T^a the generators of SU(3) that satisfy

$$(T^a)^\dagger = -T^a, \quad \mathrm{tr}(T^aT^b) = -\tfrac{1}{2}\delta^{ab}. \tag{A.11}$$

The field tensor is

$$F_{\mu\nu}^a = \partial_\mu A_\nu^a - \partial_\nu A_\mu^a + g f^{abc}A_\mu^b A_\nu^c, \tag{A.12}$$

with the coupling constant g and the structure constants of QCD f^{abc}.

B Analytic computations

In the free field case, where all gauge links are set to unity, one can compute the correlators introduced in chapter 5 analytically. Then, one can compare the results to the numeric output of the program for the given setup. Thus, the analytic computation provides a valuable tool for checking the correctness of the numeric code. We will work in the free theory with all gauge links set to unity. Thus, we can neglect the gauge field average $\langle . \rangle_{\mathrm{G}}$. First, we discuss explicitly the static cases and then in the following sections we address the $O(1/m_{\mathrm{h}})$ insertions.

Throughout this chapter, for notational simplicity, we set the lattice spacing $a = 1$.

B.1 The static case

First, we discuss explicitly the computation of the static three-point function, defined as in equation (5.4) as

$$\begin{aligned} \mathcal{C}_{\mu}^{\mathrm{B_s}\to\mathrm{K}}(t_{\mathrm{K}}, t_{\mathrm{B_s}}; \vec{p}, \vec{\theta}) &= -\frac{1}{V_3} \sum_{\{\vec{x}\}} \mathrm{e}^{-\mathrm{i}\,\vec{p}\cdot(\vec{x}_f - \vec{x}_v)} \left\langle P_{\mathrm{du}}(x_f) V^{\mu}_{\mathrm{ub}}(x_v) P_{\mathrm{bd}}(x_i) \right\rangle_{\mathrm{F}} \\ &= -\frac{1}{V_3} \sum_{\{\vec{x}\}} \mathrm{e}^{-\mathrm{i}\,\vec{p}\cdot(\vec{x}_f - \vec{x}_v)} \left\langle \overline{\psi}_{\mathrm{s}}(x_f)\gamma_5\psi_{\mathrm{u}}(x_f)\overline{\psi}_{\mathrm{u}}(x_v)\gamma_{\mu}\psi_{\mathrm{b}}(x_v)\overline{\psi}_{\mathrm{b}}(x_i)\gamma_5\psi_{\mathrm{s}}(x_i) \right\rangle_{\mathrm{F}}, \end{aligned} \tag{B.1}$$

where $\{\vec{x}\} = \vec{x}_f, \vec{x}_v, \vec{x}_i$. Now we perform Wick contractions, noting that with all gauge links unity,

$$S(x, y) = S(x - y). \tag{B.2}$$

In the next step we Fourier transform the propagators to the time-momentum representation, inserting the definition of the HQET heavy quark propagator of equation (4.16) setting $m_{\mathrm{h}} = 0$, to obtain

$$\begin{aligned} &\mathcal{C}_{\mu}^{\mathrm{B_s}\to\mathrm{K}}(t_{\mathrm{K}}, t_{\mathrm{B_s}}; \vec{p}, \vec{\theta}) = \\ &= +\frac{1}{V_3} \sum_{\{\vec{x}\}} \mathrm{e}^{-\mathrm{i}\,\vec{p}\cdot(\vec{x}_f - \vec{x}_v)} \operatorname{tr}\left\{\gamma_5 S_{\mathrm{u}}(x_f - x_v)\gamma_{\mu} S_{\mathrm{b}}(x_v - x_i)\gamma_5 S_{\mathrm{s}}(x_i - x_f)\right\} \\ &= \frac{1}{(V_3)^3}\Theta(t_v - t_i)\delta(\vec{x}_v - \vec{x}_i) \sum_{\{\vec{x}\}} \sum_{\vec{k}_{\mathrm{s}}, \vec{k}_{\mathrm{u}}} \mathrm{e}^{-\mathrm{i}\,\vec{p}\cdot(\vec{x}_f - \vec{x}_v)}\, \mathrm{e}^{\mathrm{i}\,\vec{k}_{\mathrm{s}}\cdot(\vec{x}_i - \vec{x}_f)}\, \mathrm{e}^{\mathrm{i}\,\vec{k}_{\mathrm{u}}\cdot(\vec{x}_f - \vec{x}_v)} \times \\ &\times \operatorname{tr}\left\{\gamma_5 \tilde{S}_{\mathrm{u}}(t_f - t_v; \vec{k}_{\mathrm{u}})\gamma_{\mu}\left(\tfrac{1+\gamma_0}{2}\right)\gamma_5 \tilde{S}_{\mathrm{s}}(t_i - t_f; \vec{k}_{\mathrm{s}} + \vec{\theta})\right\}. \end{aligned} \tag{B.3}$$

Next, we evaluate the delta function and reorder the exponentials:

$$\begin{aligned}
&\mathcal{C}_{\mu}^{\mathrm{B_s}\to\mathrm{K}}(t_{\mathrm{K}}, t_{\mathrm{B_s}}; \vec{p}, \vec{\theta}) = \\
&= \frac{1}{(V_3)^3}\Theta(t_v - t_i) \sum_{\vec{x}_f, \vec{x}_v} \sum_{\vec{k}_{\mathrm{s}}, \vec{k}_{\mathrm{u}}} \mathrm{e}^{\mathrm{i}\,\vec{x}_f\cdot(-\vec{p}-\vec{k}_{\mathrm{s}}+\vec{k}_{\mathrm{u}})}\, \mathrm{e}^{\mathrm{i}\,\vec{x}_v\cdot(\vec{p}-\vec{k}_{\mathrm{u}}+\vec{k}_{\mathrm{s}})} \times \\
&\times \mathrm{tr}\left\{\gamma_5 \tilde{S}_{\mathrm{u}}(t_f - t_v; \vec{k}_{\mathrm{u}})\gamma_\mu \left(\tfrac{1+\gamma_0}{2}\right) \gamma_5 \tilde{S}_{\mathrm{s}}(t_i - t_f; \vec{k}_{\mathrm{s}} + \vec{\theta})\right\} \\
&= \frac{1}{(V_3)^3}\Theta(t_v - t_i) \sum_{\vec{k}_{\mathrm{s}}, \vec{k}_{\mathrm{u}}} \delta(-\vec{p} - \vec{k}_{\mathrm{s}} + \vec{k}_{\mathrm{u}})\, \mathrm{e}^{\mathrm{i}\,\vec{x}_v\cdot(\vec{p}-\vec{k}_{\mathrm{u}}+\vec{k}_{\mathrm{s}})} \times \\
&\times \mathrm{tr}\left\{\gamma_5 \tilde{S}_{\mathrm{u}}(t_f - t_v; \vec{k}_{\mathrm{u}})\gamma_\mu \left(\tfrac{1+\gamma_0}{2}\right) \gamma_5 \tilde{S}_{\mathrm{s}}(t_i - t_f; \vec{k}_{\mathrm{s}} + \vec{\theta})\right\}. \qquad \text{(B.4)}
\end{aligned}$$

We evaluate the delta function, $\vec{k}_{\mathrm{u}} = \vec{p} + \vec{k}_{\mathrm{s}}$, adopt the notation of equations (5.1) and change notation $\vec{k}_{\mathrm{s}} \to \vec{j}$:

$$\begin{aligned}
&\mathcal{C}_{\mu}^{\mathrm{B_s}\to\mathrm{K}}(t_{\mathrm{K}}, t_{\mathrm{B_s}}; \vec{p}, \vec{\theta}) = \\
&= \frac{1}{(V_3)^2}\Theta(t_{\mathrm{B_s}}) \sum_{\vec{j}} \mathrm{tr}\left\{\gamma_5 \tilde{S}_{\mathrm{u}}(t_{\mathrm{K}}; \vec{p} + \vec{j})\gamma_\mu \left(\tfrac{1+\gamma_0}{2}\right) \gamma_5 \tilde{S}_{\mathrm{s}}(-(t_{\mathrm{B_s}} + t_{\mathrm{K}}); \vec{\theta} + \vec{j})\right\}. \qquad \text{(B.5)}
\end{aligned}$$

For the two-point light-light function, a very similar computation leads to:

$$\mathcal{C}^{\mathrm{K}}(t_{\mathrm{K}}; \vec{p}, \vec{\theta}) = \frac{1}{(V_3)^2} \sum_{\vec{j}} \mathrm{tr}\left\{\gamma_5 \tilde{S}_{\mathrm{u}}(t; \vec{p} + \vec{j})\gamma_5 \tilde{S}_{\mathrm{s}}(-t; \vec{\theta} + \vec{j})\right\}. \qquad \text{(B.6)}$$

Finally, for the heavy-light two-point function, the computation is just as in equation (B.6), except that we insert the heavy propagator S_{h} instead of the light propagator S_{u}. We have

$$\mathcal{C}^{\mathrm{B_s}}(t_{\mathrm{B_s}}; \vec{\theta}) = \frac{1}{(V_3)^2} \sum_{\vec{j}} \Theta(t)\, \mathrm{tr}\left\{\gamma_5 \left(\tfrac{1+\gamma_0}{2}\right) \gamma_5 \tilde{S}_{\mathrm{s}}(-t; \vec{\theta} + \vec{j})\right\}. \qquad \text{(B.7)}$$

The Wilson light quark propagator is given by

$$S(x) = \frac{1}{L^3 T} \sum_{p} \frac{\mathrm{e}^{\mathrm{i}\,px}}{\mathrm{i}\,\gamma_\mu \tilde{p}_\mu + m + \frac{1}{2}\hat{p}_\mu^2}, \qquad \text{(B.8)}$$

where

$$\tilde{p}_\mu = \sin p_\mu, \qquad \text{(B.9a)}$$

$$\hat{p}_\mu^2 = 2\sum_{\mu}(1 - \cos(p_\mu)). \qquad \text{(B.9b)}$$

Fourier transforming, we get

$$\tilde{S}(t;\vec{q}) = \frac{1}{L^3T}\sum_{q_0}\frac{\mathrm{e}^{\mathrm{i}\,q_0 t}\left(-\mathrm{i}\,\gamma_k\tilde{q}_k - \mathrm{i}\,\gamma_0\tilde{q}_0 + m + \frac{1}{2}\hat{q}_k^2 + \frac{1}{2}\hat{q}_0^2\right)}{\left(-\mathrm{i}\,\gamma_k\tilde{q}_k - \mathrm{i}\,\gamma_0\tilde{q}_0 + m + \frac{1}{2}\hat{q}_k^2 + \frac{1}{2}\hat{q}_0^2\right)}\times \\ \times\frac{1}{\left(\mathrm{i}\,\gamma_k\tilde{q}_k + \mathrm{i}\,\gamma_0\tilde{q}_0 + m + \frac{1}{2}\hat{q}_k^2 + \frac{1}{2}\hat{q}_0^2\right)} \\ \equiv \frac{1}{L^3T}\sum_{q_0}\frac{\mathrm{e}^{\mathrm{i}\,q_0 t}\,N(q)}{D(q)}, \quad \text{(B.10)}$$

with

$$N(q) = \left(-\mathrm{i}\,\gamma_k\tilde{q}_k - \mathrm{i}\,\gamma_0\tilde{q}_0 + m + \tfrac{1}{2}\hat{q}_k^2 + \tfrac{1}{2}\hat{q}_0^2\right), \quad \text{(B.11)}$$

$$D(q) = \left(-\mathrm{i}\,\gamma_k\tilde{q}_k - \mathrm{i}\,\gamma_0\tilde{q}_0 + m + \tfrac{1}{2}\hat{q}_k^2 + \tfrac{1}{2}\hat{q}_0^2\right)\left(\mathrm{i}\,\gamma_k\tilde{q}_k + \mathrm{i}\,\gamma_0\tilde{q}_0 + m + \tfrac{1}{2}\hat{q}_k^2 + \tfrac{1}{2}\hat{q}_0^2\right) \\ = \left(m + \tfrac{1}{2}\hat{q}_k^2 + \tfrac{1}{2}\hat{q}_0^2\right)^2 + \left(\tilde{q}_k^2 + \tilde{q}_0^2\right) \\ \equiv B^2(q) + Q(q), \quad \text{(B.12)}$$

with

$$B(q) = m + \tfrac{1}{2}\hat{q}_k^2 + \tfrac{1}{2}\hat{q}_0^2, \quad \text{(B.13)}$$

$$Q(q) = \tilde{q}_k^2 + \tilde{q}_0^2. \quad \text{(B.14)}$$

For periodic fermion boundary conditions, the sum over q_0 goes over $2\pi/L(0,\ldots,T-1)$, while for anti-periodic boundary conditions, it goes over $2\pi/L(-T/2+1,\ldots,T/2)$. Now, inserting equation (B.10) into equation (B.5), we have

$$\mathcal{C}_\mu^{\mathrm{B_s}\to\mathrm{K}}(t_\mathrm{K}, t_{\mathrm{B_s}};\vec{p},\vec{\theta}) = \frac{1}{(L^3T)^2}\sum_{\vec{j}}\sum_{q_{0,1},q_{0,2}}\mathrm{tr}\left\{\frac{\mathrm{e}^{-\mathrm{i}(t_{\mathrm{B_s}}+t_\mathrm{K})q_{0,1}}\,\mathrm{e}^{\mathrm{i}\,t_\mathrm{K}q_{0,2}}}{D(q_1)D(q_2)}\times \right. \\ \left. \times\left[\gamma_5 N(q_1)\gamma_5 N(q_2)\gamma_\mu\left(\tfrac{1+\gamma_0}{2}\right)\right]\right\}. \quad \text{(B.15)}$$

For the light-light and heavy-light two-point functions we perform similar computations. Here, however, we only present the results:

$$\mathcal{C}^\mathrm{K}(t_\mathrm{K};\vec{p},\vec{\theta}) = \frac{1}{(L^3T)^2}\sum_{\vec{j}}\sum_{q_{0,1},q_{0,2}}\frac{\mathrm{e}^{\mathrm{i}\,q_{0,2}t_\mathrm{K}}\,\mathrm{e}^{-\mathrm{i}\,q_{0,1}t_\mathrm{K}}}{D(q_2)D(q_1)}\,\mathrm{tr}\left\{\gamma_5 N(q_2)\gamma_5 N(q_1)\right\}; \quad \text{(B.16)}$$

$$\mathcal{C}^{\mathrm{B_s}}(t_{\mathrm{B_s}};\vec{\theta}) = \frac{1}{(L^3T)^2}\sum_{\vec{j}}\sum_{q_{0,1}}\frac{\mathrm{e}^{-\mathrm{i}\,q_{0,1}t_{\mathrm{B_s}}}}{D(q_1)}\,\mathrm{tr}\left\{\gamma_5\left(\tfrac{1+\gamma_0}{2}\right)\gamma_5 N(q_1)\right\}. \quad \text{(B.17)}$$

Equations (B.15), (B.16) and (B.17) have been implemented in the Matlab routine `analytic.m` located in `~/main/tools/`.

B.2 $O(1/m_\mathrm{h})$ insertions

Now we turn to the analytic computation of the $O(1/m_\mathrm{h})$ current insertions. The kernels that have to be inserted in the vertex in equation (B.3) are given in table 4.1, that is, we need to compute

$$\begin{aligned}
&\mathcal{C}_{\mu,j}^{\mathrm{B_s}\to\mathrm{K},1/m}(t_\mathrm{K}, t_{\mathrm{B_s}}; \vec{p}, \vec{\theta}) = \\
&= \frac{1}{(V_3)^3}\Theta(t_v - t_i)\delta(\vec{x}_v - \vec{x}_i)\sum_{\{\vec{x}\}}\sum_{\vec{k}_\mathrm{s},\vec{k}_\mathrm{u}} \mathrm{e}^{-\mathrm{i}\,\vec{p}\cdot(\vec{x}_f-\vec{x}_v)}\,\mathrm{e}^{\mathrm{i}\,\vec{k}_\mathrm{s}\cdot(\vec{x}_i-\vec{x}_f)}\,\mathrm{e}^{\mathrm{i}\,\vec{k}_\mathrm{u}\cdot(\vec{x}_f-\vec{x}_v)} \times \\
&\times \mathrm{tr}\left\{\gamma_5\tilde{S}_\mathrm{u}(t_f - t_v; \vec{k}_\mathrm{u})K_{\mu j}\left(\tfrac{1+\gamma_0}{2}\right)\gamma_5\tilde{S}_\mathrm{s}(t_i - t_f; \vec{k}_\mathrm{s} + \vec{\theta})\right\}. \qquad \text{(B.18)}
\end{aligned}$$

We start by noting that

$$\partial_k^\mathrm{S}\,\mathrm{e}^{\mathrm{i}\,\vec{p}\cdot\vec{x}} = \mathrm{i}\sin(p_k)\,\mathrm{e}^{\mathrm{i}\,\vec{p}\cdot\vec{x}} \qquad \text{(B.19)}$$

and that integration by parts on the lattice is given by

$$\sum_x g(x)\partial_k^\mathrm{S} f(x) = -\sum_x g(x)\overleftarrow{\partial}_k^\mathrm{S} f(x). \qquad \text{(B.20)}$$

We evaluate equation (B.18) schematically by writing all factors that contain $\vec{x}_v$, on which the derivatives act, explicitly, while we suppress all other factors and dependencies. We have

$$\begin{aligned}
&\sum_{\vec{x}_v}\mathrm{e}^{-\mathrm{i}\,\vec{p}\cdot(\vec{x}_f-\vec{x}_v)}\left[g\,\mathrm{e}^{\mathrm{i}\,\vec{k}_\mathrm{u}\cdot(\vec{x}_f-\vec{x}_v)}\frac{1}{2}\left\{\partial_k^\mathrm{S} \pm \overleftarrow{\partial}_k^\mathrm{S}\right\}\Gamma_{jl}^\mu f(\vec{x}_v)\right] \\
&= \pm\frac{1}{2}\sum_{\vec{x}_v}\mathrm{e}^{-\mathrm{i}\,\vec{p}\cdot(\vec{x}_f-\vec{x}_v)}\left[g\,\mathrm{e}^{\mathrm{i}\,\vec{k}_\mathrm{u}\cdot(\vec{x}_f-\vec{x}_v)}\overleftarrow{\partial}_k^\mathrm{S}\Gamma_{jl}^\mu f(\vec{x}_v)\right] \\
&\quad + \frac{1}{2}\left[-\sum_{\vec{x}_v}\mathrm{e}^{-\mathrm{i}\,\vec{p}\cdot(\vec{x}_f-\vec{x}_v)}\,g\,\mathrm{e}^{\mathrm{i}\,\vec{k}_\mathrm{u}\cdot(\vec{x}_f-\vec{x}_v)}\overleftarrow{\partial}_k^\mathrm{S}\Gamma_{jl}^\mu\right] f(\vec{x}_v) \\
&= \pm\frac{1}{2}\sum_{\vec{x}_v}\mathrm{e}^{-\mathrm{i}\,\vec{p}\cdot(\vec{x}_f-\vec{x}_v)}\,\mathrm{e}^{\mathrm{i}\,\vec{k}_\mathrm{u}\cdot(\vec{x}_f-\vec{x}_v)}\,\mathrm{i}\sin(-k_{\mathrm{u}k})g\Gamma_{jl}^\mu f(\vec{x}_v) \\
&\quad - \frac{1}{2}\sum_{\vec{x}_v}\mathrm{e}^{-\mathrm{i}\,\vec{p}\cdot(\vec{x}_f-\vec{x}_v)}\,\mathrm{e}^{\mathrm{i}\,\vec{k}_\mathrm{u}\cdot(\vec{x}_f-\vec{x}_v)}\,\mathrm{i}\sin(p_k - k_{\mathrm{u}k})g\Gamma_{jl}^\mu f(\vec{x}_v) \\
&= \frac{1}{2}\sum_{\vec{x}_v}\mathrm{e}^{-\mathrm{i}\,\vec{p}\cdot(\vec{x}_f-\vec{x}_v)}\,\mathrm{e}^{\mathrm{i}\,\vec{k}_\mathrm{u}\cdot(\vec{x}_f-\vec{x}_v)}\,g\Gamma_{jl}^\mu f(\vec{x}_v)\,\mathrm{i}\left[\sin(j_k) \mp \sin(p_k + j_k)\right]. \qquad \text{(B.21)}
\end{aligned}$$

We tabulate the explicit results for all currents in table B.1. The analytic expressions for the current insertions are then obtained by substituting the corresponding eigenvalue listed in table B.1 for a kernel $K_{\mu j}$ in equation (B.18).

Now, let us turn to the $O(1/m_\mathrm{h})$ Lagrangian insertions. If all gauge links are unity, the spin insertions of equation (4.9) vanish, because $\widehat{F}_{kj}$ of equation (3.13) vanishes. We can,

V_μ^{HQET}	$K_{\mu j}$	EV
V_0^{stat}	γ_0	γ_0
$V_{0,1}$	$\sum_l \gamma_l (1/2)(\nabla_l^{\text{S}} - \overleftarrow{\nabla}_l^{\text{S}})$	$\sum_l \frac{1}{2}\,\mathrm{i}\,[\sin(j_l) + \sin(p_l + j_l)]\,\gamma_l$
$V_{0,2}$	$\sum_l \gamma_l (1/2)(\nabla_l^{\text{S}} + \overleftarrow{\nabla}_l^{\text{S}})$	$\sum_l \frac{1}{2}\,\mathrm{i}\,[\sin(j_l) - \sin(p_l + j_l)]\,\gamma_l$
V_k^{stat}	γ_k	γ_k
$V_{k,1}$	$\sum_l (1/2)(\nabla_l^{\text{S}} - \overleftarrow{\nabla}_l^{\text{S}})\gamma_l\gamma_k$	$\sum_l \frac{1}{2}\,\mathrm{i}\,[\sin(j_l) + \sin(p_l + j_l)]\,\gamma_l\gamma_k$
$V_{k,2}$	$(1/2)(\nabla_k^{\text{S}} - \overleftarrow{\nabla}_k^{\text{S}})$	$\frac{1}{2}\,\mathrm{i}\,[\sin(j_k) + \sin(p_k + j_k)]$
$V_{k,3}$	$\sum_l (1/2)(\nabla_l^{\text{S}} + \overleftarrow{\nabla}_l^{\text{S}})\gamma_l\gamma_k$	$\sum_l \frac{1}{2}\,\mathrm{i}\,[\sin(j_l) - \sin(p_l + j_l)]\,\gamma_l\gamma_k$
$V_{k,4}$	$(1/2)(\nabla_k^{\text{S}} + \overleftarrow{\nabla}_k^{\text{S}})$	$\frac{1}{2}\,\mathrm{i}\,[\sin(j_k) - \sin(p_k + j_k)]$

Table B.1: Overview of $K_{\mu j}$ for V_μ and their eigenvalues.

however, compute the kinetic insertions. Then, equation (5.36) becomes

$$\mathcal{C}_\mu^{\text{B}_\text{s}\to\text{K,kin}}(t_\text{K}, t_{\text{B}_\text{s}}; \vec{p}, \vec{\theta}) = \frac{1}{V_3} \sum_{\{\vec{x}\},z,l} \mathrm{e}^{-\mathrm{i}\,\vec{p}\cdot(\vec{x}_f - \vec{x}_v)}\,\mathrm{tr}\Big\{\gamma_5 S_\text{u}(x_f - x_v)\gamma_\mu S_\text{b}(x_v - z)\times \Big[U_l(z)S_\text{b}(z + \hat{l} - x_i) + U_l^\dagger(z - \hat{l})S_\text{b}(z - \hat{l} - x_i) - 2S_\text{b}(z - x_i)\Big]\gamma_5 S_\text{s}(x_i - x_f)\Big\}. \quad \text{(B.22)}$$

Now let us focus on the product of the up, the heavy and the first heavy propagator in the square brackets. Since we are summing over all $\vec{z}$ and $\vec{x}$, we can shift the summation variables:

$$\begin{aligned}
&\sum_{\vec{x}_v,\vec{z}} S_\text{u}(x_f - x_v)S_\text{b}(x_v - z)U_l(z)S_\text{b}(z + \hat{l} - x_i)\,\mathrm{e}^{\mathrm{i}\,\vec{p}\cdot\vec{x}_v} \\
&\overset{z\to z-\hat{l}}{=} \sum_{\vec{x}_v,\vec{z}} S_\text{u}(x_f - x_v)S_\text{b}(x_v - (z - \hat{l}))U_l(z - \hat{l})S_\text{b}(z - x_i)\,\mathrm{e}^{\mathrm{i}\,\vec{p}\cdot\vec{x}_v} \\
&\overset{x_v\to x_v-\hat{l}}{=} \sum_{\vec{x}_v,\vec{z}} S_\text{u}(x_f - (x_v - \hat{l}))S_\text{b}(x_v - z)U_l(z - \hat{l})S_\text{b}(z - x_i)\,\mathrm{e}^{\mathrm{i}\,\vec{p}\cdot\vec{x}_v}\,\mathrm{e}^{-\mathrm{i}\,p_l}\,. \quad \text{(B.23)}
\end{aligned}$$

Performing analogous variable shifts for the second heavy propagator in the square brackets of equation (B.22) and collecting terms, we arrive at[1]

$$\begin{aligned}
\mathcal{C}_\mu^{\text{B}_\text{s}\to\text{K,kin}}(t_\text{K}, t_{\text{B}_\text{s}}; \vec{p}, \vec{\theta}) = \frac{1}{V_3} \sum_{\{\vec{x}\},z,l} \mathrm{tr}\Big\{ &\Big[S_\text{u}(x_f - x_v + \hat{l})\,\mathrm{e}^{-\mathrm{i}\,p_l}\,U_l(z - \hat{l}) + S_\text{u}(x_f - x_v - \hat{l})\,\mathrm{e}^{\mathrm{i}\,p_l}\,U_l^\dagger(z) - 2S_\text{u}(x_f - x_v)\Big] \\
&\times \gamma_\mu S_\text{b}(x_v - z)S_\text{b}(z - x_i)\gamma_5 S_\text{s}(x_i - x_f)\gamma_5\Big\}. \quad \text{(B.24)}
\end{aligned}$$

[1] Now note here, however, that a shifted s propagator means that we will get an extra factor coming from the twist which we put on the U field through which the s quark is propagating, because we pass the twisted U field to the `kin_ins` routine in our program. This is not correct, so we need to account for this by undoing this twist in the routine `kin_ins`.

We repeat the same calculation for the kinetic insertions for the heavy-light two-point function. We arrive at

$$\mathcal{C}^{\mathrm{B_s,kin}}(t_{\mathrm{B_s}};\vec{\theta}) = \frac{1}{V_3}\sum_{\{\vec{x}\},z,l}\mathrm{tr}\Big\{ \Big[S_{\mathrm{s}}(x_i - x_f + \hat{l})U_l(z) + S_{\mathrm{s}}(x_i - x_f - \hat{l})U_l^\dagger(z-\hat{l}) - 2S_{\mathrm{s}}(x_i - x_f)\Big] \times \gamma_5 S_{\mathrm{b}}(x_f - z)S_{\mathrm{b}}(z - x_i)\gamma_5\Big\}. \quad \text{(B.25)}$$

We have

$$\begin{aligned}\vec{D}^2\,\mathrm{e}^{\mathrm{i}\,\vec{p}\cdot\vec{x}} = \vec{\nabla}^*\vec{\nabla}\,\mathrm{e}^{\mathrm{i}\,\vec{p}\cdot\vec{x}} &= \sum_l \mathrm{e}^{\mathrm{i}\,\vec{p}\cdot\vec{x}}(\mathrm{e}^{\mathrm{i}\,p_l} - 2 + \mathrm{e}^{-\mathrm{i}\,p_l}) \\ &= \sum_l \mathrm{e}^{\mathrm{i}\,\vec{p}\cdot\vec{x}}(2\cos(p_l) - 2) \\ &= \sum_l -4\,\mathrm{e}^{\mathrm{i}\,\vec{p}\cdot\vec{x}}\sin^2(p_l/2). \end{aligned} \quad \text{(B.26)}$$

Note further that

$$\sum_{t_z=t_i}^{t_f}\Theta(t_f - t_z)\Theta(t_z - t_i)\psi(t_f - t_i) = (t_f - t_i + 1)\psi(t_f - t_i). \quad \text{(B.27)}$$

Then, performing the same steps of computation as for the static case, detailed in the previous section, equation (B.24) becomes

$$\begin{aligned}&\mathcal{C}_\mu^{\mathrm{B_s}\to\mathrm{K,kin}}(t_{\mathrm{K}}, t_{\mathrm{B_s}};\vec{p},\vec{\theta}) \\ &= \frac{1}{V_3}\sum_{\{\vec{x}\},t_z,l}\Theta(t_v - t_z)\Theta(t_z - t_i)\,\mathrm{e}^{-\mathrm{i}\,\vec{p}\cdot(\vec{x}_f - \vec{x}_v)} \\ &\quad\times \mathrm{tr}\Big\{\gamma_5\tilde{S}_{\mathrm{s}}(-(t_{\mathrm{K}} + t_{\mathrm{B_s}});\vec{j} + \vec{\theta})\gamma_5\tilde{S}_{\mathrm{u}}(t_{\mathrm{K}};\vec{p} + \vec{j})\gamma_\mu(\tfrac{1+\gamma_0}{2})^2\Big\} \times \\ &\quad\times \Big[\mathrm{e}^{\mathrm{i}(p_l + j_l)}\,\mathrm{e}^{-\mathrm{i}\,p_l} + \mathrm{e}^{-\mathrm{i}(p_l + j_l)}\,\mathrm{e}^{\mathrm{i}\,p_l} - 2\Big] \\ &= \frac{1}{V_3}\sum_{\{\vec{x}\},l}\mathrm{e}^{-\mathrm{i}\,\vec{p}\cdot(\vec{x}_f - \vec{x}_v)}\,\mathrm{tr}\Big\{\gamma_5\tilde{S}_{\mathrm{s}}(-(t_{\mathrm{K}} + t_{\mathrm{B_s}});\vec{j} + \vec{\theta})\gamma_5\tilde{S}_{\mathrm{u}}(t_{\mathrm{K}};\vec{p} + \vec{j})\gamma_\mu(\tfrac{1+\gamma_0}{2})^2\Big\} \times \\ &\quad\times (t_{\mathrm{B_s}} + 1) \times \Big[-4\sin^2(j_l/2)\Big]. \end{aligned} \quad \text{(B.28)}$$

We also give the expression for the kinetic insertion for the heavy-light two-point function:

$$\mathcal{C}^{\mathrm{B_s,kin}}(t_{\mathrm{B_s}};\vec{\theta}) = (t_{\mathrm{B_s}} + 1)\frac{1}{V_3}\sum_{\{\vec{x}\},l}\mathrm{tr}\Big\{\gamma_5\tilde{S}_{\mathrm{s}}(-t_{\mathrm{B_s}};\vec{j} + \vec{\theta})\gamma_5(\tfrac{1+\gamma_0}{2})^2\Big\} \times \Big[-4\sin^2(j_l/2)\Big]. \quad \text{(B.29)}$$

Equations (B.18), (B.28) and (B.29) have been implemented in the Matlab routine `analytic.m` located in `~/main/tools/`. Assuming the main program has been run, the

script `ana_check.pl` in `~/main/tools/` can be run. It will execute `analytic.m` if this has not yet been done and compare all numeric output files line by line with the corresponding analytic ones and print out whether any discrepancies between them have been detected at a given precision level. We verified agreement between analytical and numerical calculations of all quantities discussed in this chapter up to machine precision.

C Properties and tests of the code

C.1 General properties

The problem discussed in the main text of this thesis has some underlying properties. We list these here and describe how they are verified in the measurement code `hqet_btopi_all`.

- Gauge invariance

  The problem is gauge invariant, that is, invariant under random gauge transformations. If in the infile the `flag_rgt` is set to 1, a random gauge transformation is applied to the gauge field and the noise source. Comparing the output generated using the transformed fields with that of the untransformed fields, we observe that they are the same up to machine precision, so that gauge invariance is fulfilled.

- Translational invariance

  Setting all gauge links $U = 1$, the problem is time-translationally invariant. That is, keeping t_{K} and $t_{\mathrm{B_s}}$ fixed, the output does not depend on the absolute positions of t_i, t_v, t_f on the lattice. To check for this, we vary the position of the noise source, which has support on time slice t_f, by modifying in the infile of the program the parameter `n_timedils`. Running the program for various `n_timedils`, we get the same output up to machine precision; hence we verify that translational invariance is fulfilled.

- Discrete rotational invariance

  Setting all gauge links $U = 1$, the problem is invariant under rotations in Dirac space. To test this, we need a set of source fields that is closed under rotation. For example, such a set is obtained by taking four sources that have support on the same space time point and colour component and each have a different Dirac component set to 1 with the other three components being zero. Once the outputs obtained employing these four sources are summed, one can test the result for rotational invariance by comparing the summed outputs of different combinations of $\vec{p}_{\mathrm{K}}, \vec{\theta}$. This has been implemented in the program by setting to 1 `flag_rotinv` in the infile and choosing a set of momenta for which one wants to test rotational invariance. In particular, we have checked for all `<tag>`s that

  - for $\mu = 0$ the result depends only on $|\vec{p}_{\mathrm{K}}|$;

- for $\{\mu = 1, \vec{p}_K = (1,0,0)\}$, $\{\mu = 2, \vec{p}_K = (0,1,0)\}$ and $\{\mu = 3, \vec{p}_K = (0,0,1)\}$ for a given j the result is the same up to rounding errors;
- for $\{\mu = 1, \vec{p}_K = (1,1,0)\}$, $\{\mu = 2, \vec{p}_K = (1,1,0)\}$, $\{\mu = 1, \vec{p}_K = (1,0,1)\}$, $\{\mu = 3, \vec{p}_K = (1,0,1)\}$, $\{\mu = 2, \vec{p}_K = (0,1,1)\}$ and $\{\mu = 3, \vec{p}_K = (0,1,1)\}$ for a given j the result is the same up to rounding errors.

C.2 Effects and properties of quark twisting

In this section we want to discuss in some more detail the effects of quark twisting as introduced in section 5.1.3. Ultimately, we twist both the b and the s quark, as discussed in section 5.1.4, such that a correlation function constructed from these two quarks does not depend on $\vec{\theta}$, compare equations (5.28) and (5.29). We point out again that the heavy quark at static order does not feel effects of the twist, since it amounts to a multiplication of space-like gauge fields with a phase, equation (5.27), but the static heavy quark moves along time-like links only, equation (4.16).

Let us therefore now consider a heavy-light two-point function at static order with a twisted light quark. Since the heavy quark is static, it is bound to a point in space $\vec{x}_0$ and propagates only in time direction, from t_0 to t_1. Thus, also the light quark is fixed at $\{\vec{x}_0, t_0\}$ and $\{\vec{x}_0, t_1\}$, while it can move away from $\vec{x}_0$ between t_0 and t_1. Propagating through a twisted gauge field, it picks up a phase $\exp\{-\mathrm{i}\,\theta_k/L\}$ for each spatial link it passes along direction k. Since, however, it is required to return to $\vec{x}_0$ at t_1, at some point along its trajectory, it will move along the same link in opposite direction, thus picking up an opposite phase of $\exp\{+\mathrm{i}\,\theta_k/L\}$. This situation is sketched in figure C.1. A different possibility for the light quark to return to $\vec{x}_0$ at t_1 is sketched in figure C.2: It wraps around the lattice in direction k. In this situation, it will pick up a phase $\exp\{-\mathrm{i}\,\theta_k/L\}$ per link and, after passing through L lattice sites, end up with a total phase of $\exp\{-\mathrm{i}\,\theta_k\}$. This contribution, however, is exponentially suppressed with the lattice size L. Thus, the heavy-light two-point function is independent of the twist $\vec{\theta}$ up to exponentially suppressed finite-size effects.

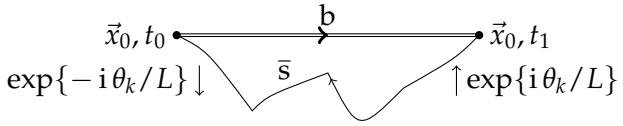

Figure C.1: Schematic representation of a B_s propagating at static order. The light quark receives no total twist.

The argument made so far holds only for the ground state contribution to the heavy-light two-point function. If we consider also excited states, we have to take into account also contributions such as the one sketched on the right in figure C.3. Here, a u-$\bar{\mathrm{u}}$-loop is formed from the sea quark background and connects to the b and $\bar{\mathrm{s}}$ quarks such that

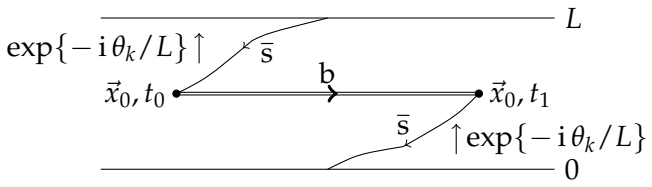

Figure C.2: Schematic representation of a B_s propagating at static order. The light quark wraps around the spatial direction k and receives a total twist $\exp\{-\mathrm{i}\,\theta_k\}$.

a B and K are propagating. If the $\bar{s}$ quark is twisted, the kaon will now have an altered momentum compared to a kaon with an untwisted $\bar{s}$ quark. Hence its energy, and therefore the energy of the combined state of the B and K, depend on the twist of the light quark. Note that while this dependece is also a finite-size effect, its suppression is only with $1/L$.

Figure C.3: Schematic representation of the heavy-light two-point function. Left: ground state contribution. Right: An excited state formed when an up quark loop is created from the sea, making for the propagation of a B and a K.

D Models of combined fits

In section 6.4, we discussed a combined fit to the three- and two-point function to obtain $\varphi_\mu^{(0,0)}$. For this fit, we made some assumptions. Here, we discuss similar fits based on different assumptions.

A.) As already noted in section 6.4, let us repeat here that in principle, it is possible to obtain $\varphi_\mu^{(0,0)}$ by fitting to equation (6.19). This is what we do to get a starting value to the final fit in section 6.4.

B.) We fix t_K to a value that is safely within the plateau region, that is, the region where only the ground state contributes significantly, $t_\mathrm{K} = t_\mathrm{K}^\mathrm{fix}$. Then, equation (6.17) simplifies to

$$\begin{aligned} \mathcal{C}_{\mu,i}^{\mathrm{B_s}\to\mathrm{K}}(t_\mathrm{K}^\mathrm{fix}, t_{\mathrm{B_s}}) &\approx \sum_{n=0}^{2} \kappa^{(0)} \varphi_\mu^{(0,n)} \beta_i^{(n)} \, \mathrm{e}^{-E_\mathrm{K}^{(0)} t_\mathrm{K}^\mathrm{fix}} \, \mathrm{e}^{-E_{\mathrm{B_s}}^{(n)} t_{\mathrm{B_s}}} \\ &\equiv \sum_{n=0}^{2} \widetilde{\varphi}_\mu^{(n)} \beta_i^{(n)} \, \mathrm{e}^{-E_{\mathrm{B_s}}^{(n)} t_{\mathrm{B_s}}}, \end{aligned} \tag{D.1}$$

with

$$\widetilde{\varphi}_\mu^{(n)} = \kappa^{(0)} \varphi_\mu^{(0,n)} \, \mathrm{e}^{-E_\mathrm{K}^{(0)} t_\mathrm{K}^\mathrm{fix}} . \tag{D.2}$$

We now perform a combined fit to equations (6.12) and (D.1), with six $\widetilde{\varphi}_\mu^{(n)}$, nine $\beta_i^{(n)}$ and three $E_{\mathrm{B_s}}^{(n)}$ as fit parameters. So, the total number of fit parameters is now eighteen. To obtain $\varphi_\mu^{(0,n)}$ from equation (D.2), we use $\kappa^{(0)}$ and $E_\mathrm{K}^{(0)}$ determined independently from the light-light two-point function as discussed in section 6.1. We remark that this fit is considerably faster than that discussed in section 6.4 in terms of CPU time, notably because only a fraction of the full set of data points enter. Still, fit parameters obtained from this fit agree remarkably well with those of the fit of section 6.4.

C.) With the approximations we make in equations (6.16) and (6.17), we neglect all excited kaon states and claim that only the ground state of the kaon contributes. While this is a reasonable approximation, we can also extend the fit to include excited kaon states. Then, we have

$$\mathcal{C}^\mathrm{K}(t_\mathrm{K}) \approx \sum_{n=0}^{1} (\kappa^{(n)})^2 \, \mathrm{e}^{-E_\mathrm{K}^{(n)} t_\mathrm{K}} = (\kappa^{(0)})^2 \, \mathrm{e}^{-E_\mathrm{K}^{(0)} t_\mathrm{K}} + (\kappa^{(1)})^2 \, \mathrm{e}^{-E_\mathrm{K}^{(1)} t_\mathrm{K}}, \tag{D.3}$$

and

$$\mathcal{C}^{\mathrm{B_s}\to\mathrm{K}}_{\mu,i}(t_\mathrm{K}, t_{\mathrm{B_s}}) = \sum_{m=0}^{1}\sum_{n=0}^{2} \kappa^{(m)} \varphi_\mu^{(m,n)} \beta_i^{(n)}\, \mathrm{e}^{-E_\mathrm{K}^{(m)} t_\mathrm{K}}\, \mathrm{e}^{-E_{\mathrm{B_s}}^{(n)} t_{\mathrm{B_s}}}, \tag{D.4}$$

adding eight additional fit parameters, $\kappa^{(1)}$, $E_\mathrm{K}^{(1)}$, $\varphi_\mu^{(1,0)}$, $\varphi_\mu^{(1,1)}$, $\varphi_\mu^{(1,2)}$, for a total of twenty-eight.

D.) We may also include finite-T effects, as discussed in section 6.5, in our fit. For this, we write the three-point function as in equation (6.28). In doing so, we can significantly increase the range of t_K that enters the fit. On the other hand, we also add a number of additional fit parameters: at least six amplitudes $\zeta_{\mu,i}$ (2×3 for $\mu = 0, 1$ and $i = 1, 2, 3$ smearing levels), depending on whether we want to include only the B^* ground state or also its first excited state. Note that at static order, $E_{\mathrm{B}^*} = E_{\mathrm{B_s}}$. Since, as we already pointed out, the t_K range is sufficiently large, we will not include finite T effects in our fit.

Let us make another general remark here. Each of the above strategies can be followed for a fixed μ. For example, if we set $\mu = 0$, in any strategy, we will obtain $\varphi_0^{(0,0)}$ and thus $f_\parallel$, compare equation (7.2a). Then, we can repeat the same for $\mu = 1$ to obtain $\varphi_1^{(0,0)}$ and thus $f_\parallel$, equation (7.2b). This reduces the total number of fit parameters in a single fit and thus stabilises it. All quantities, however, that do not have a μ dependence, that is, all β, κ, E, are then determined twice: Once in the fit for $\mu = 0$, once in the fit for $\mu = 1$. We refrained from pursuing this method.

E Finite-T effects for the ratio

We here extend the discussion of finite-T effects presented in section 6.5 to the ratio defined in equation (5.10)[1]. As in the main text, we here focus our discussion on finite-T effects in t_{K}, since in $t_{\mathrm{B_s}}$, we enter the region of large statistical noise before the wrapper contribution becomes relevant. Let us therefore remember equation (6.27) and divide it by

$$\sqrt{\left\langle P_{\mathrm{su}}(x_f)P_{\mathrm{us}}(x_v)\right\rangle \left\langle P_{\mathrm{bs}}(x_v)P_{\mathrm{sb}}(x_i)\right\rangle} \tag{E.1}$$

and obtain the ratio

$$\begin{aligned}
R_\mu \approx\ & \frac{\langle 0 \,|\, P_{\mathrm{su}} \,|\, \mathrm{K}\rangle \langle \mathrm{K} \,|\, V^\mu \,|\, \mathrm{B_s}\rangle \langle \mathrm{B_s} \,|\, P_{\mathrm{bs}} \,|\, 0\rangle \, \mathrm{e}^{-E_{\mathrm{B_s}} t_{\mathrm{B_s}}} \, \mathrm{e}^{-E_{\mathrm{K}} t_{\mathrm{K}}}}{\sqrt{\langle P_{\mathrm{su}} P_{\mathrm{us}}\rangle \langle P_{\mathrm{bs}} P_{\mathrm{sb}}\rangle}} + \\
& + \frac{\langle \mathrm{K} \,|\, P_{\mathrm{su}} \,|\, 0\rangle \langle 0 \,|\, V^\mu \,|\, \mathrm{B}^*\rangle \langle \mathrm{B}^* \,|\, P_{\mathrm{bs}} \,|\, \mathrm{K}\rangle \, \mathrm{e}^{-E_{\mathrm{B}^*} t_{\mathrm{B_s}}} \, \mathrm{e}^{-E_{\mathrm{K}}(T - t_{\mathrm{B_s}} - t_{\mathrm{K}})}}{\sqrt{\langle P_{\mathrm{su}} P_{\mathrm{us}}\rangle \langle P_{\mathrm{bs}} P_{\mathrm{sb}}\rangle}} \\
=\ & \underbrace{\langle \mathrm{K} \,|\, V^\mu \,|\, \mathrm{B_s}\rangle}_{\equiv A_0^\mu} \frac{\mathrm{e}^{-E_{\mathrm{B_s}} t_{\mathrm{B_s}}/2} \, \mathrm{e}^{-E_{\mathrm{K}} t_{\mathrm{K}}}}{\sqrt{\mathrm{e}^{-E_{\mathrm{K}} t_{\mathrm{K}}} + \mathrm{e}^{-E_{\mathrm{K}}(T - t_{\mathrm{K}})}}} + \\
& + \underbrace{\frac{\langle \mathrm{K} \,|\, P_{\mathrm{su}} \,|\, 0\rangle \langle 0 \,|\, V^\mu \,|\, \mathrm{B}^*\rangle \langle \mathrm{B}^* \,|\, P_{\mathrm{bs}} \,|\, \mathrm{K}\rangle}{\sqrt{|\langle \mathrm{K} \,|\, P_{\mathrm{su}} \,|\, 0\rangle|^2 \, |\langle \mathrm{B_s} \,|\, P_{\mathrm{bs}} \,|\, 0\rangle|^2}}}_{\equiv A_1^\mu} \frac{\mathrm{e}^{-E_{\mathrm{B}^*} t_{\mathrm{B_s}}} \, \mathrm{e}^{-E_{\mathrm{K}}(T - t_{\mathrm{B_s}} - t_{\mathrm{K}})}}{\mathrm{e}^{-E_{\mathrm{B_s}} t_{\mathrm{B_s}}/2} \sqrt{\mathrm{e}^{-E_{\mathrm{K}} t_{\mathrm{K}}} + \mathrm{e}^{-E_{\mathrm{K}}(T - t_{\mathrm{K}})}}}.
\end{aligned} \tag{E.2}$$

Here we have used equation (3.37),

$$\langle P(x)P(y)\rangle \overset{T\to\infty}{=} \sum_n |\langle n \,|\, P \,|\, 0\rangle|^2 \, \mathrm{e}^{-E_n(t_x - t_y)} \,. \tag{E.3}$$

We now multiply both sides of equation (E.2) by $\mathrm{e}^{E_{\mathrm{B_s}} t_{\mathrm{B_s}}/2} \, \mathrm{e}^{E_{\mathrm{K}} t_{\mathrm{K}}/2}$, making contact to equation (5.11), and get

$$R_\mu \, \mathrm{e}^{E_{\mathrm{B_s}} t_{\mathrm{B_s}}/2} \, \mathrm{e}^{E_{\mathrm{K}} t_{\mathrm{K}}/2} = \frac{1}{\sqrt{1 + \mathrm{e}^{-E_{\mathrm{K}}(T - 2t_{\mathrm{K}})}}} \left(A_0^\mu + A_1^\mu \, \mathrm{e}^{-(E_{\mathrm{B}^*} - E_{\mathrm{B_s}} - E_{\mathrm{K}}) t_{\mathrm{B_s}}} \, \mathrm{e}^{-E_{\mathrm{K}}(T - 2t_{\mathrm{K}})} \right). \tag{E.4}$$

Note here that at static order, $E_{\mathrm{B}^*} = E_{\mathrm{B_s}}$, so that in equation (E.4), $E_{\mathrm{B}^*} - E_{\mathrm{B_s}} = 0$ and it thus becomes independent of $E_{\mathrm{B_s}}$. To keep the discussion general here, however, we stick to the notation using both E_{B^*} and $E_{\mathrm{B_s}}$.

We note that equation (E.4) has three unknown quantities: A_0^μ, which is of physical

[1] In principle, the ratio can be constructed for any smearing level and should thus receive an index i. Here, however, we restrict ourselves to considering it for one smearing level and thus omit the index i.

interest to us, and A_1^μ and E_{B^*}, which come from the wrap-around kaon and B^* state. As expected, at moderately small t_K, equation (E.4) is dominated by the physical (plateau) term A_0^μ, while at large t_K, it is dominated by the wrapper term A_1^μ, which is enhanced with $\exp(-E_\mathrm{K}(T-2t_\mathrm{K}))$. Finally, let us write down equation (E.4) for the case of fixed $t_{\mathrm{B_s}}$:

$$R_\mu \, \mathrm{e}^{E_{\mathrm{B_s}} t_{\mathrm{B_s}}/2} \, \mathrm{e}^{E_\mathrm{K} t_\mathrm{K}/2} = \frac{1}{\sqrt{1+\mathrm{e}^{-E_\mathrm{K}(T-2t_\mathrm{K})}}} \left(A_0^\mu + \widetilde{A}_1^\mu \, \mathrm{e}^{-E_\mathrm{K}(T-2t_\mathrm{K})} \right), \tag{E.5}$$

where

$$\widetilde{A}_1^\mu = A_1^\mu \, \mathrm{e}^{-(E_{\mathrm{B}^*} - E_{\mathrm{B_s}} - E_\mathrm{K}) t_{\mathrm{B_s}}} \, . \tag{E.6}$$

We note that equation (E.5) has now only two unknown parameters, A_0^μ and $\widetilde{A}_1^\mu$.

F Fit results

In this appendix, we collect some of the results of the fits discussed in chapter 6. Let us therefore remember table 6.2, in which we show the results of all parameters of the fits using the central t ranges of given in that table for the different ensembles. In figures F.1 to F.3, we show scatter plots of all fit parameters in which we vary the fit range by one or two units in $(t_{\mathrm{B_s}})^{\mathrm{2pt}}_{\mathrm{min}}$, $(t_{\mathrm{B_s}})^{\mathrm{3pt}}_{\mathrm{min}}$ and $(t_{\mathrm{K}})^{\mathrm{3pt}}_{\mathrm{min}}$ around the central value given in table 6.2 for ensemble N6. The index on the x axis of these plots is explained in table F.1. In figure F.4, we show scatter plots of $\varphi_\mu^{(0)}$ as a function of $(t_{\mathrm{B_s}})^{\mathrm{3pt}}_{\mathrm{min}}$. In figure F.5, we show scatter plots of $\Delta\varphi_\mu^{(0)}$ as a function of $(t_{\mathrm{B_s}})^{\mathrm{3pt}}_{\mathrm{min}}$, where $\Delta\varphi_\mu^{(0)} = \varphi_\mu^{(0)}\big((t_{\mathrm{B_s}})^{\mathrm{3pt}}_{\mathrm{min}} = 13\big) - \varphi_\mu^{(0)}\big((t_{\mathrm{B_s}})^{\mathrm{3pt}}_{\mathrm{min}}\big)$ is the variation of $\varphi_\mu^{(0)}$ at a given $(t_{\mathrm{B_s}})^{\mathrm{3pt}}_{\mathrm{min}}$ from $\varphi_\mu^{(0)}$ at our central value $(t_{\mathrm{B_s}})^{\mathrm{3pt}}_{\mathrm{min}} = 13$. In figure F.6, we show plots similar to those of figures 6.5 and 6.6, comparing our fit result with the ratio method, the difference being that in figure F.6, points are obtained from ratio $R'(t_{\mathrm{K}}, t_{\mathrm{B_s}})$ as in equation (5.13), as opposed to ratio $R(t_{\mathrm{K}}, t_{\mathrm{B_s}})$, equation (5.11).

For simplicity, in this appendix we show all quantities in lattice units.

index	$\delta(t_{B_s})^{2pt}_{min}$	$\delta(t_K)^{3pt}_{min}$	$\delta(t_{B_s})^{3pt}_{min}$
1	-1	0	0
2	0	0	0
3	1	0	0
4	2	0	0
5	0	-1	0
6	0	0	0
7	0	1	0
8	0	2	0
9	0	0	-1
10	0	0	0
11	0	0	1
12	0	0	2

Table F.1: Index used on the x axis of the scatter plots in figures F.1 to F.3. Variation of times are around the central value given in table 6.2.

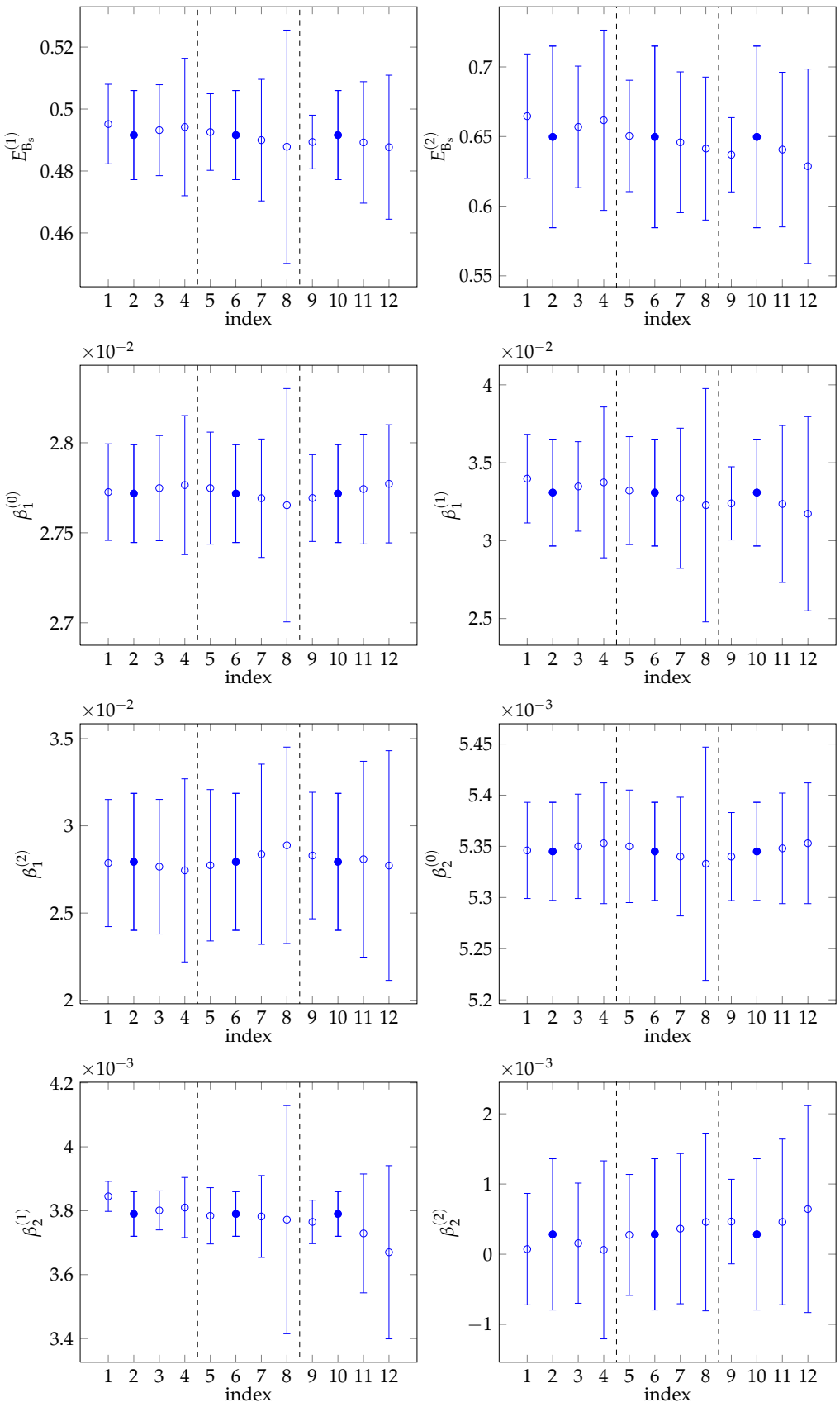

Figure F.1: Scatter plots for ensemble N6 as motivated in section 6.6. The index on the x axis is explained in table F.1. The filled points correspond to the central fit.

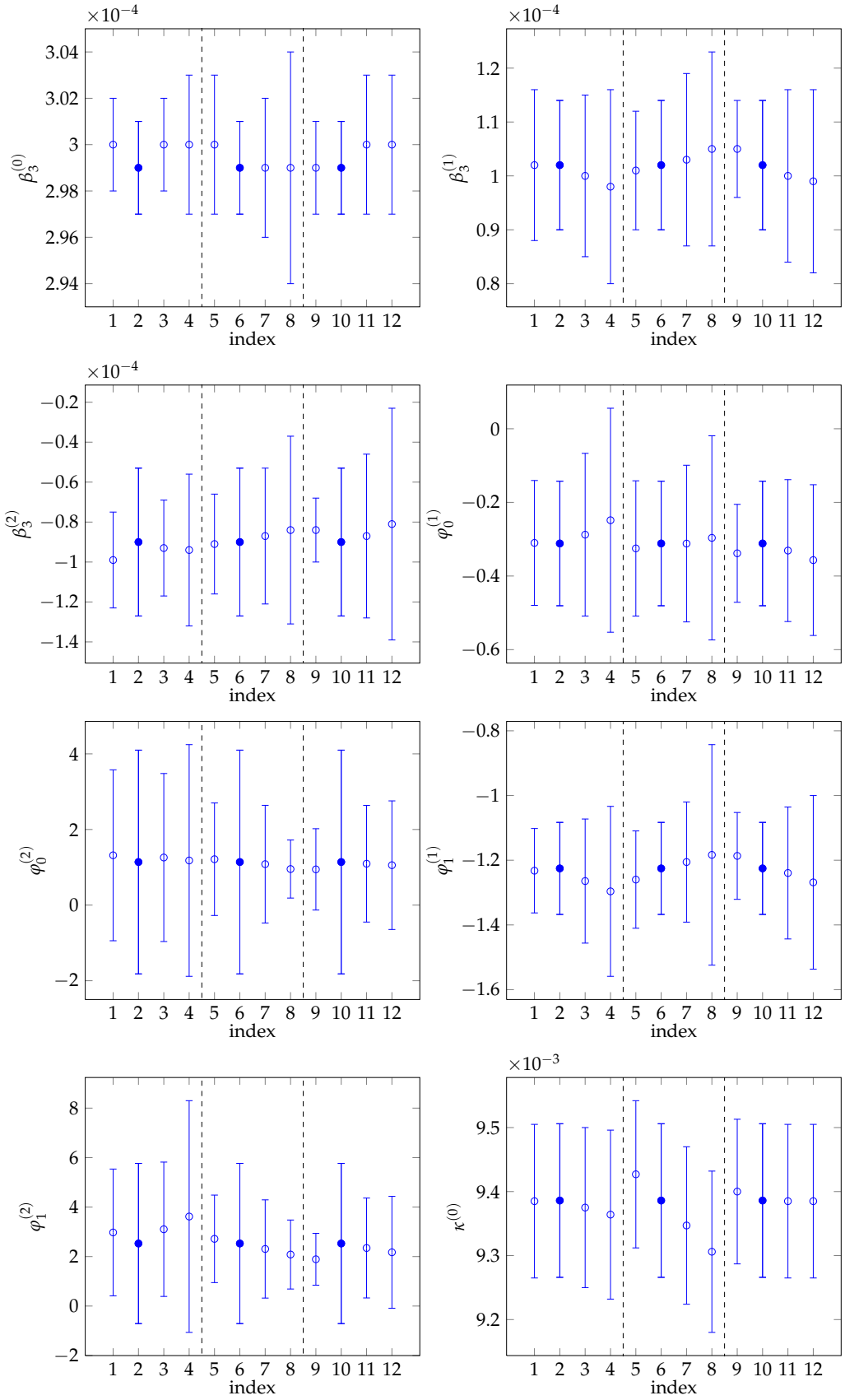

Figure F.2: Scatter plots for ensemble N6 as motivated in section 6.6. The index on the x axis is explained in table F.1. The filled points correspond to the central fit.

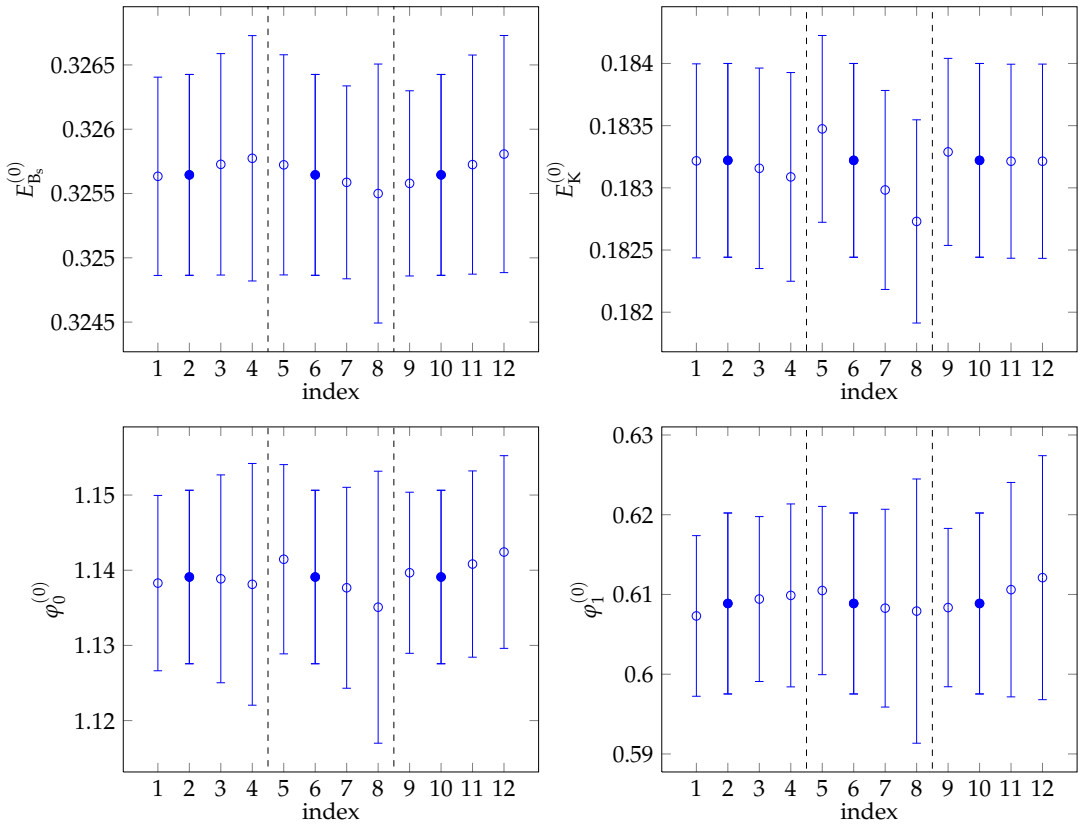

Figure F.3: Scatter plots for ensemble N6 as motivated in section 6.6. The index on the x axis is explained in table F.1. The filled points correspond to the central fit.

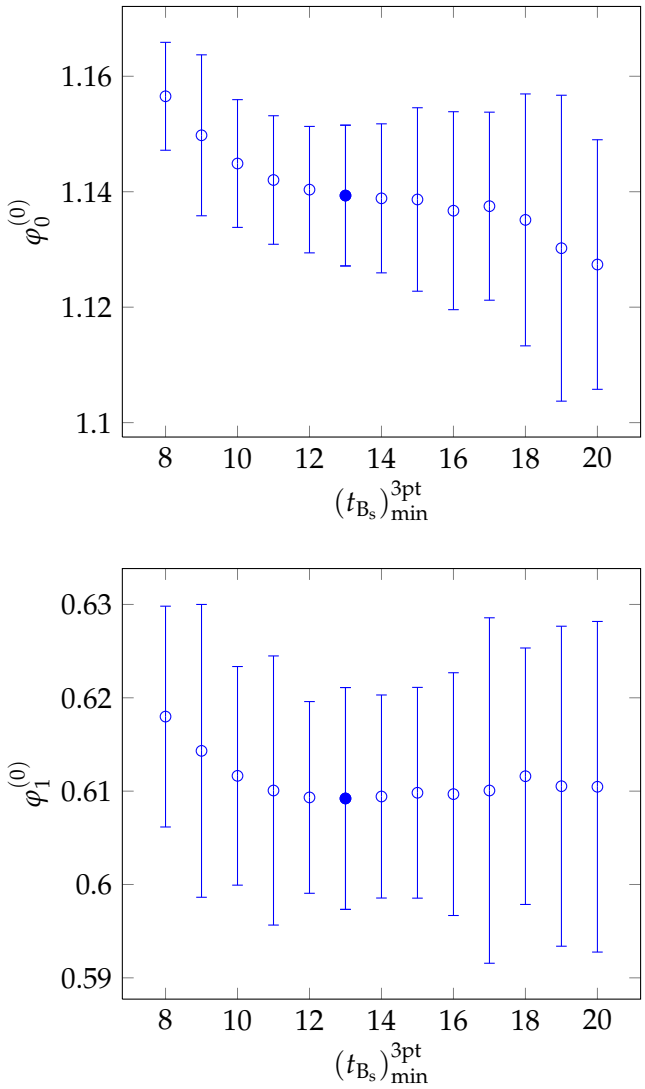

Figure F.4: Scatter plots of $\varphi_\mu^{(0)}$ for ensemble N6 as motivated in section 6.6. On the x axis is $(t_{B_s})^{3pt}_{min}$, while all other t ranges are held at their central values of table 6.2. The filled points correspond to the central fit.

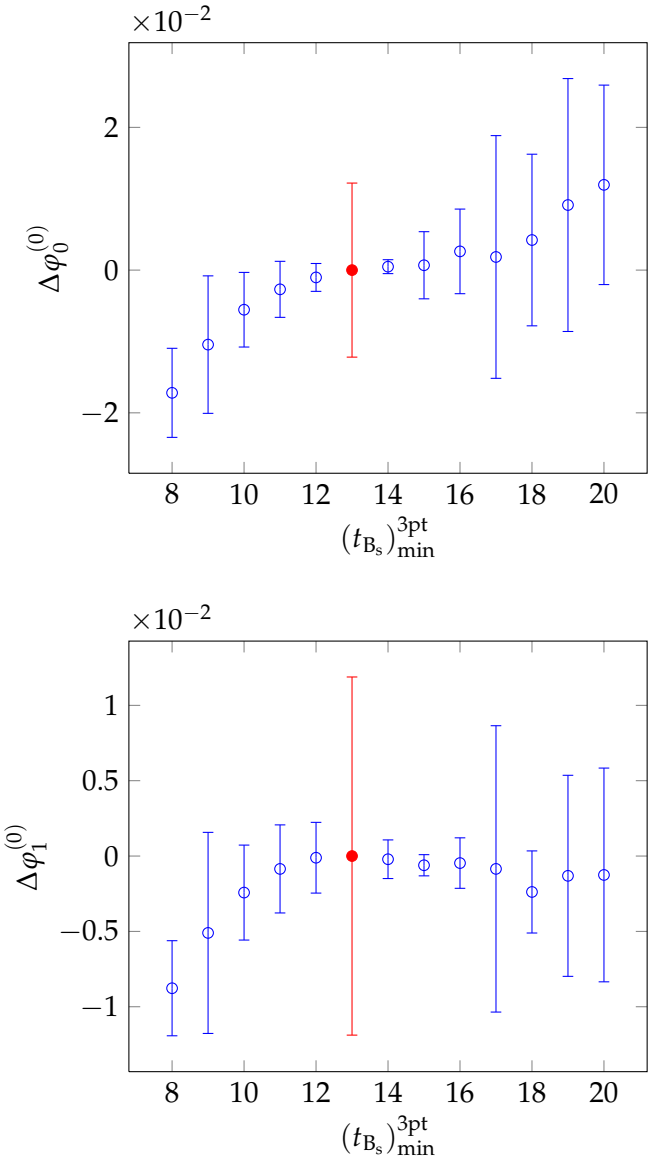

Figure F.5: Scatter plots of $\Delta\varphi_\mu^{(0)} = \varphi_\mu^{(0)}\left((t_{\mathrm{B_s}})_{\mathrm{min}}^{\mathrm{3pt}} = 13\right) - \varphi_\mu^{(0)}\left((t_{\mathrm{B_s}})_{\mathrm{min}}^{\mathrm{3pt}}\right)$ for ensemble N6 as motivated in section 6.6. That is, we here show the variations of $\varphi_\mu^{(0)}$ around the values obtained using our central fit ranges as a function of $(t_{\mathrm{B_s}})_{\mathrm{min}}^{\mathrm{3pt}}$, while all other t ranges are held at their central values of table 6.2. The red filled points correspond to the central fit with statistical errors as given in table 6.2. Compare also figure F.4, where we show $\varphi_\mu^{(0)}$ as a function of $(t_{\mathrm{B_s}})_{\mathrm{min}}^{\mathrm{3pt}}$.

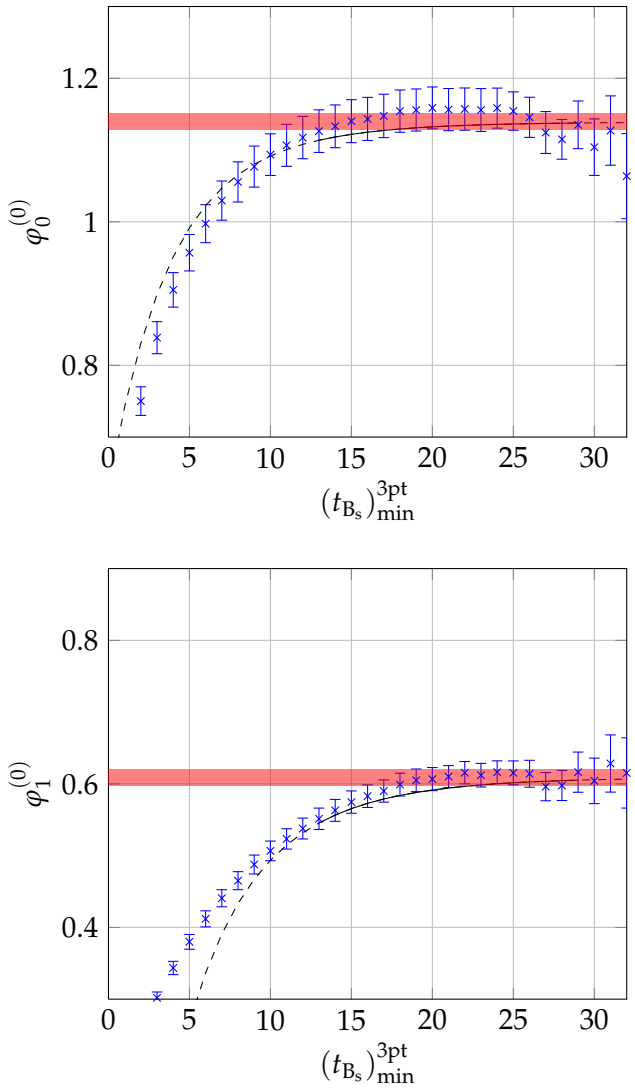

Figure F.6: Comparison of the right hand side of equation (5.13) (blue points), and the results of the fit as described in section 6.4 shown as a black solid curve in the fit range and extended as a dashed line for illustration, for ensemble N6. The red band is the fit result for $\varphi_\mu^{(0)}$. On the x axis is t_{B_s}; $t_K = 15$ is fixed. The shown points are constructed from the correlators with the highest smearing level, $i = 3$. Compare figures 6.5 and 6.6, where points are obtained from equation (5.11); the black curves are the same. The error of the blue points is dominated by that of $\kappa^{(0)}$, see section 6.1.

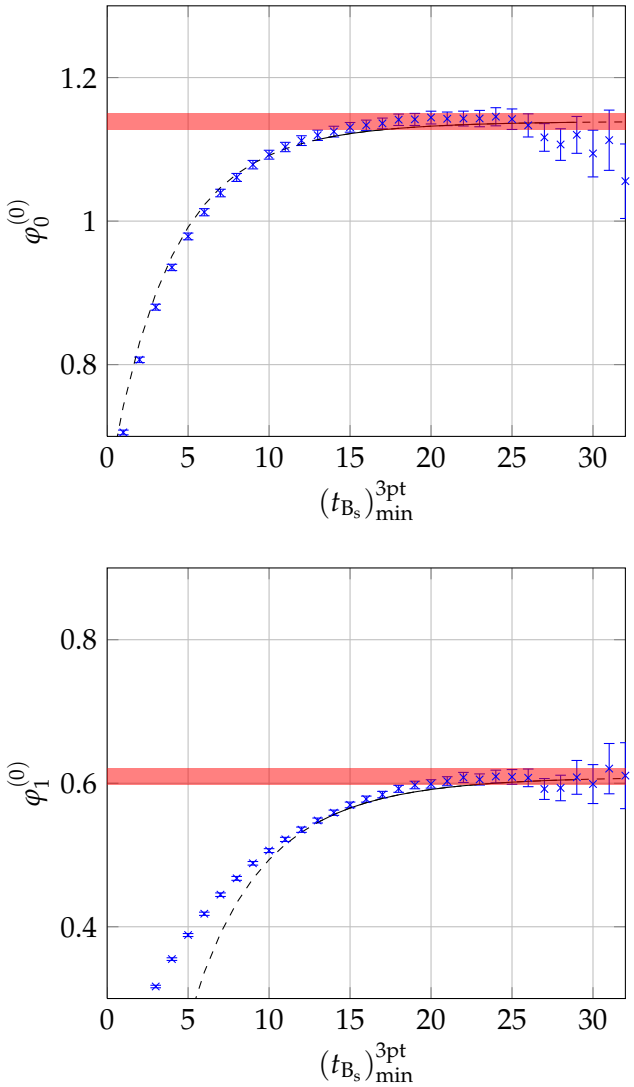

Figure F.7: Comparison of the right hand side of equation (5.11) (blue points), and the results of the fit as described in section 6.4 shown as a black solid curve in the fit range and extended as a dashed line for illustration, for ensemble N6. The red band is the fit result for $\varphi_\mu^{(0)}$. On the x axis is t_{B_s}; $t_K = 15$ is fixed. The shown points are constructed from the correlators with the highest smearing level, $i = 3$. Compare figures 6.5 and 6.6, where the energies that enter equation (5.11) were determined independently from the two-point functions as discussed in sections 6.1 and 6.2. Here, we take the energies determined in our final fit, table 6.2; the black curves are the same.

References

[1] **N. Cabibbo.** Unitary Symmetry and Leptonic Decays. *Phys. Rev. Lett. 10, 531 (1963).*

[2] **M. Kobayashi and T. Maskawa.** CP Violation in the Renormalizable Theory of Weak Interaction. *Prog. Theor. Phys. 49, 652 (1973).*

[3] **K. Olive *et al.*** (Particle Data Group)**.** Review of Particle Physics. *Chin. Phys. C 38, 090001 (2014).*

[4] **C. Jarlskog.** Commutator of the Quark Mass Matrices in the Standard Electroweak Model and a Measure of Maximal CP Violation. *Phys. Rev. Lett. 55, 1039 (1985).*

[5] **L.-L. Chau and W.-Y. Keung.** Comments on the Parametrization of the Kobayashi-Maskawa Matrix. *Phys. Rev. Lett. 53, 1802 (1984).*

[6] **A. J. Buras, M. E. Lautenbacher and G. Ostermaier.** Waiting for the top quark mass, $K^+ \to \pi^+ \nu\bar{\nu}$, $B_s^0 - \bar{B}_s^0$ mixing and CP asymmetries in B-decays. *Phys. Rev. D 50, 3433 (1994).* arXiv:hep-ph/9403384.

[7] **L. Wolfenstein.** Parametrization of the Kobayashi-Maskawa Matrix. *Phys. Rev. Lett. 51, 1945 (1983).*

[8] **J. Charles *et al.*** (CKMfitter Group)**.** CP violation and the CKM matrix: Assessing the impact of the asymmetric B factories. *Eur. Phys. J. C 41, 1 (2005).* Updated results and plots available at: http://ckmfitter.in2p3.fr. arXiv:hep-ph/0406184.

[9] **BELLE II Collaboration**. http://belle2.kek.jp/.

[10] **The LHCb collaboration**. http://lhcb.web.cern.ch/lhcb/.

[11] **BaBar**. http://www-public.slac.stanford.edu/babar/.

[12] **C. Bouchard.** Testing the Standard Model under the weight of heavy flavors *(2015).* arXiv:1501.03204.

[13] **G. Ricciardi.** Progress on semi-leptonic $B_{(s)}$ decays. *Mod. Phys. Lett. A 29, 1430019 (2014).* arXiv:1403.7750.

[14] **W. Wang.** Recent Developments on the CKM Matrix. *Int. J. Mod. Phys. A 29, 1430040 (2014).* arXiv:1407.6868.

[15] **A. Bevan *et al.*** (BaBar, Belle)**.** The Physics of the B Factories. *Eur. Phys. J. C 74(11), 3026 (2014)*. arXiv:1406.6311.

[16] **S. Aoki, Y. Aoki, C. Bernard, T. Blum, G. Colangelo *et al.*** Review of lattice results concerning low-energy particle physics. *Eur. Phys. J. C 74, 2890 (2014)*. arXiv:1310.8555.

[17] **A. Abdesselam *et al.*** (Belle Collaboration)**.** Measurement of the branching fraction of $B^+ \to \tau^+\nu_\tau$ decays with the semileptonic tagging method and the full Belle data sample. *Proceedings of the 8th International Workshop on the CKM Unitarity Triangle (CKM 2014) (2014)*. arXiv:1409.5269.

[18] **I. Adachi *et al.*** (Belle Collaboration)**.** Evidence for $B^- \to \tau^-\bar{\nu}_\tau$ with a Hadronic Tagging Method Using the Full Data Sample of Belle. *Phys. Rev. Lett. 110(13), 131801 (2013)*. arXiv:1208.4678.

[19] **B. Aubert *et al.*** (BaBar Collaboration)**.** A Search for $B^+ \to \ell^+\nu_\ell$ Recoiling Against $B^- \to D^0\ell^-\bar{\nu}X$. *Phys. Rev. D 81, 051101 (2010)*. arXiv:0912.2453.

[20] **J. Lees *et al.*** (BaBar Collaboration)**.** Evidence of $B \to \tau\nu$ decays with hadronic B tags. *Phys. Rev. D 88, 031102 (2013)*. arXiv:1207.0698.

[21] **A. Abada, C. Allton, P. Boucaud, D. Carpenter, M. Crisafulli *et al.*** Semileptonic decays of heavy flavors on a fine grained lattice. *Nucl. Phys. B 416, 675 (1994)*. arXiv:hep-lat/9308007.

[22] **D. Burford *et al.*** (UKQCD Collaboration)**.** Form-factors for $B \to \pi$ lepton anti-lepton-neutrino and $B \to K^*$ gamma decays on the lattice. *Nucl.Phys. B447, 425–440 (1995)*. arXiv:hep-lat/9503002.

[23] **C. Allton *et al.*** (APE Collaboration)**.** Lattice calculation of D and B meson semileptonic decays using the Clover action at $\beta = 6.0$ on APE. *Phys. Lett. B 345, 513 (1995)*. arXiv:hep-lat/9411011.

[24] **S. Hashimoto, K.-I. Ishikawa, H. Matsufuru, T. Onogi and N. Yamada.** Lattice study of $B \to \pi$ semileptonic decay using nonrelativistic lattice QCD. *Phys. Rev. D 58, 014502 (1998)*. arXiv:hep-lat/9711031.

[25] **A. Abada, D. Becirevic, P. Boucaud, J. Leroy, V. Lubicz *et al.*** Heavy → light semileptonic decays of pseudoscalar mesons from lattice QCD. *Nucl. Phys. B 619, 565 (2001)*. arXiv:hep-lat/0011065.

[26] **A. X. El-Khadra, A. S. Kronfeld, P. B. Mackenzie, S. M. Ryan and J. N. Simone.** The Semileptonic decays $B \to \pi$ lepton neutrino and $D \to \pi$ lepton neutrino from lattice QCD. *Phys. Rev. D 64, 014502 (2001)*. arXiv:hep-ph/0101023.

[27] **S. Aoki *et al.*** (JLQCD Collaboration)**.** Differential decay rate of $B \to \pi$ lepton neutrino semileptonic decay with lattice NRQCD. *Phys. Rev. D 64, 114505 (2001)*. arXiv:hep-lat/0106024.

[28] **J. Flynn, T. Izubuchi, T. Kawanai, C. Lehner, A. Soni *et al.*** (RBC and UKQCD Collaborations)**.** The $B \to \pi\ell\nu$ and $B_s \to K\ell\nu$ form factors and $|V_{ub}|$ from 2+1-flavor lattice QCD with domain-wall light quarks and relativistic heavy quarks *(2015)*. arXiv:1501.05373.

[29] **J. A. Bailey, C. Bernard, C. E. DeTar, M. Di Pierro, A. El-Khadra *et al.*** (Fermilab Lattice and MILC Collaborations)**.** The $B \to \pi\ell\nu$ semileptonic form factor from three-flavor lattice QCD: A Model-independent determination of $|V_{ub}|$. *Phys. Rev. D 79, 054507 (2009)*. arXiv:0811.3640.

[30] **E. Dalgic, A. Gray, M. Wingate, C. T. Davies, G. P. Lepage *et al.*** (HPQCD Collaboration)**.** B meson semileptonic form-factors from unquenched lattice QCD. *Phys. Rev. D 73, 074502 (2006)*. arXiv:hep-lat/0601021.

[31] **C. Bouchard, G. P. Lepage, C. Monahan, H. Na and J. Shigemitsu.** $B_s \to K\ell\nu$ form factors from lattice QCD. *Phys. Rev. D 90(5), 054506 (2014)*. arXiv:1406.2279.

[32] **J. A. Bailey *et al.*** (Fermilab Lattice and MILC Collaborations)**.** $|V_{ub}|$ from $B \to \pi\ell\nu$ decays and (2+1)-flavor lattice QCD *(2015)*. arXiv:1503.07839.

[33] **Y. Liu, R. Zhou, J. A. Bailey, A. Bazavov, C. Bernard *et al.*** (Fermilab Lattice and MILC Collaborations)**.** Heavy-meson semileptonic decays for the Standard Model and beyond. *PoS LATTICE2013, 386 (2013)*. arXiv:1312.3197.

[34] **C. Bouchard, G. P. Lepage, C. J. Monahan, H. Na and J. Shigemitsu** (HPQCD Collaboration)**.** *B and Bs semileptonic decay form factors with NRQCD/HISQ quarks (2013)*. arXiv:1310.3207.

[35] **D. Du, J. A. Bailey, A. Bazavov, C. Bernard, A. El-Khadra *et al.*** (Fermilab Lattice and MILC Collaborations)**.** $B \to \pi\ell\nu$ and $B \to \pi\ell^+\ell^-$ semileptonic form factors from unquenched lattice QCD. *PoS LATTICE2013, 383 (2013)*. arXiv:1311.6552.

[36] **T. Kawanai, R. S. Van de Water and O. Witzel.** The form factors for $B \to \pi\ell\nu$ semileptonic decay from 2+1 flavors of domain-wall fermions *(2013)*. arXiv:1311.1143.

[37] **J. Bailey, A. Bazavov, C. Bernard, C. Bouchard, C. DeTar *et al.*** (Fermilab Lattice and MILC Collaborations)**.** $B \to \pi\ell\nu$ semileptonic form factors from unquenched lattice QCD and determination of $|V_{ub}|$ *(2014)*. arXiv:1411.6038.

[38] **P. Ball and R. Zwicky.** New results on $B \to \pi, K, \eta$ decay formfactors from light-cone sum rules. *Phys. Rev. D 71, 014015 (2005)*. arXiv:hep-ph/0406232.

[39] **G. Duplančić, A. Khodjamirian, T. Mannel, B. Melić and N. Offen.** Light-cone sum rules for $B \to \pi$ form factors revisited. *JHEP 0804, 014 (2008)*. arXiv:0801.1796.

[40] **A. Khodjamirian, R. Rückl, S. Weinzierl and O. I. Yakovlev.** Perturbative QCD correction to the $B \to \pi$ transition form-factor. *Phys. Lett. B 410, 275 (1997)*. arXiv:hep-ph/9706303.

[41] **A. Khodjamirian, T. Mannel, N. Offen and Y.-M. Wang.** $B \to \pi \ell \nu_l$ Width and $|V_{ub}|$ from QCD Light-Cone Sum Rules. *Phys. Rev. D 83, 094031 (2011)*. arXiv:1103.2655.

[42] **I. Sentitemsu Imsong, A. Khodjamirian, T. Mannel and D. van Dyk.** Extrapolation and unitarity bounds for the $B \to \pi$ form factor. *JHEP 1502, 126 (2015)*. arXiv:1409.7816.

[43] **M. Lüscher.** Volume Dependence of the Energy Spectrum in Massive Quantum Field Theories. 1. Stable Particle States. *Commun. Math. Phys. 104, 177 (1986)*.

[44] **G. Colangelo, S. Dürr and C. Haefeli.** Finite volume effects for meson masses and decay constants. *Nucl. Phys. B 721, 136 (2005)*. arXiv:hep-lat/0503014.

[45] **E. Eichten and B. Hill.** An effective filed theory for the calculation of matrix elements involving heavy quarks. *Phys. Lett. B 234, 511 (1990)*.

[46] **E. Eichten and B. Hill.** Renormalization of heavy-light bilinears and f_{B} for Wilson fermions. *Phys. Lett. B 240, 193 (1990)*.

[47] **E. Eichten and B. Hill.** Static effective field theory: $1/m$ corrections. *Phys. Lett. B 243, 427 (1990)*.

[48] **E. Eichten.** Heavy Quarks on the Lattice. *Nucl. Phys. Proc. Suppl. 4, 170 (1988)*.

[49] **R. Sommer.** Introduction to Non-perturbative Heavy Quark Effective Theory. *Published in: Les Houches Summer School in Theoretical Physics, Modern perspectives in lattice QCD, Les Houches, France, 3 – 28 August 2009. Oxford University Press, Oxford (2010)*. arXiv:1008.0710.

[50] **C. Bourrely, I. Caprini and L. Lellouch.** Model-independent description of $\mathrm{B} \to \pi \ell \nu$ decays and a determination of $|V_{\mathrm{ub}}|$. *Phys. Rev. D 79, 013008 (2009)*. arXiv:0807.2722.

[51] **K. G. Wilson.** Confinement of Quarks. *Phys. Rev. D 10, 2445 (1974)*.

[52] **C. Gattringer and C. B. Lang.** Quantum Chromodynamics on the Lattice: An Introductory Presentation. *Springer, Heidelberg (2009)*.

[53] **I. Montvay and G. Münster.** Quantum Fields on a Lattice. *Cambridge University Press, Cambridge (1997)*.

[54] **M. Lüscher, S. Sint, R. Sommer and P. Weisz.** Chiral symmetry and $O(a)$ improvement in lattice QCD. *Nucl. Phys. B 478, 365 (1996)*. arXiv:hep-lat/9605038.

[55] **M. Lüscher, S. Sint, R. Sommer, P. Weisz and U. Wolff.** Nonperturbative O(a) improvement of lattice QCD. *Nucl. Phys. B 491, 323 (1997)*. arXiv:hep-lat/9609035.

[56] **K. Jansen and R. Sommer** (ALPHA collaboration)**.** $O(\alpha)$ improvement of lattice QCD with two flavors of Wilson quarks. *Nucl. Phys. B 530, 185 (1998)*. arXiv:hep-lat/9803017.

[57] **K. Symanzik.** Continuum Limit and Improved Action in Lattice Theories. (I). Principles and ϕ^4 theory. *Nucl. Phys. B 226, 187 (1983)*.

[58] **K. Symanzik.** Continuum Limit and Improved Action in Lattice Theories. (II). $O(N)$ non-linear sigma model in perturbation theory. *Nucl. Phys. B 226, 205 (1983)*.

[59] **B. Sheikholeslami and R. Wohlert.** Improved Continuum Limit Lattice Action for QCD with Wilson Fermions. *Nucl. Phys. B 259, 572 (1985)*.

[60] **M. Lüscher.** Construction of a Selfadjoint, Strictly Positive Transfer Matrix for Euclidean Lattice Gauge Theories. *Commun. Math. Phys. 54, 283 (1977)*.

[61] **M. Albanese *et al.*** (APE Collaboration)**.** Glueball Masses and String Tension in Lattice QCD. *Phys. Lett. B 192, 163 (1987)*.

[62] **G. P. Lepage.** Simulating heavy quarks. *Nucl. Phys. Proc. Suppl. 26, 45 (1992)*.

[63] **S. Hashimoto.** Computation of the heavy - light decay constant using nonrelativistic lattice QCD. *Phys. Rev. D 50, 4639 (1994)*. arXiv:hep-lat/9403028.

[64] **M. Lüscher.** Computational Strategies in Lattice QCD. *Published in: Les Houches Summer School in Theoretical Physics, Modern perspectives in lattice QCD, Les Houches, France, 3 – 28 August 2009. Oxford University Press, Oxford (2010)*. arXiv:1002.4232.

[65] **A. Hasenfratz and F. Knechtli.** Flavor symmetry and the static potential with hypercubic blocking. *Phys. Rev. D 64, 034504 (2001)*. arXiv:hep-lat/0103029.

[66] **A. Hasenfratz, R. Hoffmann and F. Knechtli.** The Static potential with hypercubic blocking. *Nucl. Phys. Proc. Suppl. 106, 418 (2002)*. arXiv:hep-lat/0110168.

[67] **M. Della Morte, A. Shindler and R. Sommer** (ALPHA Collaboration)**.** On lattice actions for static quarks. *JHEP 0508, 051 (2005)*. arXiv:hep-lat/0506008.

[68] **M. Della Morte, S. Dürr, J. Heitger, H. Molke, J. Rolf, A. Shindler and R. Sommer** (ALPHA Collaboration)**.** Lattice HQET with exponentially improved statistical precision. *Phys. Lett. B 581, 93 (2004)*. arXiv:hep-lat/0307021.

[69] **L. Maiani, G. Martinelli and C. T. Sachrajda.** Nonperturbative subtractions in the heavy quark effective field theory. *Nucl. Phys. B 368, 281 (1992).*

[70] **J. Heitger and R. Sommer** (ALPHA Collaboration)**.** Non-perturbative heavy quark effective theory. *JHEP 0402, 022 (2004).* arXiv:hep-lat/0310035.

[71] **F. Bernardoni, B. Blossier, J. Bulava, M. Della Morte, P. Fritzsch *et al.*** (ALPHA collaboration)**.** The b-quark mass from non-perturbative $N_f = 2$ Heavy Quark Effective Theory at $O(1/m_h)$. *Phys. Lett. B 730, 171 (2014).* arXiv:1311.5498.

[72] **F. Bernardoni *et al.*** (ALPHA Collaboration)**.** Decay constants of B-mesons from non-perturbative HQET with two light dynamical quarks. *Phys. Lett. B 735, 349 (2014).* arXiv:1404.3590.

[73] **J. Körner and G. Thompson.** The heavy mass limit in field theory and the heavy quark effective theory. *Phys. Lett. B 264, 185 (1991).*

[74] **M. Neubert.** Heavy quark symmetry. *Phys. Rept. 245, 259 (1994).* arXiv:hep-ph/9306320.

[75] **R. Sommer.** Non-perturbative QCD: Renormalization, $O(a)$-improvement and matching to Heavy Quark Effective Theory. *Nara Lectures (2006).* arXiv:hep-lat/0611020.

[76] **M. Della Morte, J. Heitger, H. Simma and R. Sommer.** Non-perturbative Heavy Quark Effective Theory: An application to semi-leptonic B-decays *(2015).* arXiv:1501.03328.

[77] **M. Della Morte, S. Dooling, J. Heitger, D. Hesse and H. Simma** (ALPHA collaboration)**.** Matching of heavy-light flavour currents between HQET at order $1/m$ and QCD: I. Strategy and tree-level study. *JHEP 1405, 060 (2014).* arXiv:1312.1566.

[78] **M. Della Morte, P. Fritzsch and J. Heitger** (ALPHA Collaboration)**.** Non-perturbative renormalization of the static axial current in two-flavour QCD. *JHEP 0702, 079 (2007).* arXiv:hep-lat/0611036.

[79] **P. Fritzsch, N. Garron and J. Heitger** (ALPHA Collaboration)**.** Non-perturbative tests of continuum HQET through small-volume two-flavour QCD. *Unpublished (2013).*

[80] **J. Heitger, A. Jüttner, R. Sommer and J. Wennekers** (ALPHA Collaboration)**.** Non-perturbative tests of heavy quark effective theory. *JHEP 0411, 048 (2004).* arXiv:hep-ph/0407227.

[81] **M. A. Shifman and M. B. Voloshin.** On Annihilation of Mesons Built from Heavy and Light Quark and anti-B0 <—> B0 Oscillations. *Sov. J. Nucl. Phys. 45, 292 (1987).*

[82] **H. D. Politzer and M. B. Wise.** Leading Logarithms of Heavy Quark Masses in Processes with Light and Heavy Quarks. *Phys. Lett. B 206, 681 (1988).*

[83] **S. Capitani, M. Lüscher, R. Sommer and H. Wittig** (ALPHA Collaboration)**.** Non-perturbative quark mass renormalization in quenched lattice QCD. *Nucl. Phys. B 544, 669 (1999)*. arXiv:hep-lat/9810063.

[84] **M. Della Morte *et al.*** (ALPHA Collaboration)**.** Non-perturbative quark mass renormalization in two-flavor QCD. *Nucl. Phys. B 729, 117 (2005)*. arXiv:hep-lat/0507035.

[85] **M. Della Morte *et al.*** (ALPHA Collaboration)**.** Computation of the strong coupling in QCD with two dynamical flavors. *Nucl. Phys. 713, 378 (2005)*. arXiv:hep-lat/0411025.

[86] **K. Chetyrkin and A. Grozin.** Three loop anomalous dimension of the heavy light quark current in HQET. *Nucl. Phys. B 666, 289 (2003)*. arXiv:hep-ph/0303113.

[87] **P. Fritzsch, F. Knechtli, B. Leder, M. Marinkovic, S. Schaefer, R. Sommer and F. Virotta** (ALPHA Collaboration)**.** The strange quark mass and Lambda parameter of two flavor QCD. *Nucl. Phys. B 865, 397 (2012)*. arXiv:1205.5380.

[88] **F. Palombi.** Non-perturbative renormalization of the static vector current and its $O(a)$-improvement in quenched QCD. *JHEP 0801, 021 (2008)*. arXiv:0706.2460.

[89] **C. Alexandrou, F. Jegerlehner, S. Güsken, K. Schilling and R. Sommer.** B meson properties from lattice QCD. *Phys. Lett. B 256, 60 (1991)*.

[90] **S. Güsken, U. Löw, K. Mütter, A. Patel, K. Schilling and R. Sommer.** Non-singlet Axial Vector Couplings of the Baryon Octet in Lattice QCD. *Phys. Lett. B 227, 266 (1989)*.

[91] **S. Güsken.** A Study of smearing techniques for hadron correlation functions. *Nucl. Phys. Proc. Suppl. 17, 361 (1990)*.

[92] **R. Sommer.** Leptonic decays of B and D mesons. *Nucl. Phys. Proc. Suppl. 42, 186 (1995)*. arXiv:hep-lat/9411024.

[93] **M. Foster and C. Michael** (UKQCD Collaboration)**.** Quark mass dependence of hadron masses from lattice QCD. *Phys. Rev. D 59, 074503 (1999)*. arXiv:hep-lat/9810021.

[94] **P. F. Bedaque.** Aharonov-Bohm effect and nucleon nucleon phase shifts on the lattice. *Phys. Lett. B 593, 82 (2004)*. arXiv:nucl-th/0402051.

[95] **G. de Divitiis, R. Petronzio and N. Tantalo.** On the discretization of physical momenta in lattice QCD. *Phys. Lett. B 595, 408 (2004)*. arXiv:hep-lat/0405002.

[96] **C. Sachrajda and G. Villadoro.** Twisted boundary conditions in lattice simulations. *Phys. Lett. B 609, 73 (2005)*.

[97] **D. Guadagnoli, F. Mescia and S. Simula.** Lattice study of semileptonic form-factors with twisted boundary conditions. *Phys. Rev. D 73, 114504 (2006)*. arXiv:hep-lat/0512020.

[98] **A. Grimbach, D. Guazzini, F. Knechtli and F. Palombi** (ALPHA collaboration)**.** O(a) improvement of the HYP static axial and vector currents at one-loop order of perturbation theory. *JHEP 0803, 039 (2008)*. arXiv:0802.0862.

[99] **M. Lüscher**. http://luscher.web.cern.ch/luscher/DD-HMC/index.html**.**

[100] **M. Lüscher.** Schwarz-preconditioned HMC algorithm for two-flavour lattice QCD. *Comput. Phys. Commun. 165, 199 (2005)*. arXiv:hep-lat/0409106.

[101] **M. Lüscher.** Deflation acceleration of lattice QCD simulations. *JHEP 0712, 011 (2007)*. arXiv:0710.5417.

[102] **M. Lüscher.** Solution of the Dirac equation in lattice QCD using a domain decomposition method. *Comput. Phys. Commun. 156, 209 (2004)*. arXiv:hep-lat/0310048.

[103] **M. Lüscher.** Local coherence and deflation of the low quark modes in lattice QCD. *JHEP 0707, 081 (2007)*. arXiv:0706.2298.

[104] **G. Colangelo *et al.*** Review of lattice results concerning low energy particle physics. *Eur. Phys. J. C 71, 1695 (2011)*. arXiv:1011.4408.

[105] **G. P. Engel, L. Giusti, S. Lottini and R. Sommer.** Chiral Symmetry Breaking in QCD with Two Light Flavors. *Phys. Rev. Lett. 114(11), 112001 (2015)*. arXiv:1406.4987.

[106] **B. Blossier, M. Della Morte, G. von Hippel, T. Mendes and R. Sommer** (ALPHA Collaboration)**.** On the generalized eigenvalue method for energies and matrix elements in lattice field theory. *JHEP 0904, 094 (2009)*. arXiv:0902.1265.

[107] **J. Bulava, M. Donnellan and R. Sommer** (ALPHA Collaboration)**.** On the computation of hadron-to-hadron transition matrix elements in lattice QCD. *JHEP 1201, 140 (2012)*. arXiv:1108.3774.

[108] **M. Lüscher and U. Wolff.** How to Calculate the Elastic Scattering Matrix in Two-dimensional Quantum Field Theories by Numerical Simulation. *Nucl. Phys. B 339, 222 (1990)*.

[109] **P. Boucaud *et al.*** (ETM Collaboration)**.** Dynamical Twisted Mass Fermions with Light Quarks: Simulation and Analysis Details. *Comput. Phys. Commun. 179, 695 (2008)*. arXiv:0803.0224.

[110] **U. Wolff** (ALPHA collaboration)**.** Monte Carlo errors with less errors. *Comput. Phys. Commun. 156, 143 (2004)*. arXiv:hep-lat/0306017.

[111] **F. Virotta.** Critical slowing down and error analysis of lattice QCD simulations. *PhD thesis, Humboldt-Universität zu Berlin (2012).*

[112] **S. Schaefer, R. Sommer and F. Virotta** (ALPHA Collaboration)**.** Critical slowing down and error analysis in lattice QCD simulations. *Nucl. Phys. B 845, 93 (2011).* arXiv:1009.5228.

[113] **S. Lottini and R. Sommer.** Data Analysis in Lattice Field Theory. *Lectures at Lattice Practices (2014).*

[114] **N. Madras and A. D. Sokal.** The Pivot algorithm: a highly efficient Monte Carlo method for selfavoiding walk. *J. Statist. Phys. 50, 109 (1988).*

[115] **A. D. Sokal.** Monte Carlo Methods in Statistical Mechanics: Foundations and New Algorithms. *NATO Adv. Sci. Inst. Ser. B Phys. 361, 131 (1997).*

[116] **M. Bruno, D. Djukanovic, G. P. Engel, A. Francis, G. Herdoiza *et al.*** (CLS)**.** Simulation of QCD with $N_f = 2 + 1$ flavors of non-perturbatively improved Wilson fermions. *JHEP 1502, 043 (2015).* arXiv:1411.3982.

List of publications

[P1] **F. Bahr, F. Bernardoni, J. Bulava, A. Ramos, H. Simma and R. Sommer** (ALPHA Collaboration)**.** B $\to \pi$ form factor with 2 flavours of $O(a)$ improved Wilson quarks. *PoS LATTICE2012, 110 (2012).* arXiv:1210.3478.

[P2] **F. Bahr *et al.*** (ALPHA Collaboration)**.** $|V_{ub}|$ determination in lattice QCD. *PoS ICHEP2012, 424 (2013).* arXiv:1211.6327.

[P3] **F. Bahr, F. Bernardoni, J. Bulava, A. Joseph, A. Ramos, H. Simma and R. Sommer** (ALPHA Collaboration)**.** Form factors for $B_s \to K\ell\nu$ decays in Lattice QCD *(2014).* arXiv:1411.3916.

Acknowledgements

Many people have helped me realise this thesis. I wish to thank all of them here. Specifically, I would like to thank

- my family.
- my supervisor Rainer Sommer. He spent countless hours on helping and supporting me and my work, answering questions and explaining concepts.
- my collaborators for numerous fruitful discussions, inspiring comments and motivating guidance. Particularly, thanks to Hubert Simma and Anosh Joseph who always had time for discussions. Special thanks go to Fabio Bernardoni who was a very patient mentor to me.
- Stefano Lottini for pointing me to the results of the interpolations for κ_s discussed in section 5.2 not explicitly given in the reference.
- Mattia Bruno for providing his routine `derfit.m` that helps speeding up the fits discussed in this thesis only by like a factor 1000 or so.
- everybody at DESY Zeuthen who made time at DESY somewhat enjoyable.
- Nora.

Selbstständigkeitserklärung

Ich erkläre, dass ich die vorliegende Arbeit selbstständig und nur unter Verwendung der angegebenen Literatur und Hilfsmittel angefertigt habe.

Berlin, den

Felix Tobias Bahr